Maksym Dosta

Dynamic Flowsheet Simulation of Solids Processes and its Application to Fluidized Bed Spray Granulation

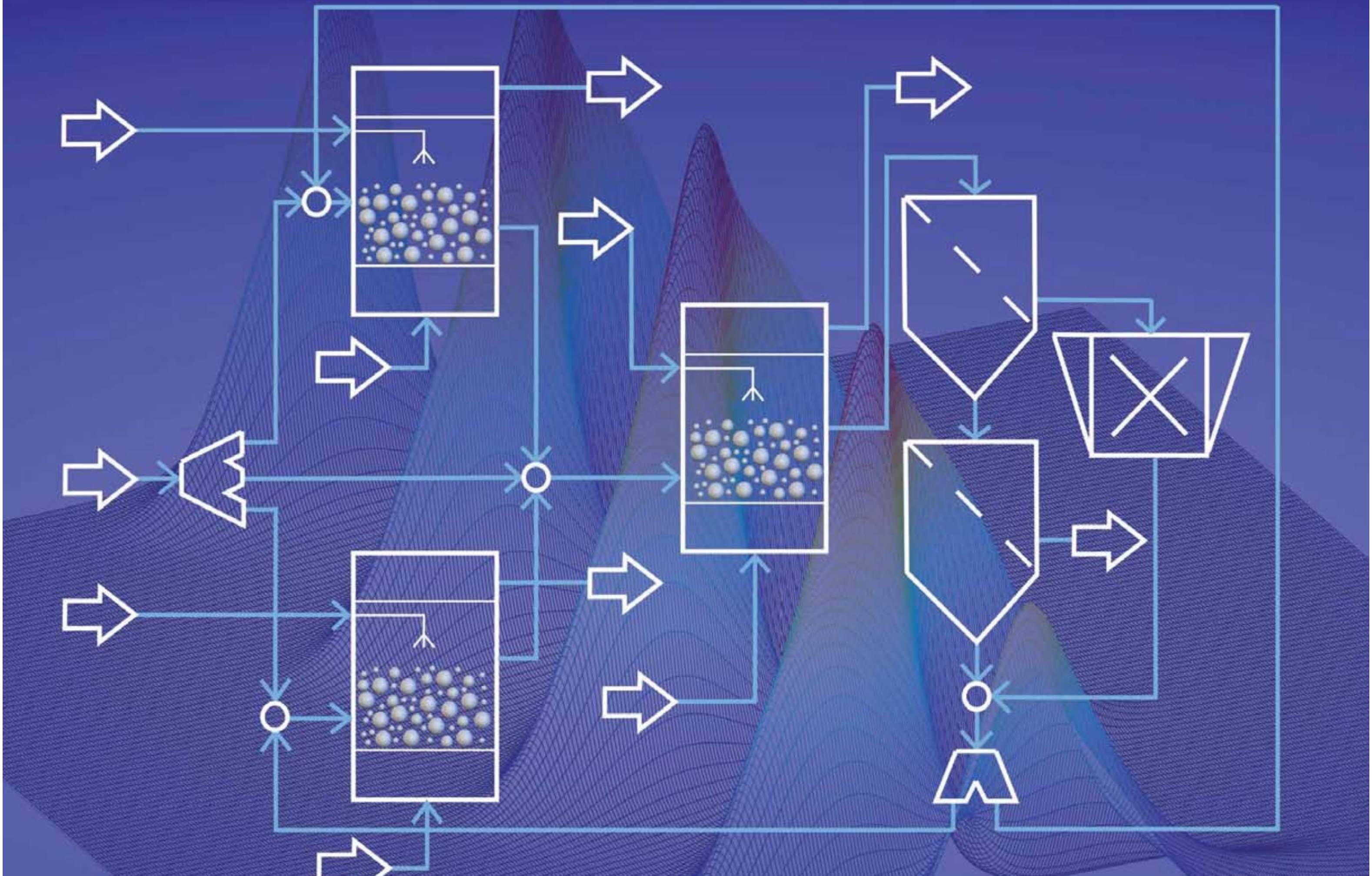

Cuvillier Verlag Göttingen
Internationaler wissenschaftlicher Fachverlag

Dynamic Flowsheet Simulation of Solids Processes and its Application to Fluidized Bed Spray Granulation

Dieses Werk ist copyrightgeschützt und darf in keiner Form vervielfältigt werden noch an Dritte weitergegeben werden.
Es gilt nur für den persönlichen Gebrauch.

Dieses Werk ist copyrightgeschützt und darf in keiner Form vervielfältigt werden noch an Dritte weitergegeben werden.
Es gilt nur für den persönlichen Gebrauch.

Dynamic Flowsheet Simulation of Solids Processes and its Application to Fluidized Bed Spray Granulation

Vom Promotionsausschuss der
Technischen Universität Hamburg-Harburg
zur Erlangung des akademischen Grades

Doktor-Ingenieur (Dr.-Ing.)
genehmigte Dissertation

von
M. Sc. **Maksym Dosta**

aus
Donezk, Ukraine

2012

Dieses Werk ist copyrightgeschützt und darf in keiner Form vervielfältigt werden noch an Dritte weitergegeben werden.
Es gilt nur für den persönlichen Gebrauch.

Bibliografische Information der Deutschen Nationalbibliothek
Die Deutsche Nationalbibliothek verzeichnet diese Publikation in der
Deutschen Nationalbibliografie; detaillierte bibliografische Daten sind im Internet
über http://dnb.d-nb.de abrufbar.
1. Aufl. - Göttingen : Cuvillier, 2013
Zugl.: (TU) Hamburg-Harburg, Univ., Diss., 2012

978-3-95404-335-4

Gutachter

1. Prof. Dr.-Ing. habil. Stefan Heinrich, Technische Universität Hamburg-Harburg
2. Prof. Dr.-Ing. Volodymyr Svyatnyy, Nationalen Technischen Universität Donezk

Tag der mündlichen Prüfung

20.12.2012

© CUVILLIER VERLAG, Göttingen 2013
Nonnenstieg 8, 37075 Göttingen
Telefon: 0551-54724-0
Telefax: 0551-54724-21
www.cuvillier.de

Alle Rechte vorbehalten. Ohne ausdrückliche Genehmigung des Verlages ist
es nicht gestattet, das Buch oder Teile daraus auf fotomechanischem Weg
(Fotokopie, Mikrokopie) zu vervielfältigen.
1. Auflage, 2013
Gedruckt auf säurefreiem Papier

978-3-95404-335-4

Dieses Werk ist copyrightgeschützt und darf in keiner Form vervielfältigt werden noch an Dritte weitergegeben werden.
Es gilt nur für den persönlichen Gebrauch.

Acknowledgments

This contribution is based on the results which have been received during my employment as a research fellow in the Institute of Solids Process Engineering and Particle Technology of Hamburg University of Technology.

First and foremost I wish to express my profound and gratitude to the supervisor of my PH.D. Thesis Prof. Dr.-Ing. Stefan Heinrich. His patient guidance, great encouragement and enthusiasm were very helpful and important for me. The friendship and strong support of Prof. Heinrich were invaluable to me on personal and academic level. It was an honor to work with him and to be a part of his team.

For the significant support and good advices I would like to thank Prof. Dr.-Ing. Joachim Werther one of the prominent researchers, who in the recently years has done plenty of work in the area of flowsheet simulation of solids processes. I would like to extend my appreciation to Dr.-Ing. Claus Reimer, Dr.-Ing. Matthias Pogodda and Dr.-Ing. Ernst-Ulrich Hartge. Their in-depth knowledge and experience in the area of steady-state flowsheet simulation of solids processes and their support were very helpful to me.

I want to thank my committee member Prof. Dr.-Ing. Volodymyr Svyatnyy for his time, interest, helpful comments and insightful questions.

Separately I would like to express acknowledge to my friend and colleague Dr.-Ing. Sergiy Antonyuk for his persistent support, helpful advices and valuable conversations.

Special thanks to the whole my family for their love and encouragements. I wish to express my gratitude to my parents for their support, understanding and for the given opportunity to obtain an excellent education. And of course, I would like to express a lot of thanks to my beloved wife for her strong support.

Finally, I want to express thanks to all my colleagues for spirited discussion, helpful advices and great working atmosphere.

Hamburg, 08 Januar 2013

Maksym Dosta

Dieses Werk ist copyrightgeschützt und darf in keiner Form vervielfältigt werden noch an Dritte weitergegeben werden.
Es gilt nur für den persönlichen Gebrauch.

Abstract

In this contribution the novel system for the dynamic flowsheet simulation of solids processes is presented. The system is generally applicable for all types of solids processes without limitation for specific process types. In a distinction to the existing flowsheet simulation systems, which have been mainly developed with a focus on fluid processes, the novel system allows to treat multidimensional distributed parameters properly.

To perform dynamic modeling of various industrial plants the library of dynamic units has been developed. These units can be easily added per drag and drop functionality onto the flowsheet and in this way the necessary process structure can be created. To make a simulation of various granulation plants the new dynamic models of fluidized bed spray granulation have been developed and implemented.

The fluidized bed spray granulation is widely used in the chemical, pharmaceutical, food and agricultural industries. In the majority of cases the granulation plants have a complex dynamic or even unstable behavior. Therefore, the dynamic simulation is one the of most effective way to understand process transient behavior, to optimize process and to develop different control strategies.

However, for the flowsheet simulation primarily empirical or semi-empirical models are used, where material microparameters and specific apparatus properties are poorly considered. To obtain more detailed estimation of process behavior, the multiscale modeling concept of solids processes has been developed. On the basis of the multiscale modeling methodology the novel multiscale simulation environment has been created. This environment consists of several models, which describe the process on different time and length scales, and has been effectively applied to the fluidized bed spray granulation process.

Dieses Werk ist copyrightgeschützt und darf in keiner Form vervielfältigt werden noch an Dritte weitergegeben werden.
Es gilt nur für den persönlichen Gebrauch.

Contents

Nomenclature IX

1. Introduction 1

2. Flowsheet simulation of solids 4

2.1 General methodology... 4

2.2 Complexity of solids processes 8

3. Novel dynamic flowsheet simulation system 13

3.1 Main calculation approach 13

3.2 Handling of distributed multidimensional parameters 19

3.3 Object-oriented programming architecture 25

3.4 Parallelization of the SolidSim-Dynamics system..................................32

3.4.1 General strategy 32

3.4.2 Parallelization on different hierarchical levels 35

4. Modeling of fluidized bed spray granulation 38

4.1 Process fundamentals 38

4.2 Population balance modeling 41

4.3 Dynamic models of fluidized bed granulation 48

4.3.1 Granulation model based on population balances...............................48

4.3.2 Model of heat and mass transfer..51

4.4 Dynamic models of fluidized bed aggregation 58

4.4.1 Fixed discretization method...58

4.4.2 Cell average technique 60

Dieses Werk ist copyrightgeschützt und darf in keiner Form vervielfältigt werden noch an Dritte weitergegeben werden.
Es gilt nur für den persönlichen Gebrauch.

5. Multiscale treatment of solids processes ... 65

5.1 General concept and interscale communications ... 65
5.2 Modeling on the microscale ... 74
5.3 Modeling on the mesoscale ... 78

6. Applications of a novel system for fluidized bed granulation ... 83

6.1 Validation of a novel simulation system ... 83
6.2 Simulation of a complex granulation model ... 91
6.3 Multiscale process calculation ... 97

Conclusion ... 103

References ... 106

Appendix ... 113

A.1: Methods of CDAEModel class ... 113
A.2: COM middleware interfaces used in SolidSim-Dynamics ... 114
A.3: Example of parallelization on the flowsheet level ... 115
A.4: Types of coalescence kernels ... 117
A.5: Comparison of results obtained from SolidSim-Dynamics and ACM systems ... 118
A.6: Approximations of heat and mass transfer ... 119
A.7: Simulation parameters for the multiscale calculation of the granulation process ... 120

List of publications ... 121

Dieses Werk ist copyrightgeschützt und darf in keiner Form vervielfältigt werden noch an Dritte weitergegeben werden.
Es gilt nur für den persönlichen Gebrauch.

Nomenclature

Abbreviations

ACM	Aspen Custom Modeler
BDF	Backward Differentiation Formula
CA	Cell Average
CAPE	Computer Aided Process Engineering
CFD	Computational Fluid Dynamics
COM	Component Object Model
CSTR	Continuous Stirred-Tank Reactor
DAE	Differential Algebraic Equations
DEM	Discrete Element Method
EO	Equation-Oriented
FB	Fluidized Bed
GPU	Graphical Processor Unit
MIMD	Multiple Instructions Multiple Data
NLA	Nonlinear Algebraic
ODE	Ordinary Differential Equations
OOP	Object-Oriented Programming
PBE	Population Balance Equations
PBM	Population Balance Model
PFTR	Plug Flow Tubular Reactor
PSD	Particle Size Distribution
PIDE	Partial Integro-Differential Equations
TI	Time Interval
UML	Unified Modelling Language
WR	Waveform Relaxation

Dieses Werk ist copyrightgeschützt und darf in keiner Form vervielfältigt werden noch an Dritte weitergegeben werden.
Es gilt nur für den persönlichen Gebrauch.

Latin letters

Variable	Unit	Denotation
A	m^2	Surface area
A_{tol}	–	Absolute tolerance
$Attr$	m/s	Attrition rate
B	–	Birth (source) event
$\bar{b}$	–	Breakage function
c_p	J·kg/K	Heat capacity
D	–	Death (sink) event
d	m	Diameter
F	N	Force
f	–	General factor
G	m/s	Growth rate
H	–	Holdup
$\dot{H}$	J/s	Enthalpy stream
Hs	–	Heaviside step function
i	–	General index
K	–	General coefficient
L	m	Length
M	kg	Mass
Mov	–	Movement matrix
N	–	Number
Nu	–	Nusselt number
$\dot{Q}$	J/s	Heat stream
R	m	Radius
R_e	–	Reynolds number
R_{tol}	–	Relative tolerance
Sh	–	Sherwood number
T_{window}	s	Size of time interval
X	–	Fraction
x	–	Coordinate
Y	kg/kg	Gas humidity (kg water/kg dry gas)

Dieses Werk ist copyrightgeschützt und darf in keiner Form vervielfältigt werden noch an Dritte weitergegeben werden.
Es gilt nur für den persönlichen Gebrauch.

Greek letters

Variable	Unit	Denotation
α	W/(m^2·K)	Heat transfer coefficient
β	1/s	Coalescence kernel
ε	–	Porosity (void volume fraction)
η	Pa·s	Viscosity
ρ	kg/m^3	Density
σ	N/m	Surface tension
ϕ	–	Wetted surface fraction
ψ	°	Angle of wetting region
ϑ	°C	Temperature

Subscripts

Variable	Denotation
32	Used to specify Sauter-diameter
a	Air
af	Transfer from air to liquid film
agg	Aggregation
ap	Transfer from air to particle
ax	Axial
$break$	Breakage
cap	Capillary
$crit$	Critical
cs	Cross-cut surface
D	Drag
dst	Destination term
dt	Discharge tube
e	Environment
elu	Elutriation
ext	External stream
f	Liquid film
G	Gravity

Dieses Werk ist copyrightgeschützt und darf in keiner Form vervielfältigt werden noch an Dritte weitergegeben werden.
Es gilt nur für den persönlichen Gebrauch.

in	Input
l	Layer
mf	Minimal fluidization
nuc	Nucleation
os	Overspray
out	Output
p	Particle
pf	Phase interface transfer from particle to liquid film
pw	Transfer between particle and apparatus wall
rec	Recycled stream
rel	Relative
sat	Saturation
sc	Screen
scl	Scalability
spd	Speedup
src	Source term
stl	Settling
$susp$	Suspension
tol	Tolerance
tot	Total
vap	Vapor
vis	Viscous
w	Water

Dieses Werk ist copyrightgeschützt und darf in keiner Form vervielfältigt werden noch an Dritte weitergegeben werden.
Es gilt nur für den persönlichen Gebrauch.

List of Figures

Figure 2.1: General process flowsheet 4
Figure 2.2: Flowsheet of urea granulation process 5
Figure 2.3: Difference between simultaneous and modular approaches 7
Figure 2.4: Example of incorrect solids treatment 10
Figure 3.1: Main calculation algorithm implemented into SolidSim-Dynamics 15
Figure 3.2: Exemplary scheme which consists of two dynamic units 17
Figure 3.3: Results obtained after processing of the exemplary scheme 18
Figure 3.4: Parameters deviations in the tear stream 19
Figure 3.5: General structure of the material stream object 20
Figure 3.6: Example of data compression 23
Figure 3.7: Application of the movement matrix in the SolidSim-Dynamics system 24
Figure 3.8: General structure of the SolidSim simulation system 26
Figure 3.9: The class diagram of the dynamic unit (UML notation) 27
Figure 3.10: Interfaces of the material stream 30
Figure 3.11: Screenshot of GUI of the SolidSim-Dynamics system 31
Figure 3.12: Stages of the program parallelization 33
Figure 3.13: Simultaneous calculation of parallel flowsheet branches 36
Figure 4.1: Fluidized bed granulator 38
Figure 4.2: Continuous particle growth (layering) 39
Figure 4.3: Formation of an agglomerate (particle aggregation) 39
Figure 4.4: General scheme of mechanisms in the FB granulator 42
Figure 4.5: General representation of the breakage process in the PBM 44
Figure 4.6: Sources of the overspray formation 45
Figure 4.7: General representation of the agglomeration process in the PBM 46
Figure 4.8: Flowchart of calculation procedure in the unit *FBGranulatorPBM* 50
Figure 4.9: Volume element of granulator with enthalpy (H) and heat (Q) streams 52
Figure 4.10: Representation of the alternative simulation strategies of FB granulator 56
Figure 4.11: GUI of the input dialog of the *FBGranulatorPBMHM* unit 57
Figure 4.12: Typical GUI of the dynamic model. Output dialog of the *FBGranulatorPBMHM*. 57
Figure 4.13: Discretized representation of PSD 59
Figure 4.14: Discretization of the size domain by CA technique 61
Figure 5.1: Models classification according to application area 66
Figure 5.2: Multiscale model of a circulating fluidized bed 67
Figure 5.3: Coupling scheme between DEM and CFD systems 68

Dieses Werk ist copyrightgeschützt und darf in keiner Form vervielfältigt werden noch an Dritte weitergegeben werden.
Es gilt nur für den persönlichen Gebrauch.

Figure 5.4: General scheme of interscale coupling 68
Figure 5.5: Flow-chart of the multiscale calculation algorithm 70
Figure 5.6: Programming architecture of the multiscale simulation environment 72
Figure 5.7: Different types of impact of wetted particles 76
Figure 5.8: Probabilities of different collision types 77
Figure 5.9: Schematic representation of the nozzle zone model 78
Figure 5.10: Example of application of the nozzle model 80
Figure 5.11: Example of a mesh conversion 82
Figure 6.1: Flowsheet of the granulation process 83
Figure 6.2: Comparison of the simulation results: coarse milling 85
Figure 6.3: Comparison of the simulation results: fine milling 85
Figure 6.4: Flowsheet of the process which consists of three FB granulators 87
Figure 6.5: Time progression of the PSD in the first granulator 89
Figure 6.6: Equivalent flowsheet structure in the SolidSim-Dynamics and Simulink systems. 90
Figure 6.7: Comparison between results obtained with Simulink and SolidSim-Dynamics 90
Figure 6.8: Flowsheet of the granulation process with internal classification 91
Figure 6.9: Dynamic behavior of main process parameters in the start-up phase 93
Figure 6.10: Influence of process parameter perturbation (classification air mass flow) 95
Figure 6.11: Influence of external nuclei mass flow 96
Figure 6.12: Flowsheet of the production process simulated by multiscale approach 97
Figure 6.13: Time-progression of the PSD of the holdup material 98
Figure 6.14: Transient behavior of the mass streams in the flowsheet 98
Figure 6.15: Apparatus geometry used for the micro and mesoscale simulations 99
Figure 6.16: Screenshot of the liquid distribution in the fluidized bed apparatus 100
Figure 6.17: Normalized growth rate 101
Figure 6.18: Comparison between steady-state results of empirical and multiscale models 102

Figure A.1: Exemplary flowsheet 115
Figure A.2: Simulation results (Jacobi method) 116
Figure A.3: Results obtained from SolidSim-Dynamics 118
Figure A.4: Results obtained from ACM 118

Dieses Werk ist copyrightgeschützt und darf in keiner Form vervielfältigt werden noch an Dritte weitergegeben werden.
Es gilt nur für den persönlichen Gebrauch.

List of Tables

Table 2.1: Examples of solids production processes 9
Table 2.2: Flowsheet simulation systems which are able to simulate solids 12
Table 3.1: Parameters of PSD in the streams 21
Table 3.2: Comparison of the quantity of stored entries by dense and sparse formats 21
Table 4.1: Enthalpy streams and heat streams within the volume element of a FB granulator .. 53
Table 6.1: Main process parameters of the flowsheet illustrated in Figure 6.4 88
Table 6.2: Main parameters of the process with internal classification 92

Table A.1: List of the methods implemented into the *CDAEModel* class 113
Table A.2: Description of the main interfaces which are used in SolidSim-Dynamics 114
Table A.3: A short summary of different coalescence kernels given in the literature 117
Table A.4: Main simulation parameters used for the multiscale process modeling 120

Dieses Werk ist copyrightgeschützt und darf in keiner Form vervielfältigt werden noch an Dritte weitergegeben werden.
Es gilt nur für den persönlichen Gebrauch.

Dieses Werk ist copyrightgeschützt und darf in keiner Form vervielfältigt werden noch an Dritte weitergegeben werden.
Es gilt nur für den persönlichen Gebrauch.

1. Introduction

Nowadays, numerical simulation plays one of the key roles in the area of solids process engineering. It is applied to describe, to analyze and to predict process behavior and to develop control and optimization strategies.

Simulation can be performed on different time and length scales considering different phenomena which take place. This can be a microscopic scale, where for example the internal particle structure is taken into account to simulate liquid penetration into pores. Alternatively, these may be much coarser scales where the thermodynamics of a whole apparatus is calculated.

In spite of the existence of various models on the different scales, the ultimate goal of process modeling is the simulation and prediction of a plant performance (Werther et al., 2011). In order to perform a modeling of plants, which often consist of an interconnection of numerous apparatuses and process substeps, the usage of flowsheet simulation systems is state of the art for the fluid processes. The analytical solution of processes, which have complex structures and where recycled energy and mass streams exist, is in most cases impossible.

The flowsheet simulation tools have become wide applications in the area of fluid processes, where nowadays various commercial and freeware software tools does exist (Hartge et al., 2006). In comparison with it, the flowsheet calculation of particulate systems has a much shorter history. In recent years, especially for solids processes, the steady-state flowsheet simulation system SolidSim has been developed (Pogodda, 2007). This framework is applicable to general solids processes; however, the ability to perform just steady-state calculations limits considerably the application areas of it. To date, engineers do not have a general simulation tool which is able to solve the tasks concerning dynamic solids behavior effectively. This gap in the area of dynamic flowsheet simulation of particulate processes and the huge interest expressed from the side of industrial companies are the main factors of intensified researches in this direction.

The work, which is presented in this contribution, is focused on the development of a novel system for dynamic flowsheet simulation of solids. On the one hand there was an aim to develop the simulation framework, on the other hand, to derive and to implement new dynamic models for the calculation of fluidized bed granulation processes.

Dieses Werk ist copyrightgeschützt und darf in keiner Form vervielfältigt werden noch an Dritte weitergegeben werden.
Es gilt nur für den persönlichen Gebrauch.

The central role in the simulation framework plays the calculation algorithms and methods which are used to simulate flowsheet and to calculate energy and mass balances in all streams. There can be distinguished between two main methods, namely equation-oriented and sequential-modular. Each of them has its own advantages, but the modular approach can be more effectively used for the calculation of solids (Dosta et al., 2010). Due to the high complexity of the models of different apparatuses, the equation-oriented approach is confronted with insuperable difficulties. More detailed analysis of both these methods can be found in Chapter 2.

Parallel with a development of the simulation methods and architecture of the new framework, the dynamic models of numerous apparatuses and process substeps play an important role. The fluidized bed granulator was one of the first apparatuses, which was developed and added into the library of the dynamic models. The fluidized bed spray granulation is one of the widely used production processes in the chemical, pharmaceutical, food and agricultural industries (Mörl et al., 2007). In this process different production substeps, like wetting, drying, heating, etc. are combined into one apparatus. It allows producing dust-free, free-flowing particulate products with specified properties, such as particle size distribution, compounds percentage, density, etc. The description of the fluidized bed granulation is not a trivial task, because of the intensive heat and mass transfer, the huge influence of all three phases onto the behavior and complex fluid dynamics which take place. In the majority of cases the granulation plants have a complex dynamic or even unstable behavior. That is why dynamic calculations are necessary to simulate the process.

In recent years a lot of researches were performed in the area of modeling the granulation process, whereby models with different levels of detail were developed. As a first approximation, the empirical or semi-empirical models, which are based on population balance models, are used (Heinrich et al., 2002), (Hounslow et al., 1988), (Litster et al., 1995). Using the population balances, the transient behavior of the particle distribution due to the numerous events like growth, aggregation, breakage, attrition, etc. is analyzed (Ramkrishna, 2000). To obtain a more detailed description, the model can be extended by considering the heat and mass transfer which occurs in the apparatus (Heinrich and Mörl, 1999). Nevertheless, the material microproperties and apparatus geometry are poorly considered in these models.

With a purpose to perform more detailed modeling the granulation process can be described on smaller length and time scales. On the microscale a lot of particulate systems can be effectively simulated using the discrete element method, where each particle is considered as a separate entity (Cundall and Strack, 1979). The disadvantage of this approach is a huge computational effort, which does not allow performing calculation of a real apparatus on a long time interval. A

Dieses Werk ist copyrightgeschützt und darf in keiner Form vervielfältigt werden noch an Dritte weitergegeben werden.
Es gilt nur für den persönlichen Gebrauch.

possible solution of this problem is a combination of submodels from different time and length scales into one multiscale model (Ingram et al., 2003). Hence, to give the possibility for the user to perform the simulation of a granulation process with high detailing grade, the novel multiscale model of a fluidized bed granulator was developed in this work.

Dieses Werk ist copyrightgeschützt und darf in keiner Form vervielfältigt werden noch an Dritte weitergegeben werden.
Es gilt nur für den persönlichen Gebrauch.

2. Flowsheet simulation of solids

2.1 General methodology

Flowsheet simulation is used to perform quantitative modeling of industrial production processes and allows to predict properties, compositions and flowrates in the streams and main operating conditions. During flowsheet simulation the numerical solutions of energy and mass balances as well as intensive process variables for arbitrary materials and process structures can be calculated.

The investigated process is decomposed and represented as a set of individual submodels, which are coupled by energy and mass streams. In Figure 2.1 the process-flow diagram of an example structure is illustrated. The energy and raw material are introduced into the system through the input streams and after their transformation the resulting product leaves the flowsheet.

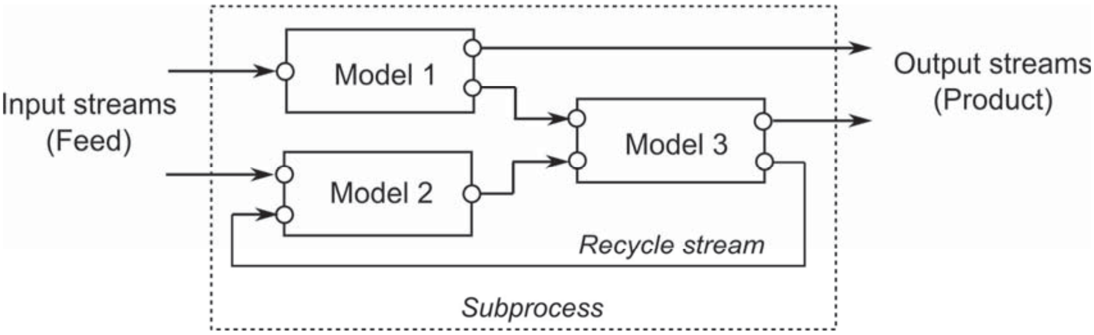

Figure 2.1: General process flowsheet

The scheme depicted in Figure 2.1 has simplified topology, while real industrial production processes can have a structure with much higher degree of complexity. In this case the main demands, which are related to the numerical simulation, are caused by the knotted network of material and energy streams and large amount of apparatuses and production substeps. In Figure 2.2 as an example, the general structure of industrial granulation process is shown. This process is used for fluidized bed granulation of urea (Uhde Fertilizer Technology). Because of the existence of a recycled material stream of milled granules the analytical prediction of the process behavior and its optimization is an unfeasible task. Therefore, the numerical solution with help of flowsheet simulation systems plays an important role in the industry.

Dieses Werk ist copyrightgeschützt und darf in keiner Form vervielfältigt werden noch an Dritte weitergegeben werden.
Es gilt nur für den persönlichen Gebrauch.

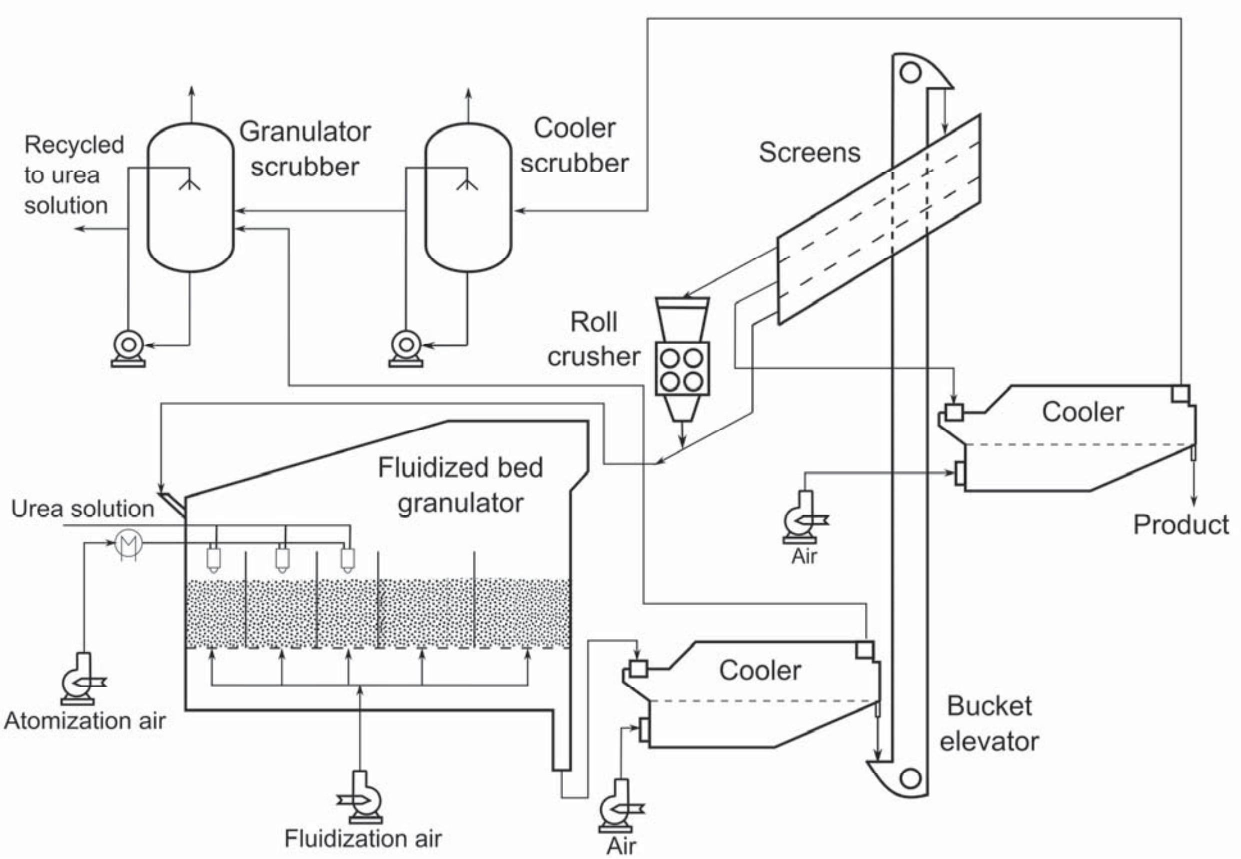

Figure 2.2: Flowsheet of urea granulation process

The flowsheet simulation can be performed in steady-state and dynamic modes. The dynamic simulation serves to obtain time dependent behavior and is much more demanding regarding computational effort. Despite the easier calculation procedure, the steady-state modeling not always allows to achieve sufficient results.

For example, transient process behavior during starting-up or shutting down phases often leads to the increased consumption of energy and raw material and cannot be modeled by a steady-state simulation tool. As a consequence, the usage of the steady-state simulation makes effective optimization infeasible. Another case, where just a dynamic simulation can be applied, is an unsteady process such as agglomeration or crystallization, which can be unsteady or can possess constant or damped oscillating behavior.

As mentioned, from the computational point of view two general classes of calculation strategies can be distinguished, which can be applied for the dynamic flowsheet simulation (Marquardt, 1991):

- equation-oriented (simultaneous) approach
- modular (sequential-modular) approach.

Dieses Werk ist copyrightgeschützt und darf in keiner Form vervielfältigt werden noch an Dritte weitergegeben werden.
Es gilt nur für den persönlichen Gebrauch.

It should also be mentioned that a combination between the methods listed above can serve as effective calculation strategy, which is used for instance in the Aspen Dynamics framework (Aspen). In the Aspen Dynamics, the modular approach is used to find consistent initial conditions (Aspen Plus) and equation-oriented approach (Aspen Custom Modeler) to perform dynamic modeling.

In the case of the simultaneous approach, equations for the description of all units (physical properties, thermodynamics, mass and energy balances, stream connectivity, etc.) are combined into one homogeneous system of Differential Algebraic Equations (DAE's) or Ordinary Differential Equations (ODE's). In most cases this is a large set of equations, where small fraction of variables is included into any single equation (sparse). This system is solved simultaneously by a suitable integration method. Usually the Newton or quasi-Newton algorithms are used. That results in iterative calculation of Jacobian matrices and solution of large non-linear equation systems (Hindmarsh et al., 2005).

This equation-oriented approach can be applied for a flowsheet process which consists of open-form models (Schopfer et al., 2004). These types of models provide all information about the internal equations set, as it is required by an external numerical algorithm.

By the modular approach (Hillestad and Hertzberg, 1986), (Helget, 1997) the units are represented as "black box" models and every unit is solved independently from each other by its own calculation procedure. The calculation sequence corresponds to the flow of material on the actual process and the connectivity equations are solved implicitly by direct data transfer from output of one unit to the input of another.

This approach can be easily applied, when the flowsheet has a simple topology and does not contain recycle streams. In the case of complex structures with a material and energy feedback the modeling procedure becomes more complex. In the first stage the structural loops should be torn to render acyclic network topology. Afterwards, iterative calculation is performed until the convergence is reached. As convergence criteria the deviations of the tear stream on successive iterations is examined.

In Figure 2.3 the general principle of both approaches is illustrated. The exemplary flowsheet consists of a fluidized bed granulator and a screen apparatus and contains one recycle stream. By simulation with an equation-oriented (EO) approach, the equations are homogenized and calculated by one solver. The modular approach gives more flexibility in the choice of the calculation procedure, because each unit is solved separately and different solvers and calculation procedures can be used simultaneously.

Dieses Werk ist copyrightgeschützt und darf in keiner Form vervielfältigt werden noch an Dritte weitergegeben werden.
Es gilt nur für den persönlichen Gebrauch.

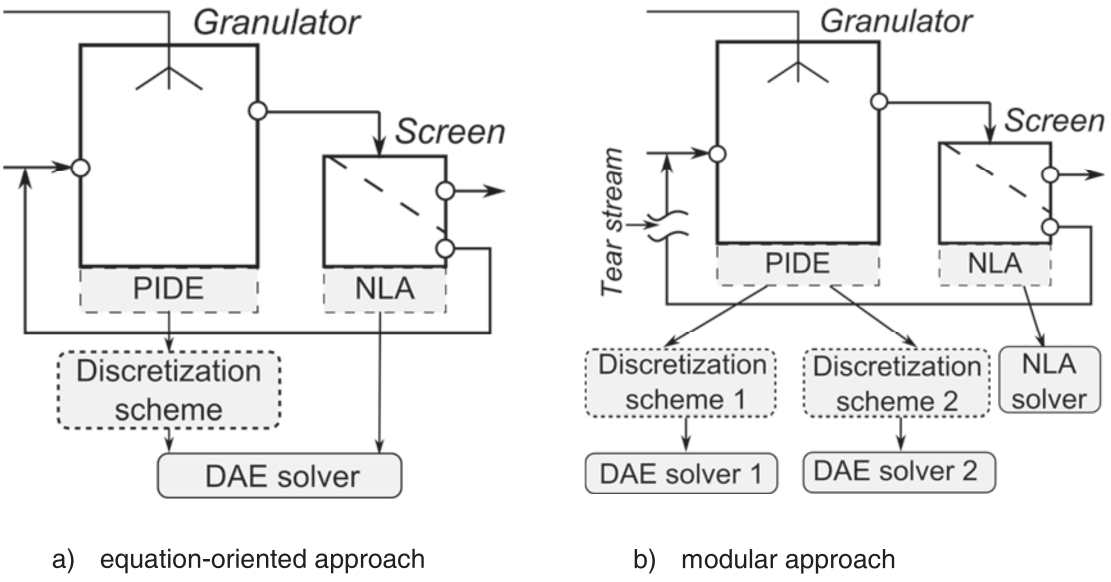

a) equation-oriented approach b) modular approach

Figure 2.3: Difference between simultaneous and modular approaches

One of the main advantages of the equation-oriented approach, compared to the modular one, are better convergence properties, which can be reached especially in the situations when the flowsheet contains large number of recycle streams (Morton, 2003). However, heterogeneity of the mathematical models, which are developed in the area of solids processes, complicate the usage of simultaneous approach. These models can be consisted of ODE's, PDE's, linear and nonlinear algebraic equations as well as they can also have implicit and explicit (time events) discontinuities, which can modify the structure of the model. Further complexity arises from various particulate processes, for instance crystallization, granulation, agglomeration, drying. Commonly these processes can be described by a population balance model (PBM) and contain the partial integro-differential equations (PIDE) (Ramkrishna, 2000).

After the comparison of both above described strategies, the conclusion can be drawn that modular strategy, according to the set of advantages, can be more effectively applied for dynamic flowsheet simulation of solids processes. From the significant advantages of sequential-modular approach the following can be marked out:

- higher flexibility in the process of model development: Any closed-form model can be added to the flowsheet;
- only this approach can be used when a certain appropriate solver for simulation of the whole system does not exist;
- it leads to an easier procedure of the consistent initialization (Biegler et al., 1997): In the case of modular simulation, the process units are executed in the sequence according

Dieses Werk ist copyrightgeschützt und darf in keiner Form vervielfältigt werden noch an Dritte weitergegeben werden.
Es gilt nur für den persönlichen Gebrauch.

to the structure of the flowsheet, which provides a reasonably good starting point for simulation;

- it allows to implement the effective methods for parallelization (Borchardt et al., 1999).

2.2 Complexity of solids processes

For many years, the usage of the flowsheet simulation frameworks is a state of the art in the area of Computer Aided Process Engineering (CAPE) (Schuler, 1995). However, in spite of the importance of solids processes, previous researches have been more focused on the fluid systems. Exactly, for the fluid processes the development of a flowsheet simulation methods was first started (Hlavacek, 1977), (Shacham et al., 1982), (Marquardt, 1991) and the first software tools for the flowsheet simulation were implemented.

Nowadays solids processes play an important role in chemical, pharmaceutical, agricultural and food industries. More than 60% of all products, which are sold by such companies as DuPont or BASF to the customers, are amorphous, crystalline or polymeric solids (Wintermantel, 1999). In order to satisfy the quality standards, these products should consist not only of specified chemical compounds, but they should also have a specific clearly defined size distribution, shape and physical microproperties. For instance, the flowability and stability of solids products play a decisive role in the minimization of transportation and storage costs.

For the transformation of the raw material into the final product, various types of processes with different conversion operations can be used. According to the classification proposed by Rumpf (1975) five mechanical treatment techniques can be categorized:

- splitting (grinding, cutting, deagglomeration, etc.);
- separation (classification, screening, sedimentation, etc.);
- agglomeration (compacting, tabletting, granulation, etc.);
- mixing (homogenization, stirring, dispersing, etc.);
- transport, storage and dosing of disperse material.

The above described basic operations sequentially or simultaneously appear in the industrial processes. In Table 2.1 some process examples from different industries are listed.

Dieses Werk ist copyrightgeschützt und darf in keiner Form vervielfältigt werden noch an Dritte weitergegeben werden.
Es gilt nur für den persönlichen Gebrauch.

Table 2.1: Examples of solids production processes

Process description	Industry
alumina calcination process	chemical
fluidized bed combustion process (Ratschow, 2009)	energy
urea granulation process (Uhde Fertilizer Technology) (see Figure 2.2)	agricultural
separation of contaminated dredged material into clean sand fraction and silt fraction with high contamination degree (Detzner, 1995)	environmental

Each of the listed examples consists of a complex interconnection of different apparatuses and basic process steps (unit operations), like screening, crushing, solids transportation, etc. To minimize the production costs and to create effective plant structures the material and energy streams are often re-used in the processes. Because of the existence of additional recycled streams this leads to an increase of the structure complexity. That is why in most cases even coarse analytical prediction of process steady-state and transient behavior are not possible. To solve this problem, the numerical calculations in form of flowsheet simulation should be used.

The necessity to distinguish the solids processes from liquid-vapor systems is not just by an additional phase, but rather by new simulation methods, was pointed out by numerous authors (Rossister and Douglas, 1986), (Barton and Perkins, 1988), (Evans, 1989), (Hartge et al., 2006), etc.). In the case of solids processes it is necessary to handle with a set of multidimensional distributed properties, which describe particle distribution by size, shape, habit, solid moisture content, etc. According to the complexity of the data, properties can be divided into three main categories (Pogodda, 2007) :

- distributed properties generally used for all types of distributed parameters such as PSD or stream composition;
- single-value properties have following data fields: numeric value, dimension and name. Each stream has at least four single-value properties such as temperature, pressure, mass flow and phase fractions of each phase;
- dependent single-value properties can have a different value for each individual interval of certain distributed property. For example, moisture content or density can be for different for different size fractions.

Dieses Werk ist copyrightgeschützt und darf in keiner Form vervielfältigt werden noch an Dritte weitergegeben werden.
Es gilt nur für den persönlichen Gebrauch.

Application of the simulation methods developed for liquid-vapor systems can cause an incorrect process modeling or even the loss of required information. In Figure 2.4 a schematic representation of the calculation of the screen unit and appeared incorrectness are shown. Here, the separation diameter of the screen is 2 mm and the inlet solid stream consists of particles which are distributed by dissimilar color and size. To illustrate the appeared incorrectness it is assumed that the inlet stream consists of just four fractions, which are depicted in Figure 2.4.

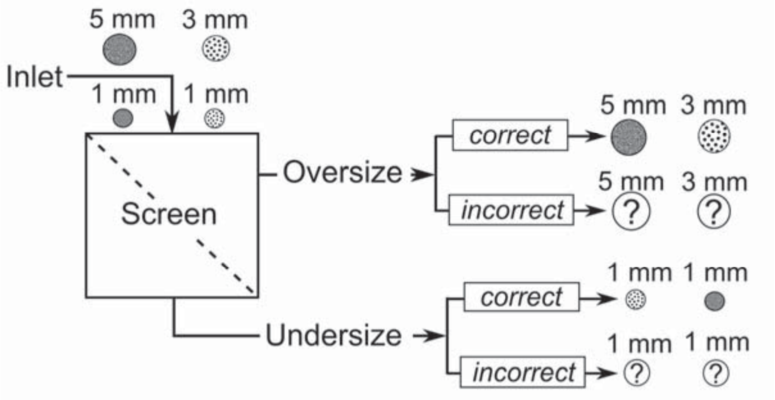

Figure 2.4: Example of incorrect solids treatment

If the inlet stream in Figure 2.4 is treated on the same manner like a fluid, the multidimensional properties will be mixed and as a consequence incorrect results will be received. One of the possible solutions of this problem was proposed and implemented in the SolidSim simulation environment (Pogodda, 2007). In order to achieve correct handling of multidimensional parameters the approach based on the stream transformation was developed. Instead of explicit calculation of models, in the SolidSim system a movement matrix is generated for every unit. This matrix is used to perform transformation of inlet to outlet stream.

A further question is how the distributed solid properties, as, for instance, the particle size distribution (PSD), are represented in the system. The conventional way to describe such parameters is the usage of the discretized form of PSD’s. In this case, the variables are represented by a set of intervals along internal coordinates and assigned to them values. The application of a coarse grid can lead to a large simulation error, induced by numerical diffusion. Hounslow and Wynn (1992) have pointed out the disadvantages of the usage of the discretized PSD and have proposed a functional description of PSD as continuous parameter. However, in the case of flowsheet simulation the exact representation of parameter values in terms of functions is a challenging task (Többermann, 1999). Furthermore, the discretization by a sufficiently fine grid decreases the numerical error to the values, which are significantly smaller in comparison with the inaccuracies, which arise due to the process simplification in the used empirical models.

Dieses Werk ist copyrightgeschützt und darf in keiner Form vervielfältigt werden noch an Dritte weitergegeben werden.
Es gilt nur für den persönlichen Gebrauch.

Further challenge of processing of solids processes is induced by the complexity of the existing models and the necessity to use different numerical techniques to solve them. For instance, to describe the time evolution of the particle assemblies during various production processes, the usage of the population balance models (PBM's) is a state of the art (Ramkrishna, 2000) (Gerstlauer et al., 2006). They have been introduced into the area of chemical engineering by Hulburt and Katz (1964) and since that time they have experienced wide expansion and have been applied for many processes like granulation, crystallization, grinding, drying, etc. The general form of the PBM is represented as a partial integro-differential equation, the numerical calculation of which can be rather tedious.

Similar to other listed above demands, in the case of solids processes the apparatus geometry has a bigger influence on to the process behavior then in the case of fluids. For instance, the number of nozzles and their spraying angle or exact positions in the fluidized bed granulator can have a decisive influence on the growth kinetics of granules. Another example is a hydrocyclone, which separation characteristics of which depends on the apparatus diameter.

Werther et al., (2004) have formulated a set of requirements to the flowsheet simulation system of solids processes. The main necessary criteria are:

- general application to all types of processes which involve solids;
- consideration of liquid and vapour phases;
- existence of a unit library for numerous apparatuses and subprocesses;
- user-friendly graphical interface;
- documentation with information about implemented models and calculation methods.

Over the last few years, various flowsheet simulation programs have been developed particularly for solids processes and already existing systems were modified to handle solids. In Table 2.2 the most well-known systems are listed.

Despite the large number of entries listed in Table 2.2, neither of the above mentioned systems can be effectively used for dynamic simulation of general solids processes. Some of the programs are applicable just for processes with fixed structure or for a strongly limited number of unit operations, while other software tools can be used just for steady-state calculations. Therefore, after analysis of the state of the art, the conclusion about the necessity to develop a new modeling environment for the dynamic flowsheet simulation of solids processes can be drawn.

Dieses Werk ist copyrightgeschützt und darf in keiner Form vervielfältigt werden noch an Dritte weitergegeben werden.
Es gilt nur für den persönlichen Gebrauch.

Table 2.2: Flowsheet simulation systems which are able to simulate solids

Program	Simulation type	Main application area	Last release
Metsim (Metsim)	Steady-state (some process can be modelled dynamically)	Chemical industry	2001 (Metsim ver. 19.01)
PMP FS Sim PMP FS Disp (Grainsoft)	Steady-state	Different size-reduction processes with classification units	2004
CHEOPS (Kulikov et al., 2005)	Tools integration framework for dynamic simulation	General solids processes	2005
JKSimMet (Morrison and Richardson, 2002)	Steady-state	Mining processing	2006
USimPack (Brochot et al., 2002)	Steady-state	Mineral processing	2007
Parsival (Wulkow et al., 2001)	Dynamic	Industrial crystallization, granulation processes	2009
Pro II (Invensys)	Steady-state	Polymer, fine-chemical and food industries	2010
FBSim	Dynamic	Fluidized bed granulation with predefined process structure	2006
gSolids (PSE)	Steady-state and dynamic	General solids processes	2012
AggFlow (AggFlow)	Steady-state	Mining industry	2011
SolidSim (Hartge et al., 2006)	Steady-state	General solids processes	2012
Aspen Plus, Aspen Dynamics, Aspen Custom Modeler	Steady-state, dynamic	Fluid processes with solid and gas phases	2012

Dieses Werk ist copyrightgeschützt und darf in keiner Form vervielfältigt werden noch an Dritte weitergegeben werden.
Es gilt nur für den persönlichen Gebrauch.

3. Novel dynamic flowsheet simulation system

3.1 Main calculation approach

The basic simulation concept, which is used in the SolidSim-Dynamics framework, is based on the sequential-modular calculation approach with the usage of the waveform relaxation (Picard-Lindelöf iteration) method (Lelarasmee, 1982). Originally the waveform relaxation (WR) method was applied for the simulation of Very Large Scale Integrated (VLSI) circuits. It was developed as a new decomposition method for solving a system of mixed differential algebraic equations (DAE) over a successive time horizon (time window). Here, the total equation set is divided into subsystems and over a certain time window all subsystems are simulated independently. Unknown values of connection variables are approximated using the solutions (waveforms) from previous iterations.

There exist several modifications of the relaxation scheme, such as the Gauss-Jacobi WR or Gauss-Seidel WR (Crow and Ilic, 1990). In the SolidSim-Dynamics environment the Gauss-Seidel method has been used, which possesses better convergence properties compared to the Gauss-Jacobi approach. One of the main advantages of the implemented method is that different solvers or calculation algorithms with different internal differentiation steps can be simultaneously used for the solution of the flowsheet. In situations, where fast changing units as well as slower ones occur in a flowsheet, this method can reduce the computational effort. In the same time, the strong coupling between the subsystems may result in a poor convergence rate (Dosta et al., 2008).

In the area of solids processes not all apparatuses reveal a pronounced transient behavior. This concerns apparatuses with relatively small holdup, like screen, mill or mixer. These types of transformations of a raw material can be effectively simulated by steady-state units. To allow the usage of the steady-state units in the dynamic simulation environment the “quasi-dynamic” processing of such units was developed and implemented. In the initialization or calculation phases, the distinction between units of different types is done. During dynamic simulation with a sequential-modular approach, the units are processed one by one in some specified sequence. By simulation with the dynamic model, the control is transferred from the modeling environment to the unit and the unit initiates its own calculation procedure on the current time interval. The dynamic unit determines itself the time points where the calculation of the model is performed. This array of points may not match up with the points specified in the inlet streams.

Dieses Werk ist copyrightgeschützt und darf in keiner Form vervielfältigt werden noch an Dritte weitergegeben werden.
Es gilt nur für den persönlichen Gebrauch.

In this case a linear interpolation is applied to approximate the missing values in the input stream.

In distinction to the dynamic units, the steady-state units are not able to handle time-dependent properties. Therefore, each steady-state model is processed for every point of time, for which the input stream is specified. Consequently, the output stream will inherit the time points from the input. In the case when the unit has more than one inlet, the time points from all input streams are merged into the sorted list of unique values, which is afterwards transferred to the output.

In Figure 3.1 the flowchart of the main simulation algorithm, which has been implemented into SolidSim-Dynamics system, is illustrated. In the first step the flowsheet is initialized. This is an iterative procedure, which is repeated until the convergence in block *(18)* is reached. During this procedure the initialization of all units in the process is carried out. In the case of steady-state units, the calculation of the implemented model is performed *(17)*.

For the dynamic models the consistent initial conditions are approximated *(16)*. The consistency requires that for a system of DAE, which can be expressed in general form as Eq. (3.1), a set of initial values of y_0 and y_0' Eq. (3.2) should be found for a start time point t_0.

$$G(t, y, y') = 0, \text{ where } G, y, y' \in R^N \tag{3.1}$$

$$G(t_0, y_0, y_0') = 0 \tag{3.2}$$

One DAE solver has been implemented into the SolidSim-Dynamics environment. This solver is able to find consistent initial conditions automatically using the Newton iterations method combined with a line search algorithm (Brown et al., 1998). There exist two available modes of the initialization:

- to compute all components of y by given y';
- to obtain differential components of y' and algebraic components of y, by given value of differential components of y.

Dieses Werk ist copyrightgeschützt und darf in keiner Form vervielfältigt werden noch an Dritte weitergegeben werden.
Es gilt nur für den persönlichen Gebrauch.

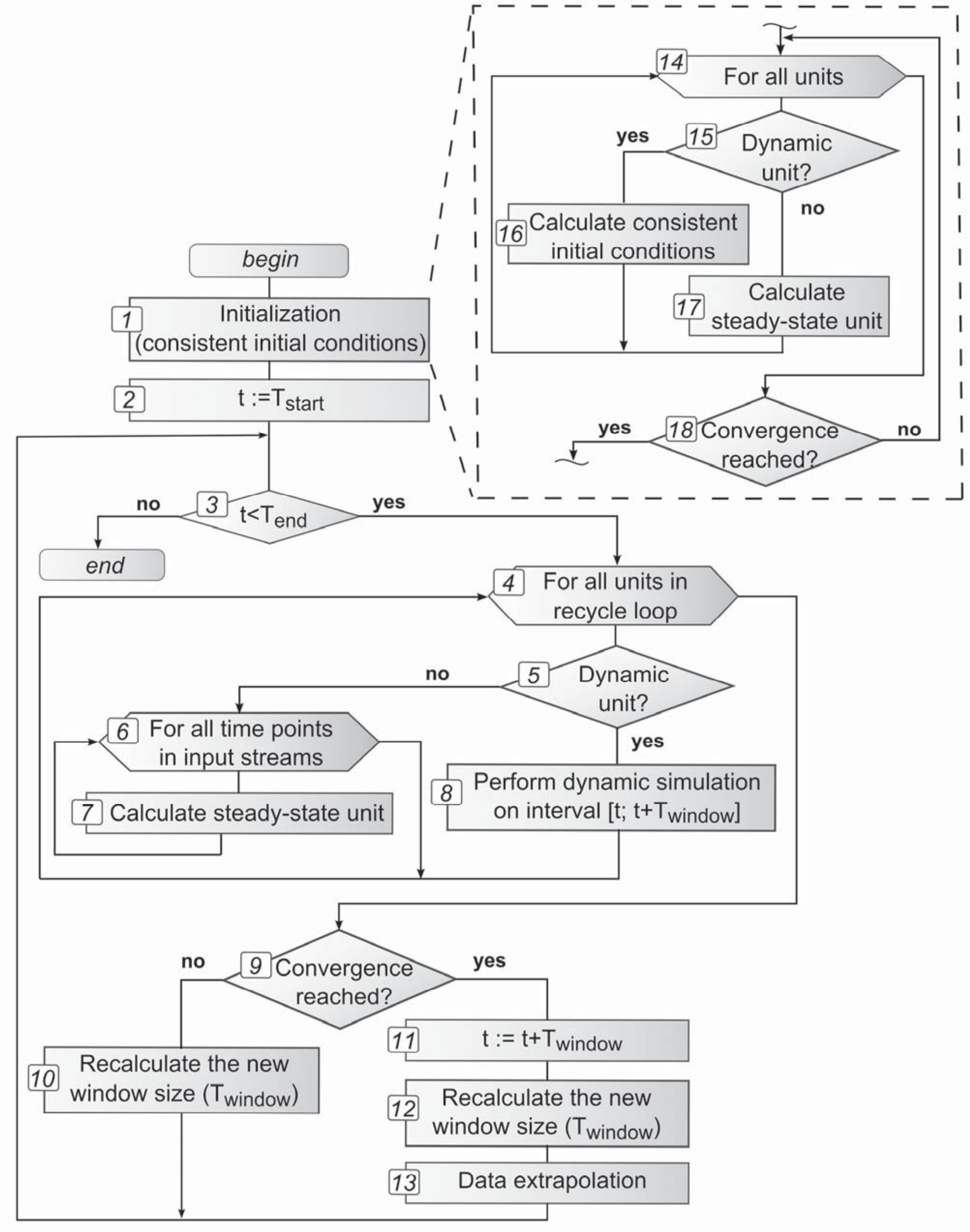
14 For all units
15 Dynamic unit?
yes
no
16 Calculate consistent initial conditions
17 Calculate steady-state unit
18 Convergence reached?
yes
no
begin
1 Initialization (consistent initial conditions)
2 t :=T_{start}
3 t<T_{end}
no
yes
end
4 For all units in recycle loop
5 Dynamic unit?
no
yes
6 For all time points in input streams
7 Calculate steady-state unit
8 Perform dynamic simulation on interval [t; t+T_{window}]
9 Convergence reached?
no
yes
10 Recalculate the new window size (T_{window})
11 t := t+T_{window}
12 Recalculate the new window size (T_{window})
13 Data extrapolation

Figure 3.1: Main calculation algorithm implemented into SolidSim-Dynamics

Dieses Werk ist copyrightgeschützt und darf in keiner Form vervielfältigt werden noch an Dritte weitergegeben werden.
Es gilt nur für den persönlichen Gebrauch.

The convergence analysis in the conditional blocks *(9)* and *(18)* is based on value deviations in all tear streams. For every tear stream, the difference between the values of all variables in the current (*j*) and previous iteration (*j-1*) are compared with the convergence criteria. For the analysis, which is performed in the conditional block *(18),* data for just one time step are used. In the case of block *(9)* the whole waveforms (values in all time points on the current time interval $[t; t + T_{window}]$) are compared. As the dynamic units are simulated by solvers with variable step size, the tear streams on successive iterations can be defined for different points in time. In this case a linear interpolation is used.

If R_{tol} and A_{tol} are the predetermined relative and absolute tolerances respectively, then the convergence criterion can be obtained from the following relation:

$$\begin{gathered} \left|Y^j[t; t + T_{window}] - Y^{j-1}[t; t + T_{window}]\right| < \\ \left|Y^j[t; t + T_{window}]\right| \cdot R_{tol} + A_{tol}, \end{gathered} \tag{3.3}$$

where Y^j is the vector of variables in all tear streams on the iteration *j*.

After the initialization phase the main calculation loop is started from T_{start} and repeated until the end time point T_{end} will be reached *(3)*. The calculations in the loop are divided into a set of smaller time intervals $[t; t + T_{window}]$, where T_{window} is the interval size.

By simulation of dynamic units the calculation is carried out automatically *(8)* and the unit determines the time points for which the output stream should be defined. Processing of steady-state units is implemented in another way. Due to the absence of time, they are calculated for all time points, for which the input streams have been defined.

Another difference between the two unit types is an analysis of the mass conservation, which is performed just for the steady-state models. One of the basic principles of the steady-state mode is a conservation of mass:

$$\begin{pmatrix} Mass\ flow\ rate \\ out\ of\ the\ unit \end{pmatrix} = \begin{pmatrix} Mass\ flow\ rate \\ into\ the\ unit \end{pmatrix} \tag{3.4}$$

The dynamic models have another form of mass conservation equation, which can be generally expressed as:

$$\begin{pmatrix} Mass\ flow\ rate \\ out\ of\ the\ unit \end{pmatrix} = \begin{pmatrix} Mass\ flow\ rate \\ into\ the\ unit \end{pmatrix} - \begin{pmatrix} Accumulation\ rate \\ in\ the\ unit \end{pmatrix} \tag{3.5}$$

Next to the calculation of units on some time interval, the convergence is analyzed *(9)* with further possible recalculation of the length of the time interval (T_{window}). The length of this time

Dieses Werk ist copyrightgeschützt und darf in keiner Form vervielfältigt werden noch an Dritte weitergegeben werden.
Es gilt nur für den persönlichen Gebrauch.

interval plays a decisive role and defines the performance characteristics of the developed algorithm. An unreasonably large magnitude of the time window can easily lead to an enormous deviation between the waveforms obtained on the successive iterations. As a consequence, the number of iterations exponentially increases. Contrary to this, the small values of T_{window} cause unreasonably short values of the internal time steps, which are used for the models calculation. Consequently, this can lead to a considerable performance decrease.

The parameter T_{window} is approximated accordingly to the number of iterations on the current time interval. If the convergence is reached after a number of iterations which is smaller than some predetermined value, then the value of T_{window} is increased. The decreasing of T_{window} occurs when the iterations quantity exceeds some predetermined limit.

One of the advantages of the algorithm presented in Figure 3.1 is its possibility to receive and analyze results during simulation. There is no need to wait until the final time point T_{end} will be reached *(3)*. During the calculations the user has an opportunity to analyze results for the already processed time interval $[T_{start}; t]$. This feature is very helpful, because processes with complex structure and models with high detailing level can have sufficiently large computational time.

To illustrate the application of the developed algorithm, which was implemented into the SolidSim-Dynamics framework (Figure 3.1), supposes that the exemplary process consists of two coupled dynamic units, as it is shown in Figure 3.2. In this showcase the system is simulated for the time window $t \in [0; 20]$ and values of relative and absolute tolerances equal to $R_{tol} = 1e^{-2}$ and $A_{tol} = 1e^{-2}$ accordingly.

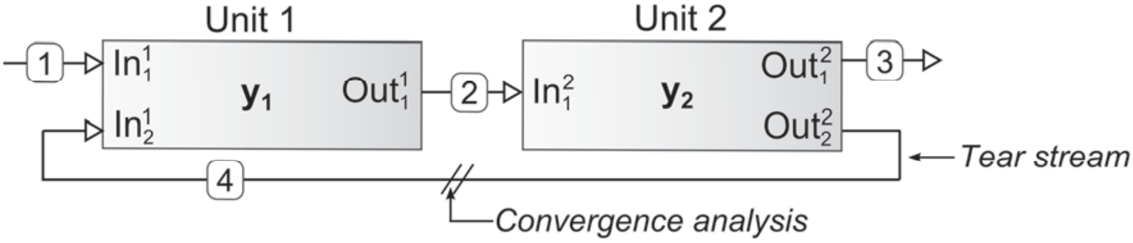

Figure 3.2: Exemplary scheme which consists of two dynamic units

Each of the above depicted units is characterized by a simple dimensionless mathematical model. The comprising set of differential algebraic equations is expressed as:

Dieses Werk ist copyrightgeschützt und darf in keiner Form vervielfältigt werden noch an Dritte weitergegeben werden.
Es gilt nur für den persönlichen Gebrauch.

$$\begin{cases} \dfrac{dy_1}{dt} = In_1^1 - y_1 + \cos(t) \cdot In_2^1; \;\; y_1(0) = 0; \; In_1^1(t) = 0 \\ \qquad In_1^2(t) = Out_1^1(t) = y(t); \; In_2^1(t) = Out_2^2(t) \\ \qquad \dfrac{dy_2}{dt} = 1 - y_2 - \sin(t) \cdot In_1^2; \;\; y_2(0) = 0 \\ \qquad\qquad Out_2^2(t) = 0.9 \cdot y_2(t) \end{cases} \tag{3.6}$$

The processing sequence is started from the Unit 1. In the first iteration the input values at the inlet stream In_2^1 are unknown, so they are set equal to the default value 0. After the calculation of the Unit 1 on the time interval $t \in [0; 20]$ the received results are transmitted into the Unit 2 and the simulation of the second unit is started. In the next step the analysis of the convergence is made, whereby the deviation of the values on the successive iteration in the stream 4 is compared with maximal allowed values. The convergence is supposed to be reached if the discrepancy on the whole time period lies within the tolerance area. In Figure 3.3 results obtained from the Unit 1 on the consequently iterations are depicted. On the left axis the value of the y_1 is plotted with a solid line. The values at the inlet $In_2^1(t)$ are shown with a dashed line.

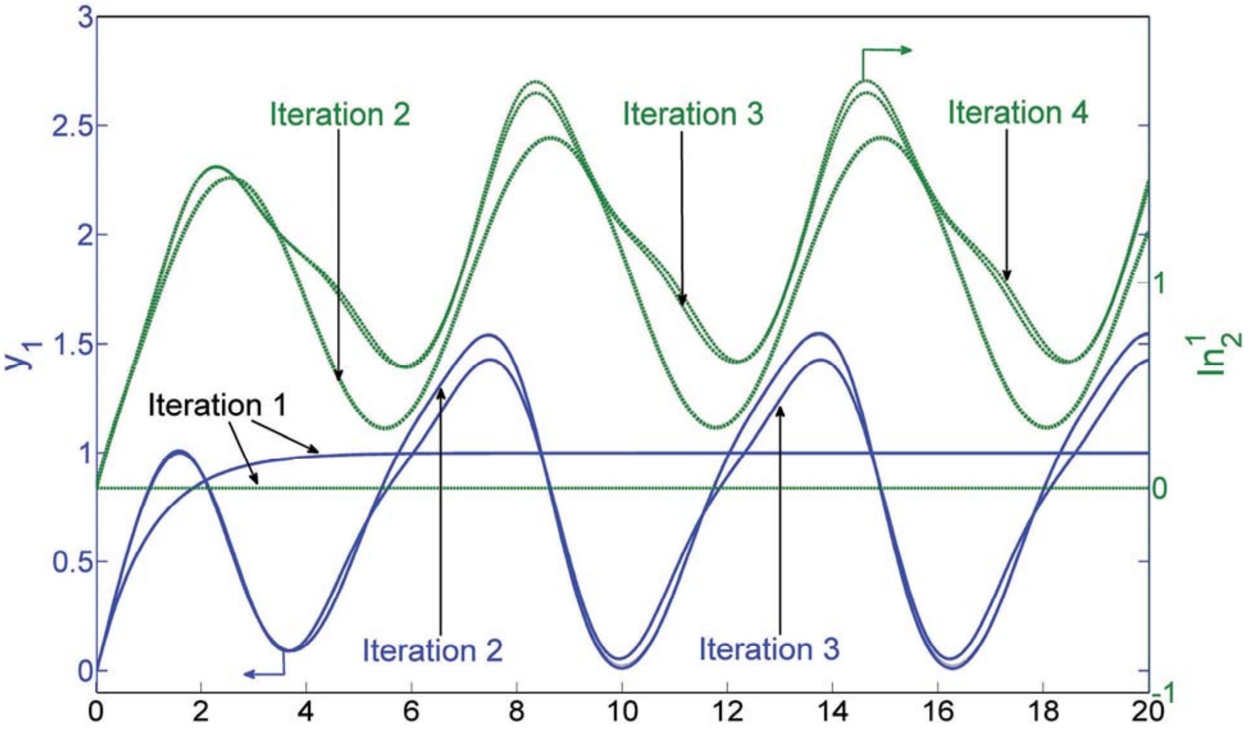

Figure 3.3: Results obtained after processing of the exemplary scheme

In Figure 3.4 the deviation of the values in the tear stream are plotted. From the analysis of illustrated results, the conclusion can be drawn that after 4 iterations the difference is smaller than a maximal allowed deviation. Thus the convergence is reached and the processing can be

Dieses Werk ist copyrightgeschützt und darf in keiner Form vervielfältigt werden noch an Dritte weitergegeben werden.
Es gilt nur für den persönlichen Gebrauch.

started for the new time interval. For the calculations on the new time window, the extrapolated values from the previous interval will be used as a first approximation of the connected stream variable $In_2^1(t)$.

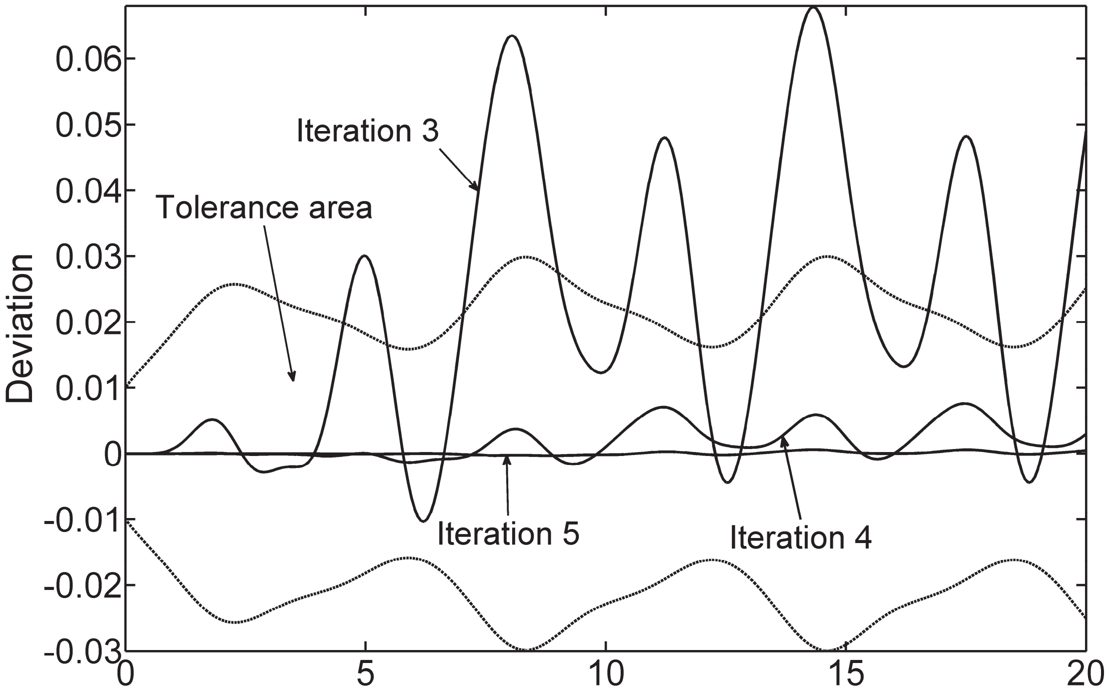

Figure 3.4: Parameters deviations in the tear stream

The example presented above is based on the Gauss-Seidel modification of the waveform relaxation algorithm. Hence, before starting its own calculation procedure the Unit 2 was waiting for the results from the Unit 1. In the case of Gauss-Jacobi method both units can be processed simultaneously. This allows to implement effective parallelization strategies into the simulation environment (Dosta et al., 2008), but on other hand exerts a negative influence on the convergence properties.

3.2 Handling of distributed multidimensional parameters

Contrary to the material streams in the liquid processes, the solids streams are defined by a set of distributed multidimensional parameters. The values which characterize the stream can be distributed through a set of internal property coordinates, such as size, moisture content, density, etc. To handle such multidimensional distributed values the Material Stream Object has been developed. The time property is included into the stream as supplementary dimension. The schematic structure of the material stream is shown in Figure 3.5.

Dieses Werk ist copyrightgeschützt und darf in keiner Form vervielfältigt werden noch an Dritte weitergegeben werden.
Es gilt nur für den persönlichen Gebrauch.

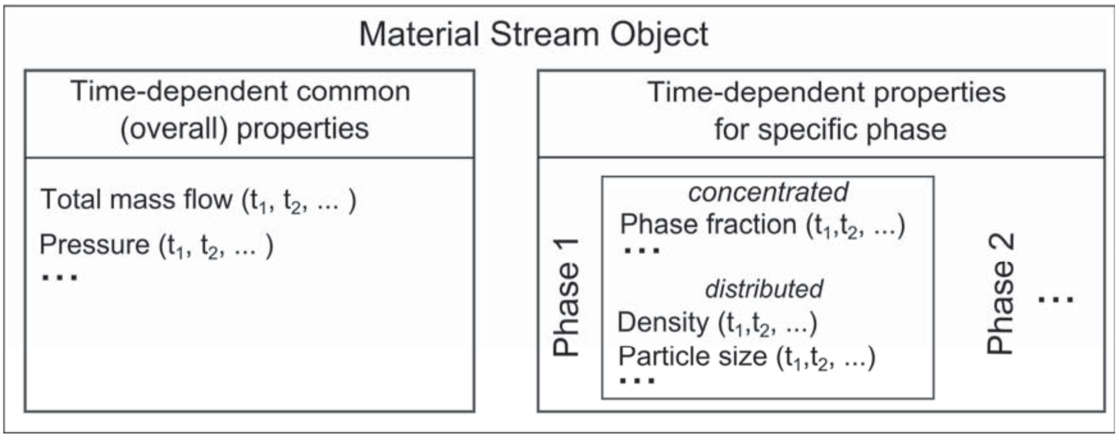
Material Stream Object
Time-dependent common (overall) properties
Total mass flow (t_1, t_2, ...)
Pressure (t_1, t_2, ...)
...
Time-dependent properties for specific phase
Phase 1
concentrated
Phase fraction (t_1,t_2, ...)
...
distributed
Density (t_1,t_2, ...)
Particle size (t_1,t_2, ...)
...
Phase 2
...

Figure 3.5: General structure of the material stream object

One part of the stream object is used to describe the common (overall) properties, such as pressure, temperature, total mass flow of the stream, etc. The other section, which is depicted on the right side of Figure 3.5, is used to characterize the variables which are specific for different phases. The description of each phase consists of concentrated and distributed values.

The various streams with different internal structures can be simultaneously defined in one flowsheet. In this case the procedure of stream generalization is performed. During the generalization procedure, the properties and components, which were common for all and unique for each input stream, are combined together into one joint structure. Afterwards, all original streams are transformed into the new general structure. Because of the existence of unique properties, this transformation step can cause a lot of zero entries. That is why, with a purpose to increase the performance of the modeling environment, the sparse data storage and handling format has been implemented. The dense matrixes, which are used in many simulation programs, store all data entries independently of values. The sparse format implies that only non-zero elements are saved and processed.

To increase the performance characteristics of the simulation environment, into SolidSim-Dynamics a modified sparse format has been implemented. The saving is performed just for the data entry Y_i, whose amplitude is greater than some predefined constant criteria min_Y ($|Y_i| > min_Y$). The user has a possibility to specify different values of min_Y for different processes. However, the criteria value cannot be varied during calculations.

The usage of sparse format causes the necessity to store supplementary data. Simultaneously to the original data entries, the index values should be saved. The indexes determine the position of data in the multidimensional parameter space. The processing of them can cause a negative effect and can lead to a noticeable performance decrease. This negative effect mostly

Dieses Werk ist copyrightgeschützt und darf in keiner Form vervielfältigt werden noch an Dritte weitergegeben werden.
Es gilt nur für den persönlichen Gebrauch.

arises by processing of schemes where material streams are described with relative small dimensions of distributed variables. In other situations, when the streams consist of a large number of distributed properties, the usage of the sparse format leads to a sufficient increase of the computational performance.

The main advantage of the sparse format can be illustrated by the following example. Suppose, the abstract unit has two input streams and the particle size distribution in each stream is described by a discretized form of the Gauss function (see Eq. (3.7)). The parameters of the PSD in the streams are listed in Table 3.1.

$$f(x_i) = \frac{1}{\sqrt{2\pi\sigma^2}} \cdot e^{-\frac{(x_i-\mu)^2}{2\sigma^2}} \qquad (3.7)$$

Table 3.1: Parameters of PSD in the streams

	Size classes	Interval of PSD [mm]	Deviation [mm] (σ)	Median [mm] (μ)
Stream 1	200	[0..5]	0.05	1
Stream 2	200	[0..5]	0.1	3

In Table 3.2 the summarized comparison between quantities of stored entries by different magnitudes of parameter min_Y are listed. From the analysis of received data, the conclusion can be drawn that even for the case of one-component stream and relative small values of min_Y the sparse format contains a sufficiently smaller amount of stored data. As a consequence, this leads to the reduction of calculations and significant performance increase.

Table 3.2: Comparison of the quantity of stored entries by dense and sparse formats

MIN_y [mm]	Dense	Values (sparse)	Indexes (sparse)	Total (sparse)
$1e^{-15}$	400	102	102	204
$1e^{-12}$	400	92	92	184
$1e^{-10}$	400	84	168	168
$1e^{-9}$	400	80	80	160
$1e^{-6}$	400	68	68	136

The implementation of the sparse matrices format improves the performance characteristics of SolidSim-Dynamics. However, there exists another deficiency with regard to the optimal

Dieses Werk ist copyrightgeschützt und darf in keiner Form vervielfältigt werden noch an Dritte weitergegeben werden.
Es gilt nur für den persönlichen Gebrauch.

memory usage. To perform post-processing and analysis of received simulation results, the calculation of flowsheets requires to store the data for all time points. In situations when the stream consists of a large number of distributed properties and the simulation is started for a long time interval, the volume of stored data is significantly increased. However, there is no necessity to store the whole data sets for all time points. A major part of the parameters can reveal time-independent behavior or their gradients can have different orders of magnitudes. In both of these cases the volume of stored data can be sufficiently reduced.

To decrease the volume of needed memory and as a consequence to decrease processing time, the stream compression algorithm was implemented. The developed algorithm is based on values of relative (R_{tol}) and absolute (A_{tol}) tolerances and works as follows:

1. For each value y_{i+1} on the time point t_{i+1}.
2. Verify following condition:

$$|y_{i+1} - y_{i+1}^{*}| \leq R_{tol} \cdot |y_{i+1}| + A_{tol}, \tag{3.8}$$

   where

$$y_{i+1}^{*} = y_i + \frac{y_i - y_{i-1}}{t_i - t_{i-1}}(t_{i+1} - t_i) \tag{3.9}$$

3. The value for this time point should be stored just in the case, when the condition is not satisfied.

In Figure 3.6 the application of the compression algorithm to the dimensionless parameter is shown. The values of relative and absolute tolerances in the illustrated example are equal to $R_{tol} = 1e^{-2}$ and $A_{tol} = 1e^{-1}$ accordingly. From the depicted results the conclusion can be drawn, that in order to represent the given function on the interval [0; 6] just 14 values are needed.

Dieses Werk ist copyrightgeschützt und darf in keiner Form vervielfältigt werden noch an Dritte weitergegeben werden.
Es gilt nur für den persönlichen Gebrauch.

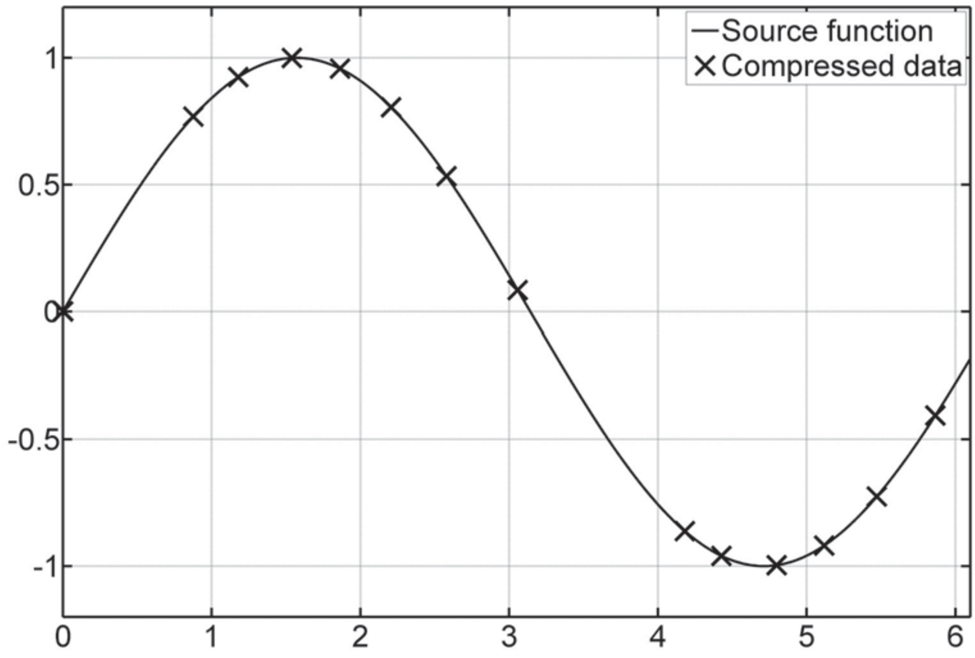

Figure 3.6: Example of data compression

As it was mentioned above, the solids streams in SolidSim-Dynamics are represented by a set of distributed multidimensional parameters. The interdependency between the parameters complicates their correct processing. The direct application of the sequential-modular simulation approach can lead to the loss of required information in the outlet material stream. In Figure 2.4 the illustrative example of this problem was shown and explained.

In order to implement a correct modeling of particulate materials, the concept of movement matrix is used in SolidSim-Dynamics. In the current version of the simulation environment exist two main approaches to approximate the values in the outlet material streams. Regardless of the current simulation mode (dynamic or steady-state) the stream entries can be obtained by two different ways:

- explicit calculation. Independently on the data structure of the inlet, the outlet stream is specified directly;
- generation of movement matrix (Mov). The entries in this matrix ($Mov_{src,dst}$) define the mass fraction, which is moved from the source class with index src into the destination class with index dst.

The explicit approach can be effectively used when the unit is able to calculate the values of all distributed properties properly. However, due to the general applicability of the new simulation environment to the diverse types of production processes, the stream has no limitation to the number or dimensions of distributed properties. Therefore, the direct estimation output values in most cases leads to the information loss.

Dieses Werk ist copyrightgeschützt und darf in keiner Form vervielfältigt werden noch an Dritte weitergegeben werden.
Es gilt nur für den persönlichen Gebrauch.

The transformation of the streams by applying a movement matrix is much more preferable compared to the explicit data assignment. In this case, independently from the number and type of distributed properties, the correct transformation of all treated variables is made.

The generation of the movement matrix for steady-state and dynamic units can be done in different ways. The steady-state units use the movement matrix to determine the transformation laws from the input into the output streams, as it is shown in Figure 3.7. In the case of the dynamic units the movement matrix $M_H(t)$ is applied to convert the stream $H(t)$ which characterizes the holdup material. After the each successful simulation step the entries in the movement matrix are recalculated.

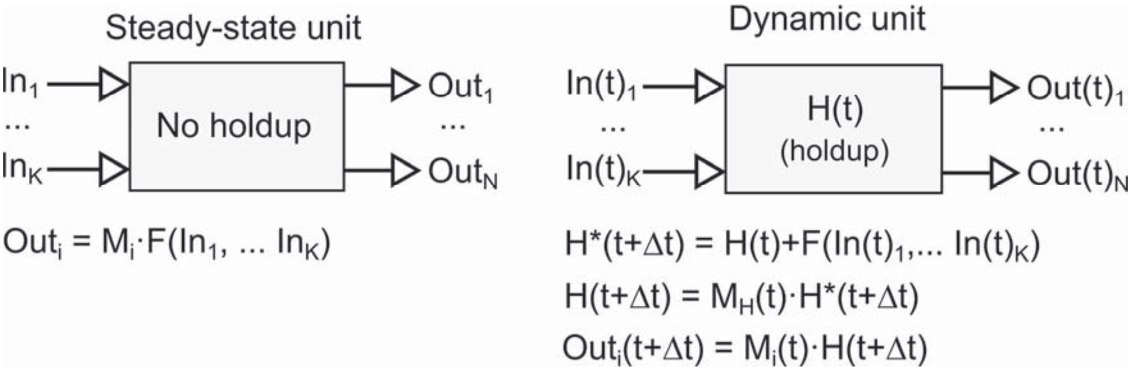
Steady-state unit
In_1
...
In_K
No holdup
Out_1
...
Out_N
$Out_i = M_i \cdot F(In_1, \ldots In_K)$
Dynamic unit
$In(t)_1$
...
$In(t)_K$
H(t)
(holdup)
$Out(t)_1$
...
$Out(t)_N$
$H^*(t+\Delta t) = H(t)+F(In(t)_1, \ldots In(t)_K)$
$H(t+\Delta t) = M_H(t) \cdot H^*(t+\Delta t)$
$Out_i(t+\Delta t) = M_i(t) \cdot H(t+\Delta t)$

Figure 3.7: Application of the movement matrix in the SolidSim-Dynamics system

In the area of solid processes most of the mathematical models of dynamic units are described by a system of DAE's. These systems are formulated just for a limited set of state variables, which complicates the implicit transformation of the holdup streams. That is why, by developing a dynamic model, further model reformulation is needed to obtain the movement matrix $M_H(t)$.

Dieses Werk ist copyrightgeschützt und darf in keiner Form vervielfältigt werden noch an Dritte weitergegeben werden.
Es gilt nur für den persönlichen Gebrauch.

3.3 Object-oriented programming architecture

Instead of an implementation of the new flowsheet simulation environment from scratch, the already existing SolidSim (Werther et al., 2004) program has been used as a conceptual basis for the development of SolidSim-Dynamics. The original architecture of the SolidSim program (Pogodda, 2007) has been extended by a set of new classes and functions to allow dynamic treatment of particulate materials. One of the main advantages of such strategy is the possibility to use already developed steady-state units on the dynamic flowsheet and to combine steady-state and transient calculations in one environment.

Another significant benefit to use SolidSim as a basis framework is the implicit inclusion of CAPE-Open interfaces. SolidSim was developed accordingly to the CAPE-Open standard (CAPE-Open). This standard defines rules and interfaces to increase the compatibility between numerous applications in the area of process engineering and to allow their interoperability. The models or solvers, which are developed according to this standard, are not implicitly implemented into the modeling framework and can be used in other software tools as an external component. For instance, this allows incorporating any previously defined SolidSim flowsheet into another process simulator.

In Figure 3.8 the general structure of the SolidSim system is illustrated (Pogodda, 2007). It consists of several components which communicate by usage Component Object Model (COM) middleware. There exist four main components:

- *Material stream object*. It contains all required data structures and methods for the sufficient description of material and energy streams. It is used for the data transfer between units and provides an access to the physical property package.
- *Unit models*. These components are used for the implementation of original process models.
- *Physical property package*. It provides standardized access to the database of compound properties and allows to obtain properties of mixtures.
- *Simulation environment*. This is a kernel of SolidSim, which is used to manage the whole calculation process. It consists of a user-friendly graphical user interface (GUI) and simulation engine. Through the interactive interface there exists the possibility to construct a flowsheet, to change the structure of existing flowsheets and to specify process parameters and boundary conditions. The simulation engine executes the main simulation algorithm and coordinates the data transfer between the units.

Dieses Werk ist copyrightgeschützt und darf in keiner Form vervielfältigt werden noch an Dritte weitergegeben werden.
Es gilt nur für den persönlichen Gebrauch.

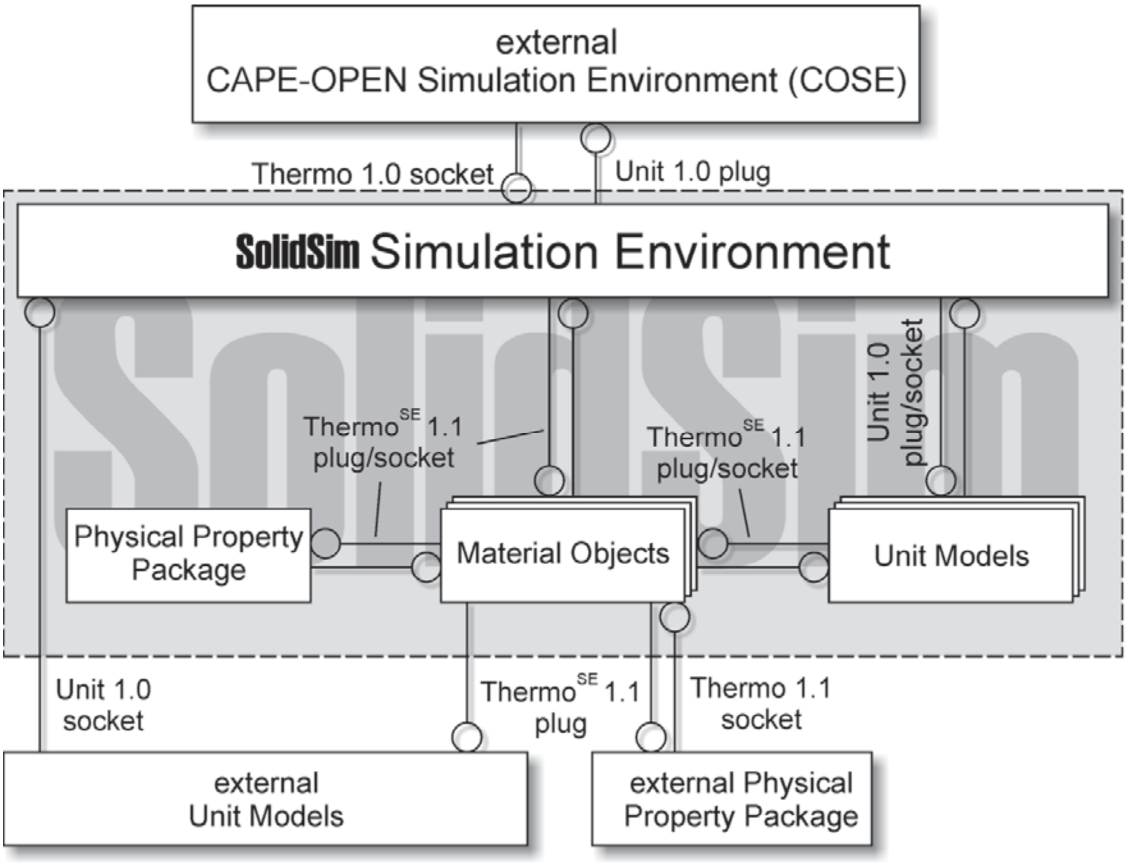
external
CAPE-OPEN Simulation Environment (COSE)
Thermo 1.0 socket
Unit 1.0 plug
SolidSim Simulation Environment
Thermo^SE 1.1 plug/socket
Thermo^SE 1.1 plug/socket
Unit 1.0 plug/socket
Physical Property Package
Material Objects
Unit Models
Unit 1.0 socket
Thermo^SE 1.1 plug
Thermo 1.1 socket
external Unit Models
external Physical Property Package

Figure 3.8: General structure of the SolidSim simulation system

The internal architecture of SolidSim-Dynamics was developed in accordance to the object-oriented programming (OOP) paradigm. Contrary to the functional programming paradigm, that treats computations as the calculation of mathematical functions, the OOP-based program consists of a set of interacting objects. These objects are instances of classes and they comprise internal data fields and methods. To increase the efficiency of the developed program, the OOP technique includes such features as polymorphism, encapsulation, data abstraction, inheritance and modularity, which allow to build flexible and scalable software tools.

One of the central roles in the OOP structure of SolidSim-Dynamics plays the object which is used to describe dynamic models. Each new dynamic unit should inherit from the abstract classes *CSolidSimBaseUnit* and *CSolidSimBaseDynamicUnit*, as it is shown in the class diagram in Figure 3.9. Due to the usage of such architecture the new dynamic models automatically obtains all required functionality for communications with the simulation environment. The access to the internal methods of the unit is carried out through the interfaces such as *ICapeUnit, ICapeUtilities, IBaseUnit, ICapeUnitReport,* etc. For example, to start a dynamic simulation the function *CalculateDynamic* should be called through *IBaseDynamicUnit* interface.

Dieses Werk ist copyrightgeschützt und darf in keiner Form vervielfältigt werden noch an Dritte weitergegeben werden.
Es gilt nur für den persönlichen Gebrauch.

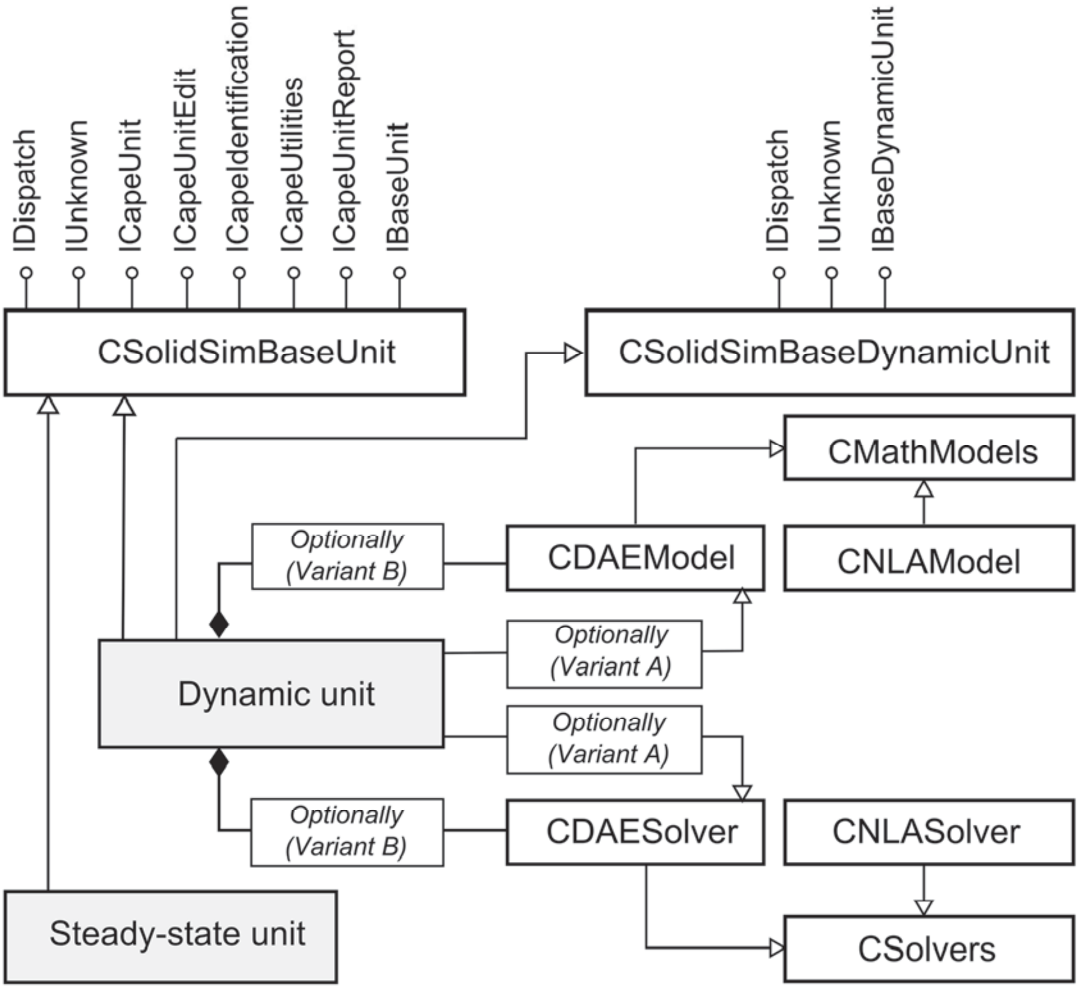

Figure 3.9: The class diagram of the dynamic unit (UML notation)

In the area of solids processes a large amount of apparatuses and process substeps are described by a system of differential algebraic equations. To standardize the mathematical models of such apparatuses the *CDAEModel* class has been introduced. This class contains all internal data fields, methods and interfaces required for successful computation of differential equations. In Table A.1 a short summary of this method is given.

The usage of the *CDAEModel* allows performing dynamic calculations directly, using objects of the *CDAESolver* class. In such case the model equations should be expressed in the implicit form and included into the function which calculates residuals. The obtained residual values are used afterwards by the solver to find the solution.

In Figure 3.9 two alternative ways of the usage of the *CDAEModel* class are illustrated. It can be used as a parent class for the dynamic object (Variant A). In this case a dynamic unit inherits all methods of the *CDAEModel* class. In the alternate version, one or several objects of the *CDAEModel* class are explicitly included into the dynamic model (Variant B). This is a very helpful optional possibility, which can be effectively used when the model consists of a set of

Dieses Werk ist copyrightgeschützt und darf in keiner Form vervielfältigt werden noch an Dritte weitergegeben werden.
Es gilt nur für den persönlichen Gebrauch.

uncoupled submodels or when implicit (state driven) or explicit (time driven) events introducing the changes in the model structure are defined. In this case the different DAE subsystems can be inserted into the one model and further simultaneous processing of them can be performed by several solvers.

In order to increase the efficiency of the simulation environment, the solver of the DAE systems was implemented into the SolidSim-Dynamics environment. This solver is based on the variable-order, variable-coefficient backward differentiation formula (BDF) method (Ascher and Petzold, 1998). The BDF approach is a linear multistep method particularly used for stiff systems. The order (k) of the implemented method is varied between one and five. In each step the BDF results in a formula of the following type:

$$h_i \cdot y_i' = \sum_{j=0}^{k} \varsigma_{i,j} \cdot y_{i-j}\,, \tag{3.10}$$

where h_i is the time step, $\varsigma_{i,j}$ the coefficients determined by the order of the method, and y_{i-j} are the values from the previous time steps. The application of the BDF method results in a set of nonlinear algebraic (NLA) equations, which are solved in every time step by the Newton iteration method.

For the automatic solution of the nonlinear algebraic systems the *CNLAModel* and the *CNLASolver* classes were introduced. With help of instances of the *CNLASolver* class the calculation of the *CNLAModel* objects can be realized. The NLA solver, which is implemented into SolidSim-Dynamics, is based on the KINSOL solver (Hindmarsh et al., 2005), where an inexact or modified Newton method is used. The *CNLASolver* solves the system $G(y) = 0, G: R^n \to R^n$ by the following calculation scheme:

1. Set the initial guess y^0
2. Until the convergence repeat:
    a. Solve $J(y^i) \cdot \delta^i = -G(y^i)$
    b. Update the values for the next iteration $(y^{i+1}) = y^i + \lambda \cdot \delta^i$,

where $J(y) = G'(y)$ is the Jacobian of the system and $0 < \lambda \leq 1$.

Another important role in the simulation environment plays the programming architecture of the stream objects. As it was mentioned above, that the original SolidSim material stream object is extended with supplementary property coordinate. This property coordinate is included to handle time specific properties. Besides it can be also effectively applied to describe the properties, which are distributed along other dimensions.

Dieses Werk ist copyrightgeschützt und darf in keiner Form vervielfältigt werden noch an Dritte weitergegeben werden.
Es gilt nur für den persönlichen Gebrauch.

Accessing the material stream can be done through a set of various interfaces, which are schematically depicted in Figure 3.10. The short description of main interfaces and their functionality is given in Table A.2. Most of the previously discussed methods were previously used during steady-state simulation in the SolidSim program. However, to get access to the time dependent properties the new interfaces *IDynamicThermoMaterial* and *IDynamicThermoMaterialXML* were developed. In the *IDynamicThermoMaterial* interface the following main methods can be underlined:

- *AddTimePoint()* – inserts new time point. At the same time the data duplication from the previous time point is performed.
- *GetTimePoints()* – returns all time points for which the data in the stream object is defined.
- *SetCurrentTime()* – specifies the current value of an independent variable.
- *Remove()* – removes all data entries from the stream.
- *RemoveValues()* – deletes all values which were defined on a specified time interval.
- *Compress()* – in order to minimize the volume of stored data and to decrease the number of computational operations, the compression algorithm can be started. Exemplary application of this algorithm is illustrated in Figure 3.6.
- *CheckConvergence()* – checks the convergence criteria for a specified time interval. If the difference on successive iterations is smaller or equal to the maximal allowed deviation then this function returns a positive result.

Dieses Werk ist copyrightgeschützt und darf in keiner Form vervielfältigt werden noch an Dritte weitergegeben werden.
Es gilt nur für den persönlichen Gebrauch.

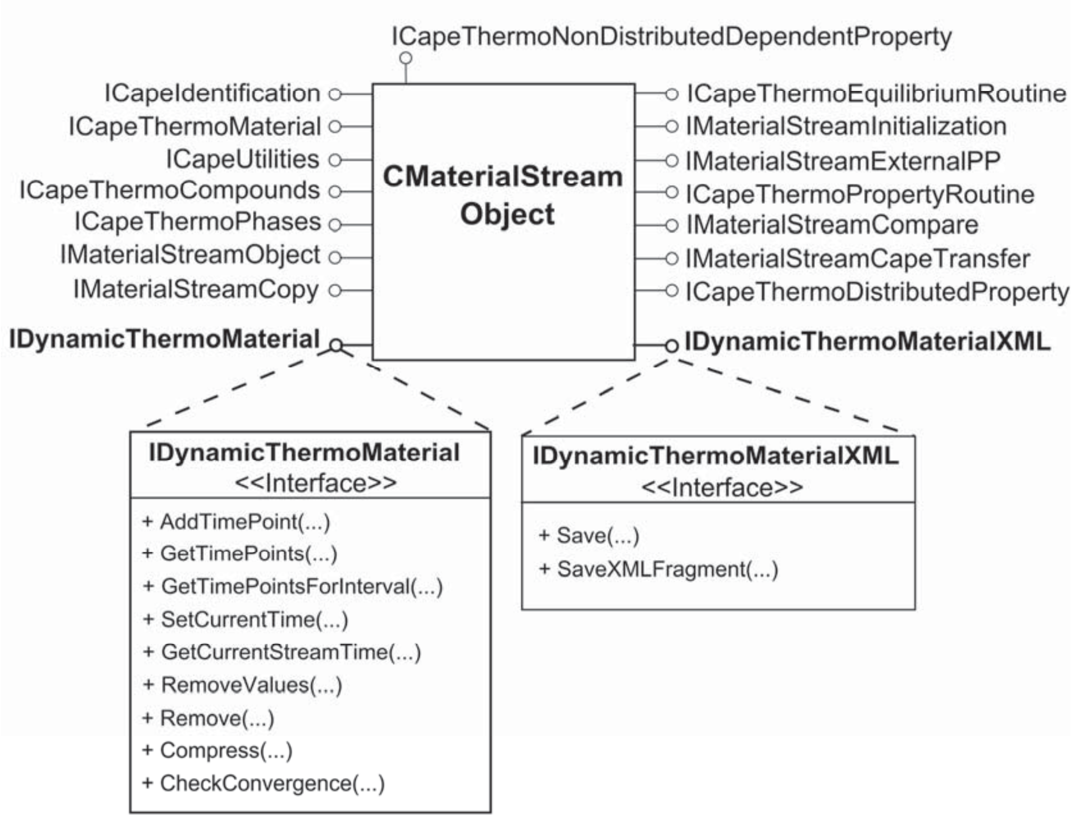

Figure 3.10: Interfaces of the material stream

Received simulation results in SolidSim-Dynamics can be visualized with two-dimensional or three-dimensional plots. This visualization feature is directly implemented into the simulation environment. Moreover, to extend the usability of the new program, the communication interface to the commercial software package Matlab (Matlab) has been developed. This interface is used to transfer the obtained results from SolidSim-Dynamics into Matlab and to perform the further post-processing.

Next to the successful flowsheet initialization in the main calculation algorithm (*Block 2* in Figure 3.1) a Matlab session is started as a separate process in a background mode. After each simulation step, the Matlab engine library is used to transmit data and to start necessary visualization and post-processing routines. In Figure 3.11 a typical screenshot of the graphical user interface (GUI) of the SolidSim-Dynamics system is shown.

Dieses Werk ist copyrightgeschützt und darf in keiner Form vervielfältigt werden noch an Dritte weitergegeben werden.
Es gilt nur für den persönlichen Gebrauch.

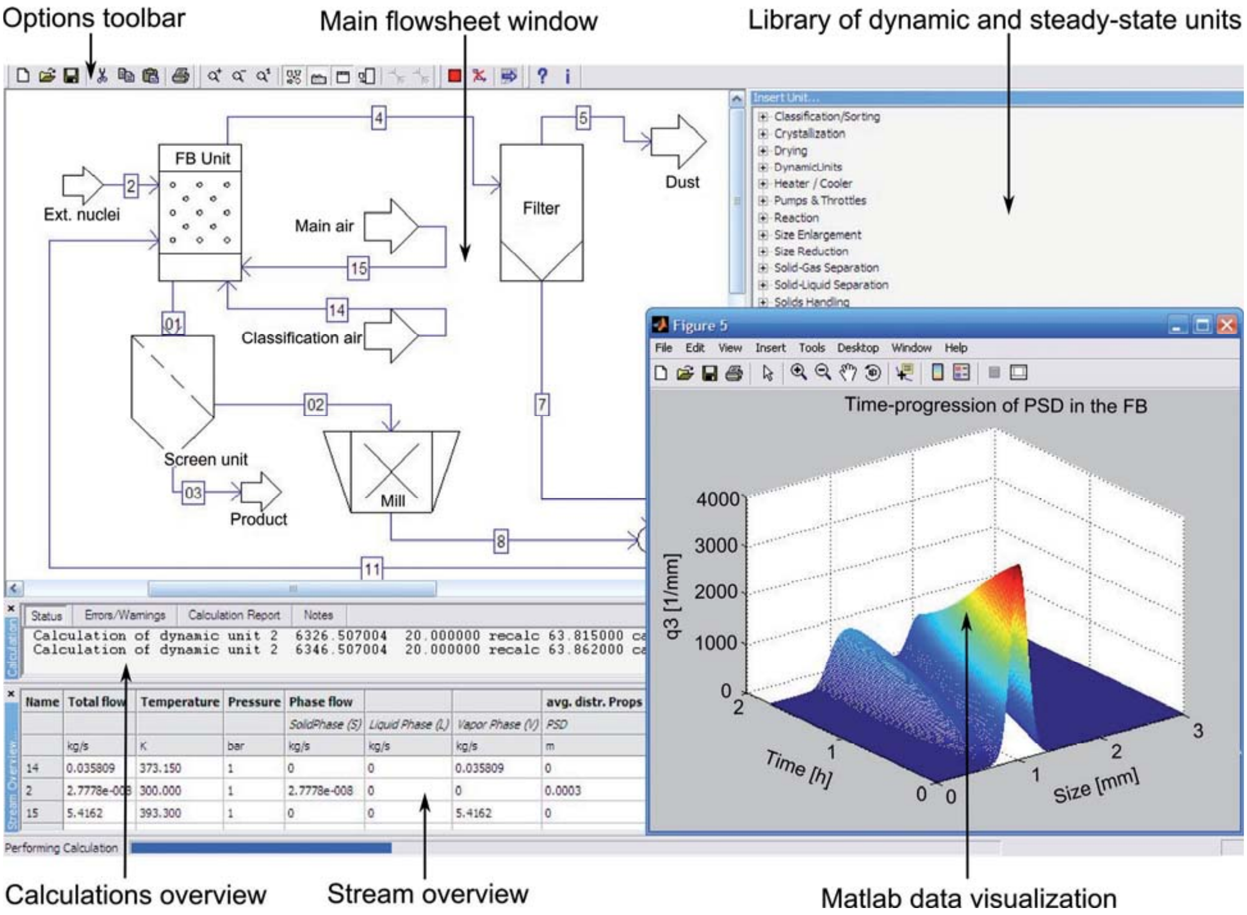

```
Calculation of dynamic unit 2  6326.507004  20.000000 recalc 63.815000 ca
Calculation of dynamic unit 2  6346.507004  20.000000 recalc 63.862000 ca
```

Name	Total flow	Temperature	Pressure	Phase flow			avg. distr. Props
				SolidPhase (S)	Liquid Phase (L)	Vapor Phase (V)	PSD
	kg/s	K	bar	kg/s	kg/s	kg/s	m
14	0.035809	373.150	1	0	0	0.035809	0
2	2.7778e-008	300.000	1	2.7778e-008	0	0	0.0003
15	5.4162	393.300	1	0	0	5.4162	0

Figure 3.11: Screenshot of GUI of the SolidSim-Dynamics system

The main window of SolidSim-Dynamics consists of a set of different dialogs, whereby each of dialogs has its own functionality. The process structure is shown in the main flowsheet window. The toolbar dialog provides a fast access to the most important functions such as starting or stopping calculations, data saving, initializing of all stream variables, etc. The total set of available steady-state and dynamic units is shown in a separate tree-coded list. The units can be transferred from this list to the current flowsheet per drag-and-drop action. The calculation overview dialog is used to analyze the current state of the simulation procedure (current process time, amount of executed iterations, deviations in tear streams, etc.). In the stream overview table the main characteristics of all flowsheet streams are expressed.

Dieses Werk ist copyrightgeschützt und darf in keiner Form vervielfältigt werden noch an Dritte weitergegeben werden.
Es gilt nur für den persönlichen Gebrauch.

3.4 Parallelization of the SolidSim-Dynamics system

3.4.1 General strategy

The computational time is one of the most important criteria to estimate the efficiency of any software tool. In the case of the SolidSim-Dynamics system, due to the extreme complexity of mathematical models of different apparatuses and the complexity of the process structures, the flowsheet processing can take an inappropriately long time. To reduce the calculation time parallelization strategies on different hierarchical levels have been developed and partially implemented into the new environment. The developed methods allow to get computational speed-up using distributed calculations on the multi-core or multiprocessor machines.

Depending on the number of simultaneously executed commands and the number of data streams, all computer systems according to Flynn (Grama et al., 2003) can be classified into four main types:

- SISD (Single Instruction Single Data) – one processor unit executes one command at a time for one data item;
- SIMD (Single Instruction Multiple Data) – several processor elements are supervised by one control unit;
- MISD (Multiple Instructions Single Data). As an example of MISD architecture the pipeline principle of data treatment in the processor or systolic arrays can be considered;
- MIMD (Multiple Instructions Multiple Data). Such architecture has more than one processor and several data streams.

The above mentioned classification of Flynn can be extended by a class of hybrid computational architectures. Such systems are a combination between SIMD and MIMD architectures and overwhelmingly used in supercomputers and at high-performance centers.

The parallelization methods, which have been developed in this work, were mainly focused for further applications on the MIMD architectures. Nowadays, the MIMD systems have become broad prevalence and can be found everywhere. For instance, any personal computer with multicore processor or even standard network of personal computers can be considered as MIMD architecture based.

In order to parallelize computations, the original computational problem should be modified and reassigned to the target topology of the computational network. In Figure 3.12 the several general phases of parallelization are illustrated. At the first stage the partitioning of the initial

Dieses Werk ist copyrightgeschützt und darf in keiner Form vervielfältigt werden noch an Dritte weitergegeben werden.
Es gilt nur für den persönlichen Gebrauch.

problem into a set of fine-grained tasks occurs. This partitioning can be based on the domain or functional decomposition. In the case of functional decomposition the main effort is to divide the computations and by domain decomposition the aim is to divide data associated with a problem.

In the second stage the communications (data dependencies) between separate components are defined and the task graph is created. This is an undirected graph with weighted edges and nodes. The weight of the node represents the volume of the computations needed to solve the problem and the weight of the edge equals the amount of transferred data between two tasks.

In order to divide computations between processors and to perform load balancing, the task graph is mapped onto the graph, which represents the communication structure of the parallel system. The nodes of the architecture graph express the processor units and the edges represent the structure of communication network. In the final stage the execution of the tasks is started on the parallel system.

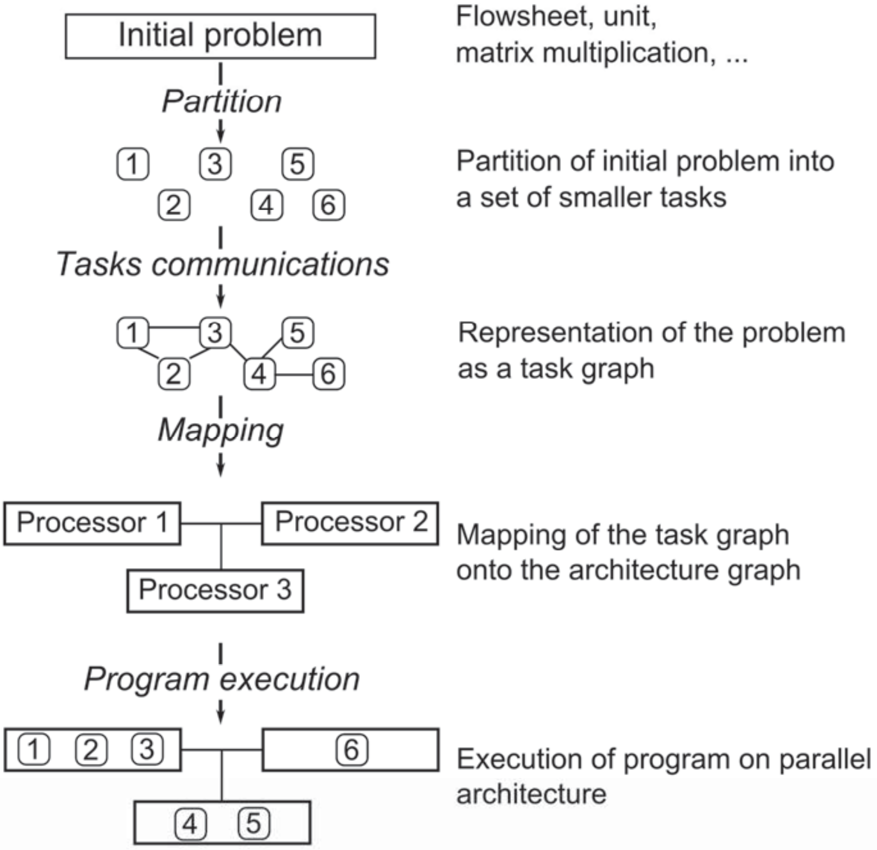
Initial problem
Flowsheet, unit, matrix multiplication, ...
Partition
1 3 5 2 4 6
Partition of initial problem into a set of smaller tasks
Tasks communications
Representation of the problem as a task graph
Mapping
Processor 1
Processor 2
Processor 3
Mapping of the task graph onto the architecture graph
Program execution
Execution of program on parallel architecture

Figure 3.12: Stages of the program parallelization

Dieses Werk ist copyrightgeschützt und darf in keiner Form vervielfältigt werden noch an Dritte weitergegeben werden.
Es gilt nur für den persönlichen Gebrauch.

The MIMD systems have various topological structures, such as hypercube, 2-D and 3-D meshes, linear array, star connected network, multistage interconnection network, etc. (Grama et al., 2003). However, just the two following topologies were considered in this work:

- bus-based network;
- completely connected network.

For the above listed topologies, the mapping problem can be reformulated into the graph partition problem. If the original problem, which is represented by a task graph $\Gamma = (\Xi, E)$, should be simultaneously executed on an N-processor system, then nodes Ξ should be divided into N subsets ξ^j $(j \in 1..N)$, where $\xi^j \cap \xi^k = 0$, for $j \neq k$. During the splitting procedure the load imbalance (Λ) and the volume of transferred data (Ψ) should be minimized. These parameters are approximated as:

$$\Lambda = max\left\{\left|\xi^j\right| - \frac{|\Xi|}{N}\right\}, \quad j \in \{1..N\} \tag{3.11}$$

$$\Psi = \sum_{\xi_m \in \xi^j,\ \xi_l \in \xi^k}^{m,l} \left|e_{m,l}\right|, \tag{3.12}$$

where $|e_{m,l}|$ is a weight of the edge which is incident to the vertices m and l, ξ_m is the weight of node with index m, $|\Xi|$ is the summarized weight of all vertices.

The formulated problem of the graph splitting can be effectively solved by a multilevel k-way partition scheme (Karypis and Kumar, 1998), where the splitting algorithm is divided into three phases. In the first phase the reduction of the graph Γ occurs, afterwards the vertices of the scaled graph are divided into N parts and finally a refinement process takes place.

The size and the structure of the task graph Γ depends on the hierarchical level on which the parallelization occurs. In the context of the system for dynamic flowsheet simulation of solids processes three hierarchy levels are distinguished. The more detailed description of the parallelization methods on each level is given below.

To measure the efficiency of the simultaneous execution of the program on the multiprocessor architecture the speedup f_{spd} and scalability f_{scl} factors are used. f_{spd} is used to evaluate the relative benefit of the parallel algorithm. It is determined as ratio of the calculation time on a single processor computer (T_s) to the processing time on a multiprocessor system (T_p).

$$f_{spd} = \frac{T_s}{T_p} \tag{3.13}$$

Dieses Werk ist copyrightgeschützt und darf in keiner Form vervielfältigt werden noch an Dritte weitergegeben werden.
Es gilt nur für den persönlichen Gebrauch.

Commonly the magnitudes of the speedup factor are in the interval $1 \leq f_{spd} \leq N$, where N is the number of processors. However, the value of f_{spd} can also be less than 1, when the parallel algorithm is developed inefficiently.

The scalability factor (f_{scl}) of the parallel program is the measure of its ability to increase speedup in the proportion to the increased number of processor elements. This factor is calculated as:

$$f_{scl} = \frac{T_s}{N \cdot T_p} \tag{3.14}$$

3.4.2 Parallelization on different hierarchical levels

The highest hierarchy level, on which the parallelization in SolidSim-Dynamics can be done, is the level of the flowsheet. The strategy on this level is based on the reformulation of the original problem and specification of units or process subparts, which can be simultaneously calculated for the same or varied time points. This can be achieved in two different ways:

- simultaneous calculation of parallel branches;
- parallelization on the base of the waveform relaxation (WR) method (Secchi et al., 1993).

The method of parallel branches determines some flowsheet units which are situated on the parallel streams of the simulated scheme. Afterwards these units are distributed between several processors or cores of one processor. The data transfer between processors occurs just during the calculation of the time points, where parallel branches are scattered or merged. In Figure 3.13 the application of the described approach to the example flowsheet is shown.

If all units in Figure 3.13 have an equal calculation time and the time for data transfer is negligibly small, then the speedup factor of the parallel algorithm on a two-processor machine will be equal to 1.5. Such speedup indicates about reasonably good efficiency of the parallelization algorithm. However, applying this strategy on the general type of flowsheets cannot be always effective. The negative effects arise due to the strong dependency on the process structure, small scalability and potential huge load imbalance.

Dieses Werk ist copyrightgeschützt und darf in keiner Form vervielfältigt werden noch an Dritte weitergegeben werden.
Es gilt nur für den persönlichen Gebrauch.

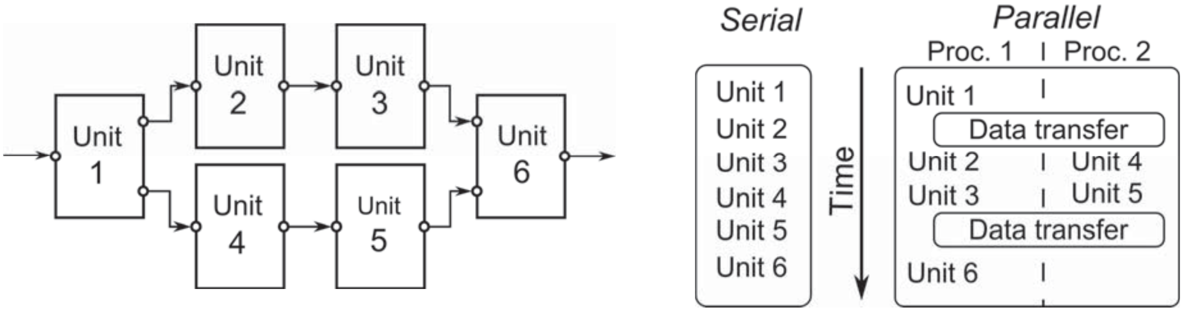

a) example flowsheet b) calculation procedure

Figure 3.13: Simultaneous calculation of parallel flowsheet branches

A more effective way to implement concurrent simulations is the usage of the Jacobi type of the waveform relaxation method. By the Jacobi WR approach all units are independently calculated on the same time interval. As an illustrative example, suppose that the abstract flowsheet consists of two dynamic units and the total process is described by the following set of differential equations:

$$\begin{cases} \frac{dy_1}{dt} = F_1(y_1, y_2) & y_1(0) = y_{10} \\ \frac{dy_2}{dt} = F_2(y_1, y_2) & y_2(0) = y_{20} \end{cases} \tag{3.15}$$

In the case of Jacobi WR algorithm the original system (3.15) on the iteration i+1 will have the following form:

$$\frac{dy_1^{i+1}}{dt} = F_1\left(y_1^{i+1}, y_2^{i}\right) \qquad y_1(0) = y_{10} \tag{3.16}$$

$$\frac{dy_2^{i+1}}{dt} = F_2\left(y_1^{i}, y_2^{i+1}\right) \qquad y_2(0) = y_{20} \tag{3.17}$$

In the every iteration, Eq. (3.16) and Eq. (3.17) are solved independently from each other. The values for unknown coupling variables are approximated from the values on previous iterations.

The next level, where the parallelization can be implemented, is the level of the flowsheet units. The main methodology of this level is applied to split the calculation of some unit between several processors. For many units the splitting of the model into weakly coupled subsystems can be used as effective solution. Such subsystems can afterwards be simultaneously calculated on a multiprocessor system (Dosta et al., 2008). However, there is no effective strategy can be developed for the general type of dynamic units.

Only one parallelization approach has been implemented into the current version of SolidSim-Dynamics system. It is based on the main advantages of sequential-modular calculation

Dieses Werk ist copyrightgeschützt und darf in keiner Form vervielfältigt werden noch an Dritte weitergegeben werden.
Es gilt nur für den persönlichen Gebrauch.

strategy and it is applied for dynamic simulation of steady-state units. Depending on the flowsheet structure and the complexity of the used mathematical models, the usage of the described approach can lead to a significant speed-up.

The dynamic simulation of the steady-state units leads to their iterative calculation on a set of time points (see main simulation algorithm in Figure 3.1). The total number of these time points depends on the quantity of time-dependent entries in all inlet streams. In the case when the input stream contains a large number of entries the processing time can increase significantly. However, the fact that the steady-state unit contains no holdup allows to distribute computations between different processors and to increase performance characteristics. The absence of the holdup implies that the state of the unit on some time point does not depend on previous values. Therefore, the calculation of the steady-state unit for different time points can be executed simultaneously.

Dieses Werk ist copyrightgeschützt und darf in keiner Form vervielfältigt werden noch an Dritte weitergegeben werden.
Es gilt nur für den persönlichen Gebrauch.

4. Modeling of fluidized bed spray granulation

In order to perform dynamic simulation of fluidized bed spray granulation process, a set of new models were implemented into the SolidSim-Dynamics simulation system. These units allow to calculate aggregation or growth processes with different detailing grade and gives a possibility to analyze transient behavior of complex granulation plants.

4.1 Process fundamentals

Since 1922, when the invention of fluidized bed technology for coal gasification was made by Fritz Winkler, this technology has been extended into many application areas, such as drying, granulation, coating, mixing, etc. (Mörl et al., 2007). One of the main advantages of the fluidized bed apparatus is an integration of diverse subprocesses like particle formulation, wetting, homogenization, drying or separation into a one single step. In Figure 4.1 the exemplary construction of a top-spray fluidized bed granulator is schematically shown.

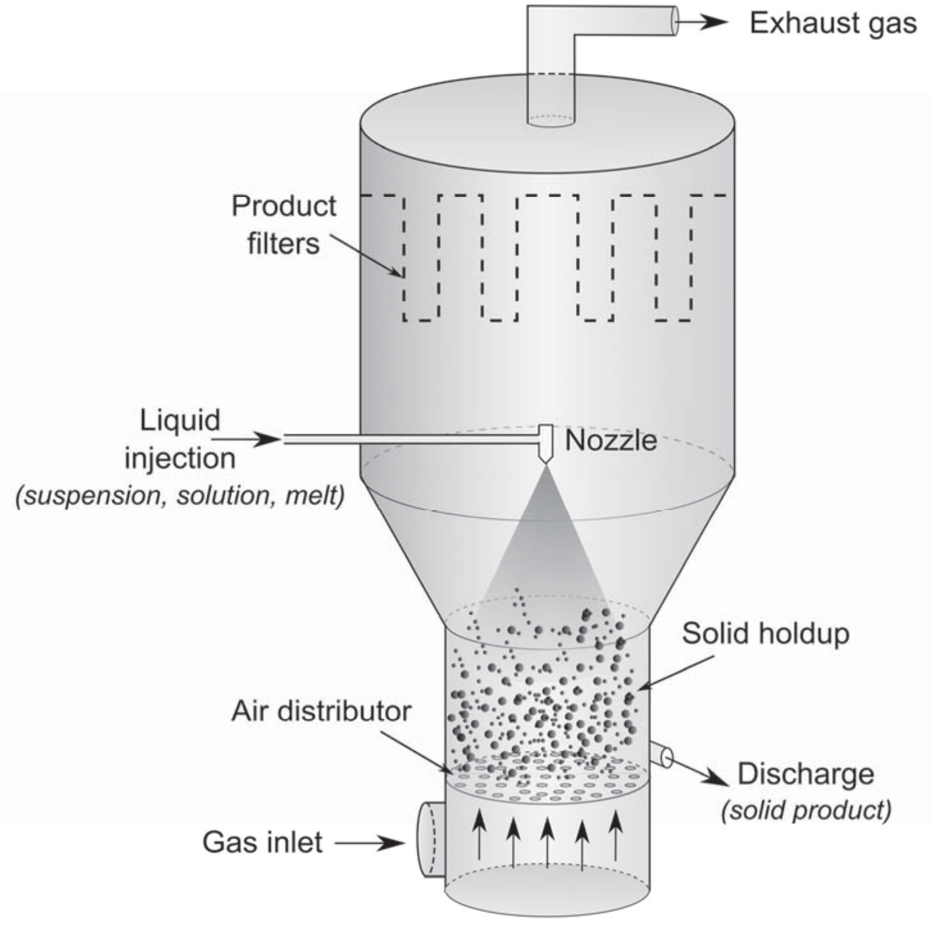

Figure 4.1: Fluidized bed granulator

Dieses Werk ist copyrightgeschützt und darf in keiner Form vervielfältigt werden noch an Dritte weitergegeben werden.
Es gilt nur für den persönlichen Gebrauch.

In the fluidized bed (FB) apparatus solid particles (holdup) are transformed into a fluid-like state after counterbalancing the gravity force by the drag force, caused by the gas flow. During the granulation process the liquid, which contains the solid, is injected into the system through one or several nozzles. After collision with a particle, the atomized liquid droplets can be deposited onto the particle surface with subsequent forming of a liquid film. Due to the existence of the solid fraction in the sprayed liquid, the drying of the liquid film leads to the continuous growth (layering) process. In Figure 4.4 the general scheme of granules formation is shown.

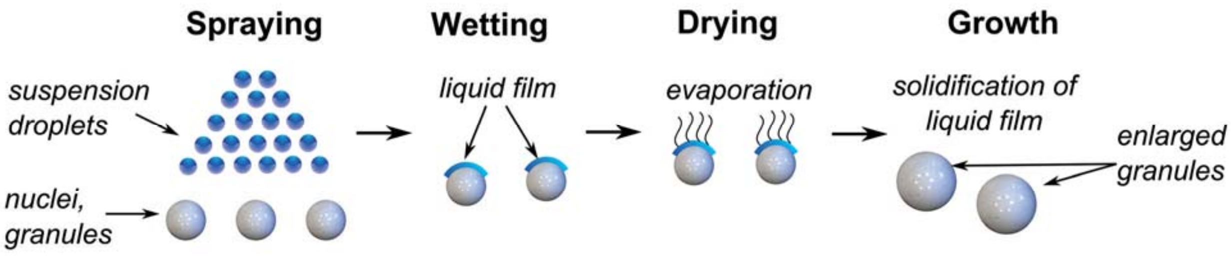

Figure 4.2: Continuous particle growth (layering)

The particles, which are covered by a liquid film, can stick together during collisions. This can happen due to the existence of viscous, capillary and surface tension forces, which appear additionally to the forces of dry contact (Antonyuk et al., 2009). Further drying of a liquid bridge between particles, which are sticking together, leads to its solidification and appearance of a solid bond. In this case an aggregation event takes place. The scheme of agglomerate formation is depicted in Figure 4.3.

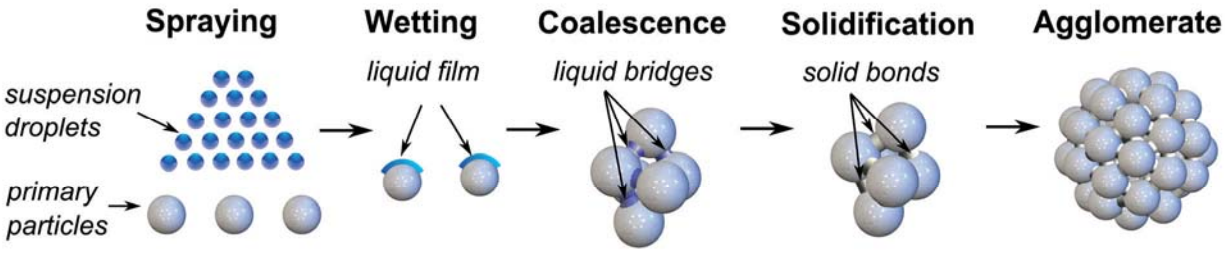

Figure 4.3: Formation of an agglomerate (particle aggregation)

It can be distinguished between different agglomeration mechanisms, such as (Rumpf, 1975):

- attraction forces between solids (molecular, electric and magnetic forces);
- solid bridges;
- interlocking bonds;
- adhesion and cohesion forces (highly viscous binders);
- surface tension and capillary forces (liquid bridges).

Dieses Werk ist copyrightgeschützt und darf in keiner Form vervielfältigt werden noch an Dritte weitergegeben werden.
Es gilt nur für den persönlichen Gebrauch.

However, in this contribution the attraction forces between solids and interlocking bonds are not considered.

In the literature a difference between definitions of granulation and agglomeration processes does exist, that can cause some uncertainty. In some publications (Flore et al., 2009), (Heinrich and Mörl, 1999), (Litster and Sarwono, 1996) granulation means the continuous increase of granules size due to the layering of particles by a sprayed liquid. The agglomeration implies a process of the particle size enlargement according to the aggregation of fine particles. In other sources no distinction between terms of agglomeration and granulation has been made (Ennis, 1996), (Le et al., 2009).

In this contribution both definitions are used synonymously to describe the particle growth. However, to distinguish the different nature of a size enlargement process, the both terms of layering (growth) and aggregation are used. In the case when the bed material and solid phase of the sprayed liquid are dissimilar substances and if the coated solid layer is very thin in comparison to the core particle the term coating is used.

Simultaneously to the aggregation and growth, the attrition, breakage and nucleation events occur in the fluidized bed apparatus. The particles can break at high impact velocities by the contact with other particles and the apparatus wall. New nuclei can be formed by overspray or by attrition of granules. The overspray is the part of the suspension droplets which do not stick on the particles surfaces. After drying of this part of suspension they can serve as a source for the new nuclei or can elutriate the apparatus as dust with the exhaust gas.

All listed micro mechanisms can occur simultaneously and should be considered in the mathematical model for the process description. Further process complexity arises due to the existence of three different phases between which intensive transport processes, like heat and mass transfer, may occur.

In order to ensure a constant product quality, to minimize energy consumption and to develop effective control strategies, an appropriate process understanding is needed. Such understanding of a process behavior can be reached through an advanced process modeling, which is performed on different time and length scales (Werther et al., 2011), (Ingram and Cameron, 2005). Among all existing calculation approaches the methodology which is based on the population balance modeling can be emphasized. It is widely used for the modeling of industrial applications and allows to predict macroscopic behavior of individual elements, like particles, bubbles and droplets in an appropriate calculation time.

Dieses Werk ist copyrightgeschützt und darf in keiner Form vervielfältigt werden noch an Dritte weitergegeben werden.
Es gilt nur für den persönlichen Gebrauch.

4.2 Population balance modeling

The population balance models (PBM) are used to describe the time evolution of populations of one or several properties, which are distributed along different coordinates (Ramkrishna, 2000), (Qamar, 2007), (Hulburt and Katz, 1964). With respect to particles it is convenient to distinguish between two types of property coordinates:

- internal – to describe respective particle property, such as particle form, size, color, charge, etc.;
- external – to characterize spatial distribution within a balance volume.

The distributed properties in the PBM are commonly represented as a density function. For example, to characterize the particle size distribution (PSD) the number density distribution $n(t,\vec{\imath},\vec{e})$ is used, whereby $\vec{\imath}$ and $\vec{e}$ are internal and external coordinates accordingly. The value $n(t,\vec{\imath},\vec{e})$ equals to the average number of particles per volume of investigated state space. In this contribution the ideally mixed systems are considered, therefore there is no distribution of number density function $n(t,\vec{\imath})$ throughout the external coordinate.

To describe the temporal change of the PSD, which occurs due to the continuous transport of the particles in the state space, the population balance equation (PBE) is used. In general form this is a partial integro-differential equation, which can be expressed as:

$$\frac{\partial f(t,x)}{\partial t} + \nabla(Vf) - B(t,x) + D(t,x) = 0, \tag{4.1}$$

where x is a phase space, $f(t,x)$ is a distribution in the multidimensional state space, $B(t,x)$ and $D(t,x)$ are integral source (birth) and integral sink (death) terms accordingly, V is a convectional velocity with:

$$V = \frac{dx}{dt} \tag{4.2}$$

The application of the PBM to the fluidized bed granulation is not a trivial task. Due to the influence of different parameters such as binder content, temperature, density, porosity, etc., the PBE can consist of several dimensions. This can lead to a significant increase of computational complexity. At the same time, very detailed process description is often redundant. In many cases the usage of a one-dimensional balance equation leads to adequate results. In this work just the particle size has been considered as a key characteristic to describe process dynamics.

Dieses Werk ist copyrightgeschützt und darf in keiner Form vervielfältigt werden noch an Dritte weitergegeben werden.
Es gilt nur für den persönlichen Gebrauch.

In terms of the PSD there can be distinguished five main mechanisms which occur during FB granulation. In Figure 4.4 the general representation of these mechanisms is shown. The abrasion transfer can be additionally considered (Sastry and Fuerstenau, 1973) as a supplementary mechanism, but in this contribution it is neglected.

The uncertainties of a classification, which is shown in Figure 4.4, can arise from the difficulty to determine the cut-off size between granular and non-granular material. In these cases the fixed size boundary can be used (Grünewald, 2011) or as an alternative Iveson et al. (2001) has proposed to classify all processes into a combination of only three sets: wetting and nucleation, consolidation and growth, attrition and breakage.

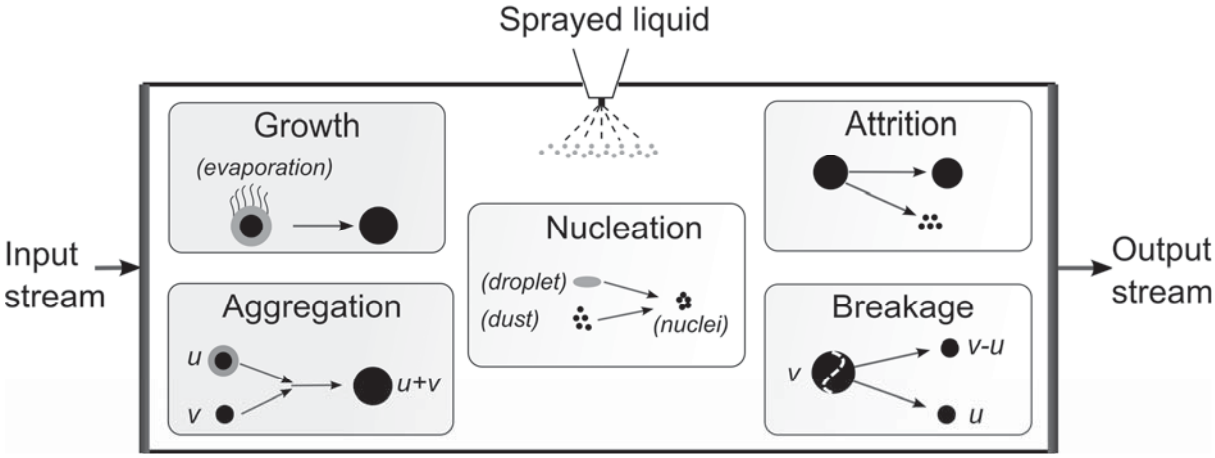

Figure 4.4: General scheme of mechanisms in the FB granulator

A general form of the one-dimensional PBE for the ideally mixed granulation system is expressed in Eq. (4.3) (Heinrich, 2001), (Green and Perry, 2007). This equation is written in terms of particle size. However it can also be reformulated in terms of granule volumes or other similar properties.

$$\begin{aligned}\frac{\partial n(t,v)}{\partial t} = \frac{\dot{Q}_{in}(t)}{V} n_{in}(t,v) - \frac{\dot{Q}_{out}(t)}{V} n_{out}(t,v) + B_{nuc}(t,v) \\ - \frac{\partial\left[\left(G(t,v) - Attr(t,v)\right)\cdot n(t,v)\right]}{\partial v} + B_{agg}(t,v) \\ - D_{agg}(t,v) + B_{break}(t,v) - D_{break}(t,v)\end{aligned} \tag{4.3}$$

Here V is the volume of the system and v represents the size of the particles. $\dot{Q}_{in}(t)$ and $\dot{Q}_{out}(t)$ are inlet and outlet flow rates from the system respectively. The terms $B(t,v)$ describe the birth of new particles and $D(t,v)$ their death. The abbreviations *nuc*, *break*, *agg* are used to distinguish between nucleation, breakage and aggregation mechanisms respectively. The growth (layering) rate is considered by the term $G(t,v)$ and the attrition rate by $Attr(t,v)$. A more detailed description of these terms is given as follows.

Dieses Werk ist copyrightgeschützt und darf in keiner Form vervielfältigt werden noch an Dritte weitergegeben werden.
Es gilt nur für den persönlichen Gebrauch.

Breakage and attrition

There can be distinguished between two main mechanisms which cause decrease of particle size, namely attrition and breakage. The sources of both mechanisms are various types of stresses which act on particles. The stresses can be divided into (Vaux and Keairns, 1980):

- thermal stress, when unequal temperatures in the particle cause intraparticle stress;
- chemical stress, which occurs due to the chemical reaction within the particle;
- static mechanical stress;
- dynamic mechanical stress by particle-particle or particle-wall collisions.

In this work the focus has been made on the last two types of influences. The attrition process, driven by mechanical stress, occurs under the influence of friction forces and small forces in the normal direction. The relatively large magnitude of the normal force is the reason of the breakage process. In the discipline of solids process engineering the breakage process is defined as an irreversible process during which the mass of the source particle is decreased by at least 10% (Schubert, 2003).

To consider the breakage process in the PBM, the fragmentation rate $S(v)$ and the breakage function $\bar{b}(v, v')$ are used. The function $\bar{b}(v, v')$ describes the fractions into which selected particles break, and represents the average number of particles with the size v produced after fracture of particles with the size v'. The rate $S(v)$ is the frequency the particles of specified size break with. The birth and the death rate can be expressed as (Ziff, 1991):

$$B_{break}(t, v) = \int_{v}^{\infty} \bar{b}(v, v') \cdot S(v') \cdot n(t, v') dv' \tag{4.4}$$

$$D_{break}(t, v) = S(v) \cdot n(t, v) \tag{4.5}$$

In the case of binary breakage, when the primary particle breaks into two unequal parts, the equations (4.4) and (4.5) can be reformulated to:

$$B_{break}(t, v) = 2 \int_{v}^{\infty} \bar{b}(v, v' - v) \cdot n(t, v') dv' \tag{4.6}$$

$$D_{break}(t, v) = n(t, v) \int_{0}^{v} b(v, v - v') dv' \tag{4.7}$$

In Figure 4.5 the general representation of the change of PSD during breakage process is shown.

Dieses Werk ist copyrightgeschützt und darf in keiner Form vervielfältigt werden noch an Dritte weitergegeben werden.
Es gilt nur für den persönlichen Gebrauch.

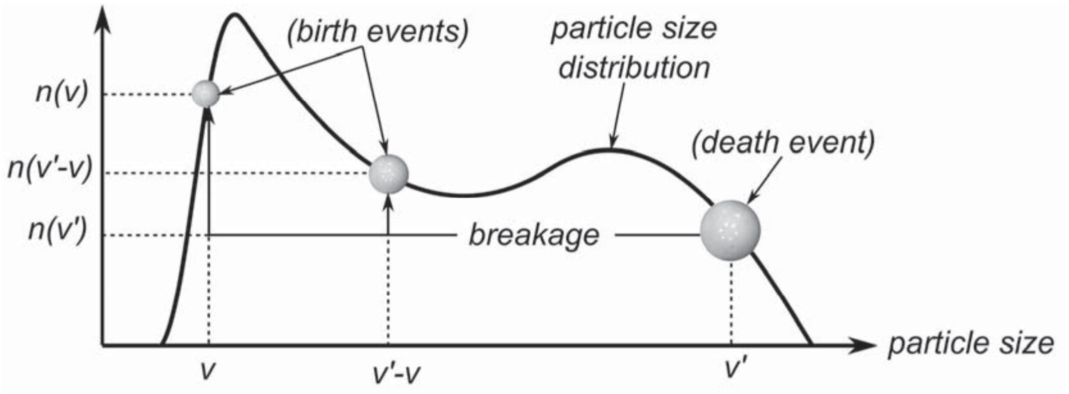

Figure 4.5: General representation of the breakage process in the PBM

The attrition of particles also causes a decrease of their size, but it is not directly included into birth $B_{break}(t,v)$ and death $D_{break}(t,v)$ events. Instead of this it can be effectively included into the PBE as a negative component of a convectional term $Attr(t,v)$ and as a secondary nucleation mechanism (Heinrich et al., 2002).

Despite the relative simple form of the equations (4.4) and (4.5) the adequate modeling of the breakage process is not a trivial task. One of the main difficulties here, is to obtain the values of such parameters as a fragmentation rate $S(v)$ and a breakage function $\bar{b}(v,v')$. The dynamics of the particles in the apparatus, their interactions, geometry of the apparatus, moisture content and many other parameters have a decisive influence on the agglomerates breakage. The microscale simulations can be used as a possible way to consider large numbers of such parameters. Nowadays, the usage of the discrete element method (DEM) is an effective way to predict the granule fracture (Thornton et al., 1996), (Reynolds et al., 2005).

Growth (layering) and nucleation

During a fluidized bed layering process the liquid is injected through one or several nozzles into the apparatus. This liquid deposits on the particle surface and, due to the further evaporation, the solid fraction remains on the particle surface and the particle growth occurs (Uhlemann, 1990) (Figure 4.2). The solvent evaporates and leaves the apparatus with the humid exhaust gas stream.

To obtain the growth rate $G(t,v)$, which is used in the population balance equation (4.3), the model of the linear size-independent growth can be used (Mörl et al., 2007). It is assumed that the particle growth rate does not depend on the size of a particle. This model has been used in many researches (Heinrich et al., 2002), (Balliu and Cameron, 2007) and has shown good agreement between experimental and simulation results. However, the constructional or design

Dieses Werk ist copyrightgeschützt und darf in keiner Form vervielfältigt werden noch an Dritte weitergegeben werden.
Es gilt nur für den persönlichen Gebrauch.

parameters can have strong influence on the growth kinetics during FB granulation. Zank et al. (2001) have shown on the basis of experimental results that the growth rate can be proportional to the size of the particles. In their work the authors have found that during bottom spraying the larger particles have significantly larger growth rates. Therefore, the usage of a size-independent growth rate cannot always give results with satisfied accuracy.

The second source of the granule growth is coverage of particles with dust. During this process, the fine particles stick to the granule surface and thus the growth occurs. Formation of dust in the apparatus is induced by the attrition of particles and by the existence of overspray. Four main sources of overspray can be distinguished (Uhlemann, 1990):

- droplet does not collide with any particle;
- reflection of the droplet with solidified surface from particle;
- destruction of the droplet after impact;
- droplet reflection from the wetted granule surface.

The possible sources of the overspray are schematically illustrated in Figure 4.6.

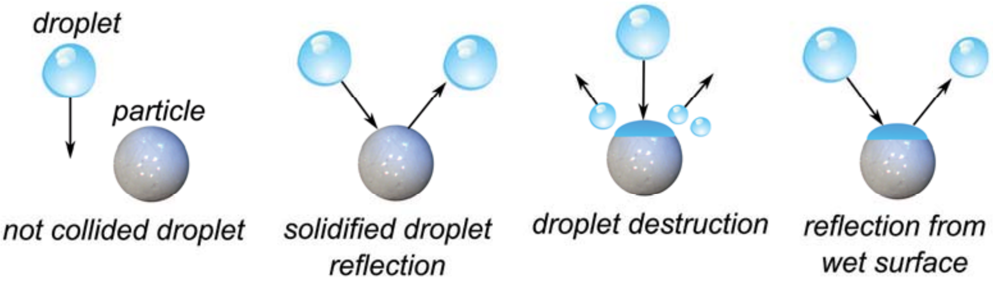

Figure 4.6: Sources of the overspray formation

The new nuclei in the FB apparatus can be generated due to the existence of the external nuclei stream (in the case of continuous process) and the presence of internal nucleation. A short summary of research works in the field of nucleation mechanisms can be found in (Iveson et al., 2001); (Grünewald, 2011). In the PBM in Eq. (4.3) the nucleation process is considered as an additional birth term $B_{nuc}(t, v)$, which describes appearance of nucleus with specified size v.

Aggregation (coalescence)

Next to the collision between particles they can aggregate and form a larger particle (Figure 4.3). It is assumed that the agglomerates have spherical form and their mass and volume are equal to the summarized mass and volume of source particles. In this case the birth rate of particles can be calculated by integration throughout a volume coordinate as:

Dieses Werk ist copyrightgeschützt und darf in keiner Form vervielfältigt werden noch an Dritte weitergegeben werden.
Es gilt nur für den persönlichen Gebrauch.

$$B_{agg}(t,v) = \frac{1}{2}\int_0^v \beta(t,v',v-v') \cdot n(t,v') \cdot n(t,v-v')dv' \tag{4.8}$$

The term $B_{agg}(t,v)$ describes how many particles with the volume v appear after aggregation of smaller particles. In Figure 4.7 the general representation of aggregation process is illustrated.

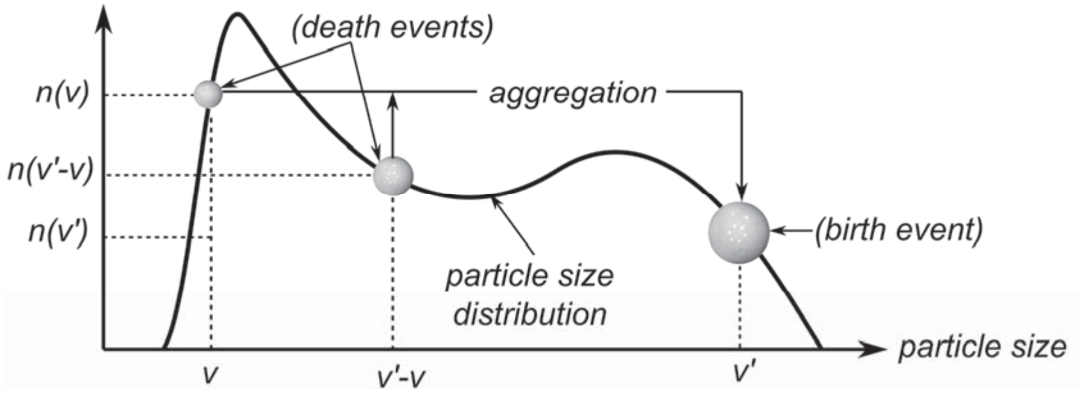

Figure 4.7: General representation of the agglomeration process in the PBM

The factor 0.5 in the Eq. (4.8) is used to avoid the double inclusion of the same aggregation event. The coalescence kernel $\beta(t,v,u)$ is an important parameter in the PBE, which represents the rate at which particles with volume v and u aggregate to form a particle with volume that equals $v+u$. This kernel is symmetric ($\beta(t,v,u) = \beta(t,u,v)$), continuous and positive ($\beta(t,v,u) \geq 0, \forall\, v,u > 0$).

Sastry has proposed (Sastry, 1975) to divide the coalescence kernel $\beta(v,u)$: into a time dependent $\beta^*(t)$ and a size dependent part:

$$\beta(t,v,u) = \beta^*(t) \cdot \beta(v,u) \tag{4.9}$$

The time dependent term is used to consider the dependence of coalescence on the operating conditions and $\beta(v,u)$ to define dependency from granule size. Several types of coalescence kernels are available in the literature. The most important ones are listed in Appendix in Table A.3 and were implemented into the dynamic model of fluidized bed agglomerator within this work. The listed correlations have been approximated for a specific, strictly limited parameter space; however, the application of inverse methods allows to obtain aggregation kernels from the experimental results (Hampel, 2010).

The death term $D_{agg}(t,v)$ defines the velocity with which the particles with volume v aggregate with other particles. The continuous form of the death events can be expressed as:

Dieses Werk ist copyrightgeschützt und darf in keiner Form vervielfältigt werden noch an Dritte weitergegeben werden.
Es gilt nur für den persönlichen Gebrauch.

$$D_{agg}(t,v) = \int_0^\infty \beta(t,v,v') \cdot n(t,v') \cdot n(t,v) dv' \tag{4.10}$$

Numerical solution of the PBE

The analytical solution of the PBE in the equation (4.3) exists just for very simplified cases. That is why for the solution of this equation, the application of some numerical approximation schemes is necessary. There can be distinguished between different classes of methods, for instance: a method of moments, Monte Carlo simulation, a method of weighted residuals, a finite difference scheme, etc. The review and comparison of the diverse approximation schemes can be found in (Ramkrishna, 2000), (Motz et al., 2002), (Kumar, 2006), (Qamar, 2007).

Many researchers in their works have tried to develop and to apply numerical schemes for calculations of separately considered mechanisms. One of the widely used techniques for simulation of the aggregation process has been proposed by Hounslow (Hounslow et al., 1988) and Kumar and Ramkrishna (Kumar and Ramkrishna, 1996). The method of Hounslow is based on the discretization scheme with the geometric grid. Afterwards it was extended by Litster (Litster et al., 1995) and Wynn (Wynn, 1996). The technique of Kumar and Ramkrishna is based on the grid with a more flexible pattern and allows to preserve any two defined properties (i.e. number and mass of particles). Balliu et al., (2004) compared both techniques by applying them to the dynamic granulation model. She pointed out that the technique of Kumar and Ramkrishna is capable to predict results for all particle size ranges more accurately. However, compared to the Hounslow technique it has higher computational effort.

In regard to the fixed-pivot method (Kumar and Ramkrishna, 1996), Kumar (Kumar et al., 2006) has proposed the cell average technique. This technique allows to simulate the aggregation process more precisely and offers the convenience of using linear, geometric and irregular meshes.

For simulation of the breakage equation numerical methods of different types have been applied. Hill and Ng (1995) have proposed a new discretized method, which allows to conserve the total mass and total number of particles. Other classes of numerical schemes, such as method of moments (Kostoglou and Karabelas, 2002) or Monte Carlo simulation (Mishra, 2000) have also been effectively used.

Dieses Werk ist copyrightgeschützt und darf in keiner Form vervielfältigt werden noch an Dritte weitergegeben werden.
Es gilt nur für den persönlichen Gebrauch.

4.3 Dynamic models of fluidized bed granulation

Two new dynamic units have been added into the SolidSim-Dynamics library in order to simulate the behavior of the pure growth process in the fluidized bed apparatus. The developed units possess different detailing levels of the process description. In the first one (*FBGranulatorPBM)* the growth is described by a one-dimensional population balance model. In the second one (*FBGranulatorPBMHM)* the PBM is extended by heat and mass transfer as by simplified fluid dynamics.

4.3.1 Granulation model based on population balances

In the developed simulation environment, the modeling of the fluidized bed granulation process can be performed with different detailing levels. As a first approximation the unit named *FBGranulatorPBM* was implemented into the SolidSim-Dynamics library. The granulation in this unit is described as a pure growth process without taking into account aggregation and breakage terms. It is additionally assumed that all particles have ideally spherical shapes, the mass of the bed material remains constant and uniform wetting of all particles (size independent growth) occurs.

For the modeling of growth the one-dimensional PBM with the particle diameter as the internal property coordinate is used. The central equation for description of the time progression of the particle size distribution (PSD) has the following form:

$$\frac{\partial n(t,d)}{\partial t} = \dot{n}_{in}(t,d) - \dot{n}_{out}(t,d) - \frac{\partial\left[\left(G(t,d) - Attr(t,d)\right)\cdot n(t,d)\right]}{\partial d}, \tag{4.11}$$

where $\frac{\partial n(t,d)}{\partial t}$ is the change of the particle number over time; the term $G(t,d)$ describes the particle growth due to the injection of solution, suspension or melted solid; $Attr(t,d)$ is used to consider attrition of granules; $\dot{n}_{in}(t,d) - \dot{n}_{out}(t,d)$ characterizes the particle fluxes entering and leaving the apparatus.

The numerical solution of the partial differential equation (4.11) is approximated with the help of a first order upwind finite difference scheme. This scheme can be relatively easily implemented, but because of numerical diffusion it has a big loss of accuracy near discontinuities (Kumar, 2006). There exist several more accurate approximation schemes for the numerical solution of PBM, which allows to avoid numerical dissipation (see, for example, method of characteristics proposed by Kumar and Ramkrishna (1996), Ramkrishna (2000)).

Dieses Werk ist copyrightgeschützt und darf in keiner Form vervielfältigt werden noch an Dritte weitergegeben werden.
Es gilt nur für den persönlichen Gebrauch.

It is assumed that the growth rate $G(t,d)$ does not depend on the particle size and is calculated by:

$$G(t) = \frac{2 \cdot \dot{M}_e(t)}{\rho_{p,susp} \cdot A_{tot}(t)}, \tag{4.12}$$

where $A_{tot}(t)$ is a total surface of particles in the apparatus; $\rho_{p,susp}$ is the density of the solid in the suspension, and $\dot{M}_e(t)$ is an effective mass stream of the injected suspension.

During the FB granulation process a part of the injected suspension may not be deposited on the bed material and leaves apparatus as dust. This can happen due to:

- geometrical properties of the apparatus. For instance, for a relative large distance between nozzle and bed material;
- process parameters, such as high gas temperature and velocity, which cause the drying of the suspension before a contact with the bed material occurs;
- material microproperties, which play an important role in the droplet-particle interaction. For example, the surface tension of the suspension and the influence of its viscosity on the dynamics of the droplet-particle impact.

To consider above mentioned events, the parameter which defines the overspray part (K_{os}) was introduced into the PBM. Depending on the overspray fraction, the effective mass stream, which covers the bed material, is calculated as:

$$\dot{M}_e(t) = \dot{M}_{susp}(t) \cdot (1 - K_w) \cdot (1 - K_{os}), \tag{4.13}$$

where K_w is the water fraction in the suspension.

The total mass flow of dust, caused by particle attrition and by overspray, is calculated as:

$$\dot{M}_{dust}(t) = \dot{M}_{susp}(t) \cdot (1 - K_w) \cdot K_{os} + R_{attr} \cdot A_{tot}(t), \tag{4.14}$$

where R_{attr} is the surface based attrition rate.

The PSD of dust is described by the normal Gaussian distribution Eq. (3.7) with specified values of median and variance, which can be specified by the user.

To develop a generally applicable unit, the concept of the implicit stream transformation with a movement matrix has been implemented (Figure 3.7). After each successful solver step, the stream for the description of the holdup is transformed by multiplication to a movement matrix. Afterwards, the input stream is added and a correction step is performed. It should also be

Dieses Werk ist copyrightgeschützt und darf in keiner Form vervielfältigt werden noch an Dritte weitergegeben werden.
Es gilt nur für den persönlichen Gebrauch.

mentioned that the entries of the movement matrix are recalculated in each time step – Eq. (4.15). In Figure 4.8 the general flowchart of the calculation procedure is shown.

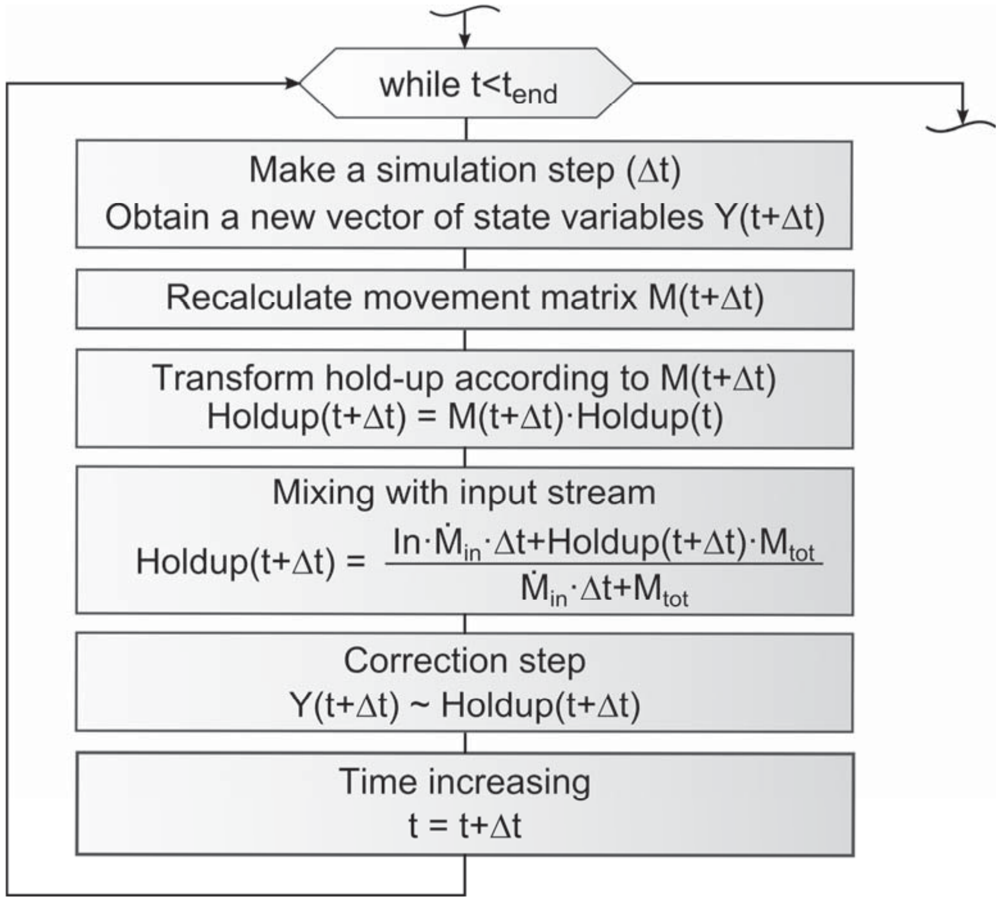
while t<t_end
Make a simulation step (Δt)
Obtain a new vector of state variables Y(t+Δt)
Recalculate movement matrix M(t+Δt)
Transform hold-up according to M(t+Δt)
Holdup(t+Δt) = M(t+Δt)·Holdup(t)
Mixing with input stream
Holdup(t+Δt) = (In·Ṁ_in·Δt+Holdup(t+Δt)·M_tot) / (Ṁ_in·Δt+M_tot)
Correction step
Y(t+Δt) ~ Holdup(t+Δt)
Time increasing
t = t+Δt

Figure 4.8: Flowchart of calculation procedure in the unit *FBGranulatorPBM*

The correction step, which is shown in the flowchart in Figure 4.8, is used to remove discrepancies between the entries in the holdup stream and internal state variables. The inconsistency between these values can appear due to the usage of different numerical schemes which are applied for calculation of holdup stream and for solution of Eq. (4.11). In the unit *FBGranulatorPBM* for the transformation of the holdup stream the Euler method is used, and for calculation of state variables the Backward Differentiation Formula (BDF) (Ascher and Petzold, 1998) approach is applied.

The movement matrix for the granulation unit is calculated according to:

$$\begin{cases} M(t+\Delta t)[i,j] = 1 - K_i & i = j \\ M(t+\Delta t)[i,j] = K_i & i = j+1 \\ M(t+\Delta t)[i,j] = 0, & \end{cases} \tag{4.15}$$

where the parameter K_i defines the mass fraction which is transferred from the interval i to the interval $i+1$. In every time step it is estimated as:

Dieses Werk ist copyrightgeschützt und darf in keiner Form vervielfältigt werden noch an Dritte weitergegeben werden.
Es gilt nur für den persönlichen Gebrauch.

$$K_i = \left(\frac{2\dot{M}_{susp} \cdot (1 - K_w) \cdot (1 - K_{os})}{\rho_{susp} \cdot A_{tot}} - R_{attr} \cdot A_{tot} \right) \cdot \Delta t \qquad (4.16)$$

The developed model *FBGranulatorPBM* can be used as a short-cut unit to perform coarse prediction of the granulation process. The relatively low computational effort allows running real-time simulations of this unit even with the fine discretization of the PSD. For more detailed modeling concerning heat and mass transfer the unit *FBGranulatorPBMHM* can be applied.

4.3.2 Model of heat and mass transfer

One of the main advantages of the fluidized bed process is the intensive heat and mass transfer (Mörl et al., 2007). Nowadays, different models predicting the thermodynamics in the FB can be found in the literature. Most of the models are characterized by the energy and material balances and describe the time-progression of the main process parameters, like temperature and humidity of fluidization gas or particle temperature. From the analysis of the energy and mass balances a set of partial differential equations (PDE’s) can be formulated. To obtain their numerical solution, the PDE’s can be spatially discretized. The discretization can be performed just through one spatial coordinate (height) as it was done in (Heinrich and Mörl, 1999) and (Ronsse et al., 2007), or additionally a radial distribution can be considered (Heinrich, 2001), (Nagaiah et al., 2007). A three-dimensional numerical study can give more predicted results and is effectively used to consider the nozzle position and its geometry (Nagaiah et al., 2007). However, because of the high computational effort, the usage of it is not always advisable.

During FB granulation the mass and heat transfer occurs on the boundaries of several phases. The liquid, which is deposited on the particle surface, is evaporated and, as a result, the humidity of environmental gas increases and the temperature of the suspension decreases. But due to the heat transfer between liquid film and particle and between liquid film and gas, the temperature of the liquid can increase. Moreover, it should be considered that FB granulation is not an adiabatic process and that is why the heat transfer through convection with the environment should be also considered.

To consider thermodynamics in the fluidized bed apparatus the novel unit named *FBGranulatorPBMHM* has been implemented into SolidSim-Dynamics. In this unit the PBM, which was previously introduced and implemented into the *FBGranulatorPBM* model, is extended with the model which takes into account heat and mass transfer as well as the fluid

Dieses Werk ist copyrightgeschützt und darf in keiner Form vervielfältigt werden noch an Dritte weitergegeben werden.
Es gilt nur für den persönlichen Gebrauch.

dynamics (Heinrich, 2011). The process in the *FBGranulatorPBMHM* model has been modelled under the following assumptions:

- total backmixing of particles (CSTR model), i.e. from a state of fluidization the particle concentration is uniform in the bed;
- ideal plug flow of the fluidization gas (PFTR model);
- no diffusion phenomena in the particles;
- cylindrical geometry of the apparatus;
- uniform distribution of the liquid load on the bed material (does not depend on location);
- the particles are covered by a liquid film with a constant thickness L_f.

To perform the calculations of heat and mass transfer, the entire apparatus volume was discretized throughout the height into a set of differential elements $[1..N_l]$. In Figure 4.9 the general representation of one layer of the apparatus with considered enthalpy ($\dot{H}$) and heat ($\dot{Q}$) streams is shown. The specification of these streams is given in Table 4.1.

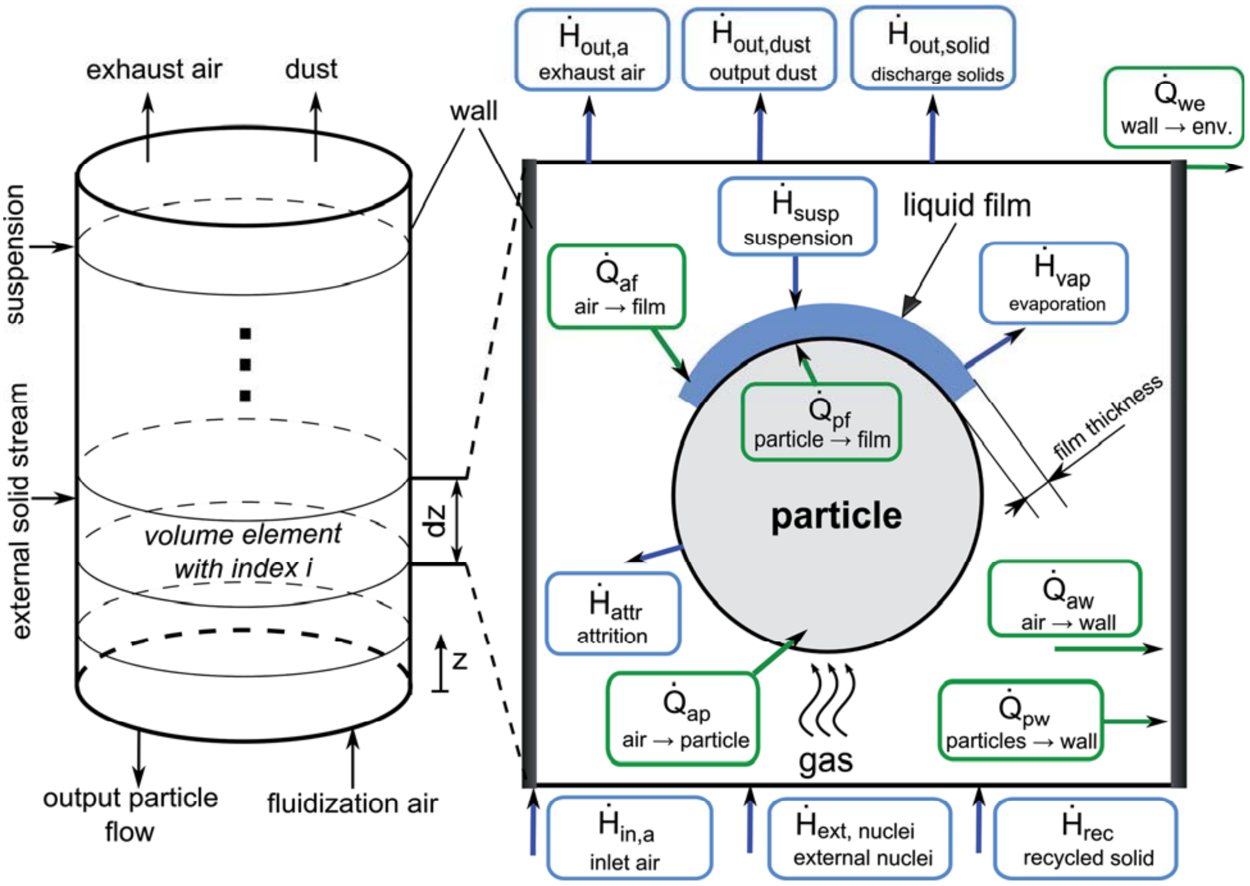
exhaust air
dust
wall
suspension
external solid stream
volume element with index i
dz
z
output particle flow
fluidization air
$\dot{H}_{out,a}$ exhaust air
$\dot{H}_{out,dust}$ output dust
$\dot{H}_{out,solid}$ discharge solids
$\dot{Q}_{we}$ wall → env.
$\dot{H}_{susp}$ suspension
liquid film
$\dot{Q}_{af}$ air → film
$\dot{H}_{vap}$ evaporation
$\dot{Q}_{pf}$ particle → film
film thickness
particle
$\dot{H}_{attr}$ attrition
$\dot{Q}_{aw}$ air → wall
$\dot{Q}_{ap}$ air → particle
gas
$\dot{Q}_{pw}$ particles → wall
$\dot{H}_{in,a}$ inlet air
$\dot{H}_{ext,\ nuclei}$ external nuclei
$\dot{H}_{rec}$ recycled solid

Figure 4.9: Volume element of granulator with enthalpy $(\dot{H})$ and heat $(\dot{Q})$ streams

Dieses Werk ist copyrightgeschützt und darf in keiner Form vervielfältigt werden noch an Dritte weitergegeben werden.
Es gilt nur für den persönlichen Gebrauch.

According to the equations of energy and mass balance of the components liquid, gas and solid particles, the system of DAE's (Eq. (4.18) - Eq. (4.22)) was formulated. This system consists of the equations for the description of:

- air temperature ϑ_a:
  derived from the energy balance of the gas and distributed above the height – Eq. (4.18);
- temperature of the liquid film ϑ_f:
  derived from the energy balance of the liquid – Eq. (4.19);
- wetted surface fraction ϕ:
  derived from the mass balance of the liquid – Eq. (4.22). The parameter ϕ is defined as a ratio between the particle surface covered with A_{cov} a liquid film and the total surface A_{tot} – Eq. (4.17);
- particle temperature ϑ_p:
  derived from the energy balance of the solid particles – Eq. (4.20);
- air humidity Y_a:
  derived from the mass balance of the gas and distributed throughout the height – Eq. (4.21).

Table 4.1: Enthalpy streams and heat streams within the volume element of a FB granulator

Enthalpy streams induced by:

exhaust and inlet air: $\dot{H}_{out,a}$ and $\dot{H}_{in,a}$
evaporation: $\dot{H}_{vap}$
sprayed suspension: $\dot{H}_{susp}$
recycled solid stream: $\dot{H}_{rec}$
discharge solids flow: $\dot{H}_{out,solid}$
output dust flow: $\dot{H}_{out,dust}$

Heat transfer between:

particle and liquid film: $\dot{Q}_{pf}$
air and liquid film: $\dot{Q}_{af}$
air and particle: $\dot{Q}_{ap}$
air and wall: $\dot{Q}_{aw}$
particle and wall: $\dot{Q}_{pw,i}$
wall and environment: $\dot{Q}_{we}$

Dieses Werk ist copyrightgeschützt und darf in keiner Form vervielfältigt werden noch an Dritte weitergegeben werden.
Es gilt nur für den persönlichen Gebrauch.

The coefficients of heat and mass transfer, which are used in the Eq. (4.18) - Eq. (4.22), were obtained with help of correlations proposed by Gnielinski (1980).

$$\phi = A_{cov}/A_{tot} \tag{4.17}$$

Film temperature:

$$\begin{aligned} \frac{d\vartheta_f}{dt} = \frac{1}{c_{p,f} \cdot L_f \cdot \rho_f \cdot A_{tot} \cdot \phi} \cdot \sum_{i=1}^{N_l} \left[\dot{Q}_{pf,i} + \dot{Q}_{af,i} + \frac{\dot{H}_{susp} - \dot{H}_{vap}}{N_l} \right] \\ - \frac{\vartheta_f}{\phi} \frac{d\phi}{dt} - \frac{\vartheta_f}{A_{tot}} \frac{dA_{tot}}{dt} \end{aligned} \tag{4.18}$$

Air temperature:

$$\begin{aligned} \frac{d\vartheta_{a,i}}{dt} = \frac{N_l}{M_{a,tot} \cdot \left(c_{p,a} + c_{p,vap} \cdot Y_{a,i} \right)} \\ \cdot \left[\dot{H}_{in,a}[i] - \dot{H}_{out,a}[i] - \dot{Q}_{ap,i} - \dot{Q}_{af,i} - \dot{Q}_{aw,i} + \frac{\dot{H}_{vap}}{N_l} \right] - \\ \frac{dY_{a,i}}{dt} \cdot \left[\frac{c_{p,vap} \cdot \vartheta_{a,i} + \Delta h_0}{c_{p,a} + c_{p,vap} \cdot Y_{a,i}} \right] \end{aligned} \tag{4.19}$$

Particle temperature:

$$\frac{d\vartheta_p}{dt} = \frac{1}{M_{tot} \cdot c_{p,p}} \left(\sum_{i=1}^{N_l} \left[\dot{Q}_{ap,i} - \dot{Q}_{pw,i} - \dot{Q}_{pf,i} \right] + \dot{H}_{rec} - \dot{H}_{out,solid} - \dot{H}_{out,dust} \right) \tag{4.20}$$

Air humidity:

$$\frac{dY_{a,i}}{dt} = - \frac{\dot{M}_a^{dry} \cdot N_l}{M_{a,tot}} \left(Y_{a,i} - Y_{a,i-1} \right) + \frac{\dot{M}_{vap}}{M_{a,tot}} \tag{4.21}$$

Wetted surface fraction:

$$\frac{d\phi}{dt} = \frac{1}{\rho_l \cdot L_f \cdot A_{tot}} \left(\dot{M}_{susp} - \dot{M}_{vap} \left[1 + \frac{\dot{M}_{vap} \cdot (1 - K_w)}{\dot{M}_{susp} \cdot K_w} \right] \right) - \frac{\phi}{A_{tot}} \cdot \frac{dA_{tot}}{dt} \tag{4.22}$$

The rates of the above described heat and mass transfers depend on the fluid dynamics in the apparatus. To predict the values of the mass and heat transfer coefficient Gnielinski (1980) proposed empirical approximations of Sherwood (*Sh*) and Nusselt (*Nu*) numbers. The equations of these approximations are given in the Appendix: (A.4)-(A.9). The correlation proposed by Gnielinski is of proven validity for regimes with high Reynolds number. For low

Dieses Werk ist copyrightgeschützt und darf in keiner Form vervielfältigt werden noch an Dritte weitergegeben werden.
Es gilt nur für den persönlichen Gebrauch.

values of Reynolds number Groenewold and Tsotsas (1999) have proposed a new model, which is related to the model of Gnielinski.

The value of the mass transfer coefficient β [m/s] depends on the coefficient of mass diffusivity D [m^2/s] and particle diameter d_p. It is calculated as:

$$\beta = \frac{Sh \cdot D}{d_p} \tag{4.23}$$

The heat transfer coefficients between air and liquid film and between air and particle are obtained with Eq. (4.24). Here λ is the thermal conductivity [W·m^{-1}·K^{-1}].

$$\alpha_{af} = \alpha_{ap} = \frac{Nu \cdot \lambda}{d_p} \tag{4.24}$$

To obtain the heat transfer between particle and liquid film α_{pf}, Reppmann (1990) and Heinrich (2001) have used a correlation factor f_a, such that:

$$\alpha_{pf} = f_a \cdot \alpha_{af} \tag{4.25}$$

To couple the model of granular material with a model of heat and mass transfer the Sauter-diameter is used as a characteristic scalar value for the average particle diameter. The Sauter-diameter d_{32} is expressed as:

$$d_{32} = \frac{6 \cdot M_{tot}}{\rho_p \cdot A_{tot}}, \tag{4.26}$$

where M_{tot} is a holdup mass.

The porosity in the bed (ε) and the Reynolds numbers at the elutriation (Re_{elu}) and the minimal fluidization (Re_{mf}) points are approximated according to the model proposed by Gorosko et al. (1958). The equations to calculate these parameters are given in the Appendix Eq. (A.10), (A.11) and (A.12). To check the correctness of the process parameters the value of the Reynolds number is compared according to the inequality (4.27). If the condition is not satisfied, a warning message is displayed during simulation.

$$Re_{elu} \geq Re \geq Re_{mf} \tag{4.27}$$

Simultaneously to the consideration of thermodynamics, the internal separation by a classification tube was included into the model. The separation of the bed material is characterized by the different settling velocity ($u_{stl}(d)$) and superficial gas velocity for particles

Dieses Werk ist copyrightgeschützt und darf in keiner Form vervielfältigt werden noch an Dritte weitergegeben werden.
Es gilt nur für den persönlichen Gebrauch.

of different sizes. During a production process the classification gas enters the apparatus through a tube. This gas flow acts on the particles and does not allow particles to leave the apparatus. However, after the particle reaches a specific diameter, the gravity force is increased to overcome gas resistance and particle leaves the apparatus. In the view of the different settling velocities, the process of the particle discharge out of the fluidized bed is specified in accordance to the separation function of Molerus and Hoffmann (1969). The output particle size distribution is based on the distribution of the bed material and on the separation function $T_{dt}(d)$, which defines the probability that particles with diameter d will be discharged from the granulator through a tube with length L_{dt}. The separation function is calculated according to the Eq. (4.28), where D_{ax} is the axial dispersion coefficient and u_{dt} is the flow velocity in the discharge tube.

$$T_{dt}(d) = \left(1 + \left(\frac{u_{dt}}{u_{stl}(d)}\right) \cdot \exp\left(-\frac{(u_{stl}(d) - u_{dt}) \cdot L_{dt}}{D_{ax}}\right)\right)^{-1} \tag{4.28}$$

For the numerical solution of the unit *FBGranulatorPBMHM* the thermodynamic equations were combined with a set of equations which were received after discretization of the PBM. The total model was represented as a set of differential algebraic equations (DAE's) and afterwards this system was simultaneously processed by a single solver, as it is schematically shown in Figure 4.10. Such approach possesses good convergence properties, but it does not allow to use specific numerical solution schemes intended for the PBM.

As an alternative, the modular strategy can be used. In the case of the granulation process the modular approach can be applied not just on the level of flowsheet, but also on the level of the unit, as illustrated in Figure 4.10. The population balance model and equations for the description of heat and mass transfer can be solved independently by different solvers with further synchronization of coupled variables. This strategy should be applied in the case when the usage of a specific numerical algorithm is needed for the calculation of PBM.

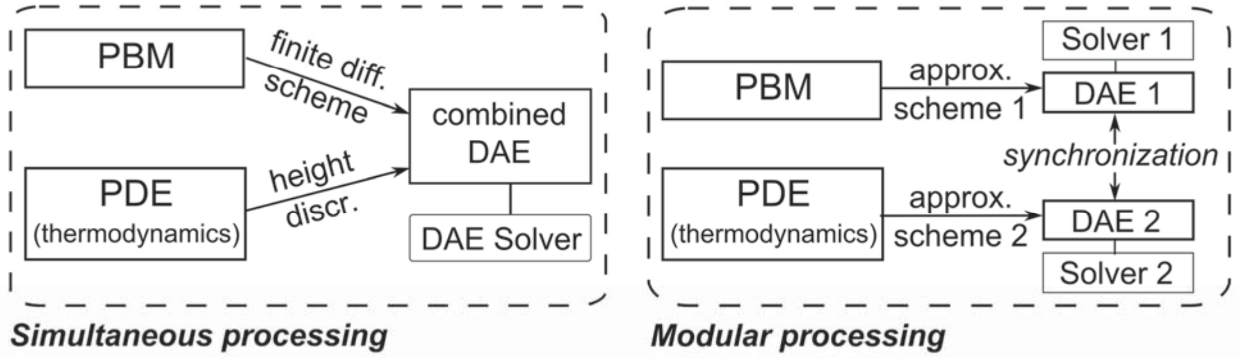

Figure 4.10: Representation of the alternative simulation strategies of FB granulator

Dieses Werk ist copyrightgeschützt und darf in keiner Form vervielfältigt werden noch an Dritte weitergegeben werden.
Es gilt nur für den persönlichen Gebrauch.

To simplify the further usage of the *FBGranulatorPBMHM* unit, the user-friendly graphical user interface (GUI) has been developed. The main dialog windows of the unit *FBGranulatorPBMHM* are illustrated in Figure 4.11 and Figure 4.12. The represented interface is typical for all dynamic units which are implemented into the model library of the SolidSim-Dynamics environment. In the input dialog (Figure 4.11) the user can specify the values which are relevant to the main model parameters such as initial bed material, thickness of the liquid film, geometry of apparatus, etc. The output dialog (Figure 4.12) displays the information about the time progressions of the important state variables. This information is represented in the form of two-dimensional plots and can be easily exported into external software tools.

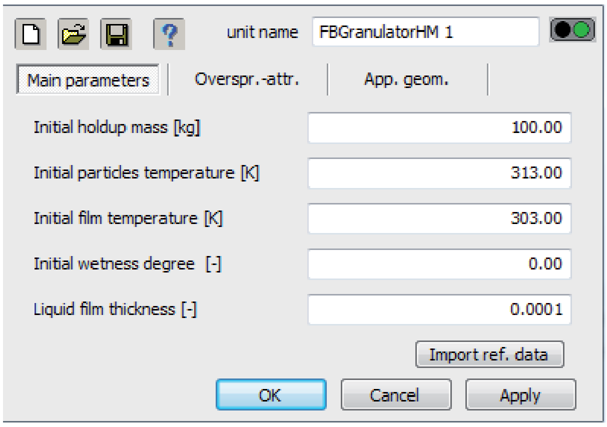

unit name: FBGranulatorHM 1

Initial holdup mass [kg]: 100.00

Initial particles temperature [K]: 313.00

Initial film temperature [K]: 303.00

Initial wetness degree [-]: 0.00

Liquid film thickness [-]: 0.0001

Figure 4.11: GUI of the input dialog of the *FBGranulatorPBMHM* unit

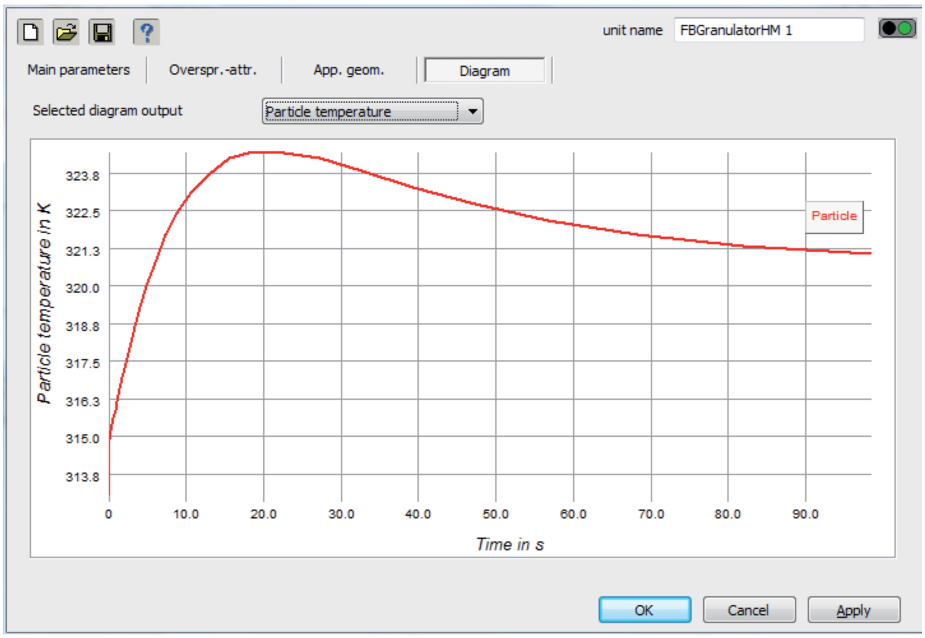

unit name: FBGranulatorHM 1

Selected diagram output: Particle temperature

Figure 4.12: Typical GUI of the dynamic model. Output dialog of the *FBGranulatorPBMHM*

Dieses Werk ist copyrightgeschützt und darf in keiner Form vervielfältigt werden noch an Dritte weitergegeben werden.
Es gilt nur für den persönlichen Gebrauch.

Compared to the unit *FBGranulatorPBM,* the developed *FBGranulatorPBMHM* model describes more precisely the dynamics of the fluidized bed granulation process. However, the larger number of differential equations in the new unit leads to significant longer computational time. Nevertheless, the *FBGranulatorPBMHM* is still a model which contains a lot of empirical approximation. In order to perform more precise modeling and to consider specific material microparameters the multiscale methodology can be applied.

4.4 Dynamic models of fluidized bed aggregation

Two different units for the modeling of pure aggregation have been implemented into SolidSim-Dynamics. The implemented units are based on the different numerical approximation schemes, which are used to obtain the numerical solution of the population balance equation expressed in the Eq. (4.29). This equation is derived from the Eq. (4.3) by assuming that there are no growth, breakage or attrition events.

$$\frac{\partial n(t,v)}{\partial t} = \frac{\dot{Q}_{in}(t)}{V} n_{in}(t,v) - \frac{\dot{Q}_{out}(t)}{V} n_{out}(t,v) + B_{agg}(t,v) - D_{agg}(t,v) \tag{4.29}$$

4.4.1 Fixed discretization method

Hounslow et al. (Hounslow et al., 1988) have proposed a discretization form of the population balance, where the PSD has been discretized above the volume into a set of unequal intervals, as it is shown in Figure 4.13. Each following grid node has been calculated as $v_{i+1} = 2 \cdot v_i$, where v_i is volume of particle in the class i. By such discretization only interactions involving particles in the *i-1*th interval can produce a particle in the *i*th interval. The usage of the equal grid intervals may result in a huge number of classes and enormous increase of computations.

Hounslow has distinguished different types of the binary interactions which modify the value of the PSD in the cell with index i:

- birth induced by the aggregation between the particles from interval *i-1* with the smaller particles;
- birth induced by the coalescence of the particles from class *i-1*;
- death of the particle after aggregation with smaller particle;
- death of the particle after aggregation with a particle of the same or larger size.

Dieses Werk ist copyrightgeschützt und darf in keiner Form vervielfältigt werden noch an Dritte weitergegeben werden.
Es gilt nur für den persönlichen Gebrauch.

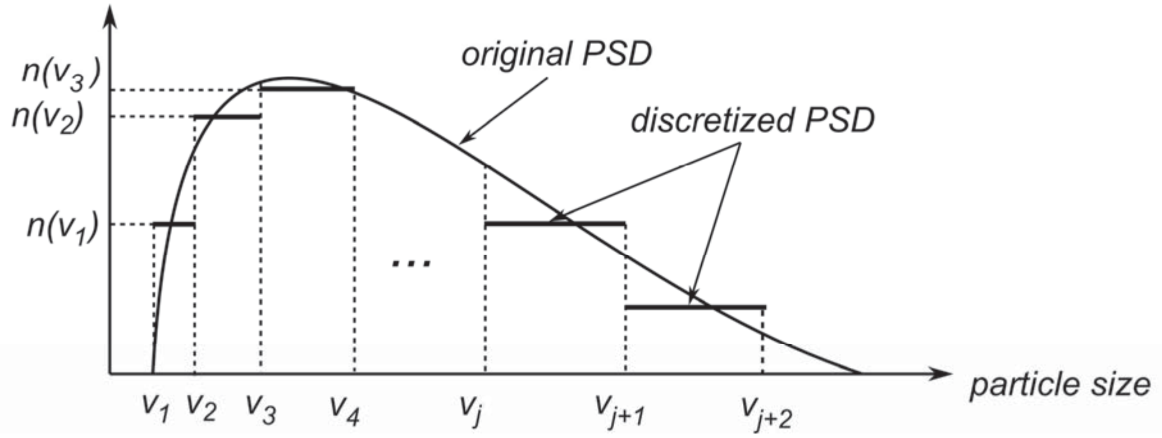

Figure 4.13: Discretized representation of PSD

Litster et al., (1995) have extended this approach for an adjustable geometry of the form $v_{i+1} = 2^{1/q} \cdot v_i$, where q is an integer which is greater than or equal to one. However, this method has a poor convergence and can be instable for order greater than four. This disadvantage has been removed in the modification proposed by Wynn (Wynn, 1996). The new formulation has more stable convergence properties than the original version, but requires larger volume of computations. The modified equation proposed by Wynn for the expression of the time progression of the PSD is given by:

$$\begin{aligned}\frac{dN_i}{dt} = &\sum_{j=1}^{i-S_1} \beta_{i-1,j} \cdot N_{i-1} \cdot N_j \frac{2^{(j-i+1)/q}}{2^{1/q}-1} \\ &+ \sum_{p=2}^{q} \sum_{j=1-S_p-1}^{i-S_p} \beta_{i-p,j} \cdot N_{i-p} \cdot N_j \frac{2^{(j-i+1)/q} - 1 + 2^{(1-p)/q}}{2^{1/q}-1} + \frac{1}{2} \\ &\cdot \beta_{i-q,i-q} \cdot N_{i-q}^2 \\ &+ \sum_{p=1}^{q-1} \sum_{j=i+1-S_p}^{i+1-S_{p+1}} \beta_{i-p,j} \cdot N_{i-p} \cdot N_j \frac{-2^{\frac{j-1}{q}} + 2^{\frac{1}{q}} - 2^{-\frac{p}{q}}}{2^{\frac{1}{q}}-1} \\ &+ \sum_{j=1}^{i-S_1+1} \beta_{i,j} \cdot N_i \cdot N_j \frac{2^{\frac{j-i}{q}}}{2^{\frac{1}{q}}-1} - \sum_{j=i-S_1+2}^{\infty} \beta_{i,j} \cdot N_i \cdot N_j ,\end{aligned} \tag{4.30}$$

where N_i is a number of particles in cell i and the parameter S_p is obtained according to the Eq. (4.31).

$$S_p = Int\left[1 - \frac{q \cdot \ln(1-2^{-p/q})}{\ln 2}\right], \tag{4.31}$$

where $Int(y)$ is a function which returns the integer value of y without the fractional part.

Dieses Werk ist copyrightgeschützt und darf in keiner Form vervielfältigt werden noch an Dritte weitergegeben werden.
Es gilt nur für den persönlichen Gebrauch.

The equations (4.30) and (4.31) have been used in SolidSim-Dynamics for the simulation of the fluidized bed agglomerator unit *FBAgglomeratorPBM*. In this unit the movement matrix for the holdup transformation was not directly obtained from the above described approximation of the PBM. Instead of this, the entries in the movement matrix were estimated from the solution of the inverse problem. In every simulation time step the following operations were executed:

- the PSD for the new time points is predicted by Eqs. (4.30) and (4.31);
- the entries in the movement matrix depend on the difference between the distributions on consecutive time steps;
- the received matrix is applied to make a holdup transformation.

The implemented graphical interface of the unit *FBAgglomeratorPBM* provides a possibility to set the value of the parameter q. To avoid the loss of information by grid conversion, this parameter should be chosen in accordance with the structure of the material stream in the investigated process flowsheet.

4.4.2 Cell average technique

Cell average (CA) technique is the approach which was developed for the numerical solution of the population balance equations (Kumar et al., 2006). Compared to the widely used fixed-pivot technique, this approach has a better consistency with respect to the first two moments and can be generalized to conserve any two moments.

The general idea of the CA method can be explained by the following example. Suppose the particles are discretized throughout a property coordinate x, as it is shown in Figure 4.14. Here, the entire size domain is divided into a set of cells with boundaries $\left(x_{i-\frac{1}{2}}; x_{i+\frac{1}{2}}\right)$.

Dieses Werk ist copyrightgeschützt und darf in keiner Form vervielfältigt werden noch an Dritte weitergegeben werden.
Es gilt nur für den persönlichen Gebrauch.

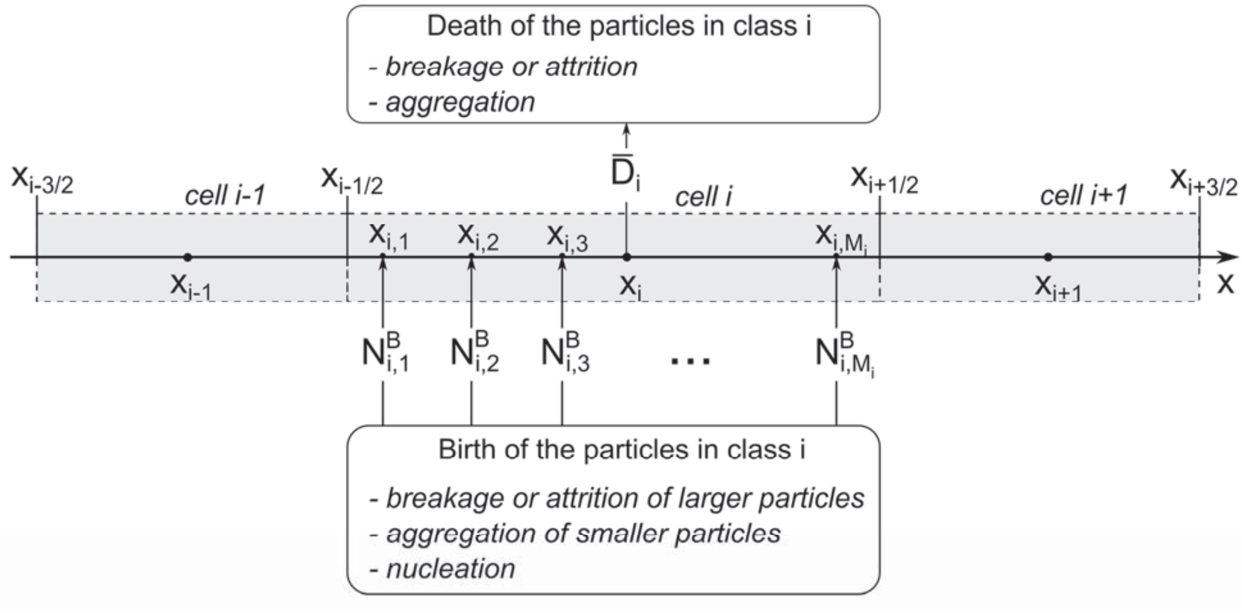

Figure 4.14: Discretization of the size domain by CA technique

The time-progression of the PSD at the grid points is expressed by the discretized form of the PBE as:

$$\frac{dN_i}{dt} = \bar{B}_i - \bar{D}_i \,, \tag{4.32}$$

where $i \in [1..N_{cl}]$; N_{cl} is a total number of classes; N_i is the number of particles in the class i; $\bar{B}_i$ and $\bar{D}_i$ are the input and output particle fluxes induced by the birth and death events accordingly.

Due to physical events like aggregation or breakage, new-born particles $N^B_{i,j}$ with different sizes $x^B_{i,j}$ are introduced into the system. To consider these processes, the total number of new-born particles N^B_i and their average size $\bar{x}_i$ are calculated as expressed in the equations (4.33) and (4.34).

$$N^B_i = \sum_{j=1}^{M_i} N^B_{i,j} \tag{4.33}$$

$$\bar{x}_i = \frac{\sum_{j=1}^{M_i} N^B_{i,j} \cdot x^B_{i,j}}{N^B_i} \tag{4.34}$$

The new average particle size $\bar{x}_i$ in the majority number of cases does not agree with the existing grid ($\bar{x}_i \neq x_i$). Therefore, it is necessary to reassign evolved particles to the neighbor grid intervals. In the Eq. (4.35) the function $\lambda^{\pm}_i(x)$ is expressed which is used to determine the fractions of newborn particles which should be moved to neighbor classes.

Dieses Werk ist copyrightgeschützt und darf in keiner Form vervielfältigt werden noch an Dritte weitergegeben werden.
Es gilt nur für den persönlichen Gebrauch.

$$\lambda_i^{\pm}(x) = \frac{x - x_{i\pm1}}{x_i - x_{i\pm1}} \tag{4.35}$$

For instance, if the condition $x_{i-\frac{1}{2}} < \bar{x}_i < x_i$ is satisfied, then the fraction, which will be reassigned to the class $i-1$ is obtained as $N_i^B \cdot \lambda_i^-(\bar{x}_i)$, and to the class i equals to the $N_i^B \cdot \lambda_{i-1}^+(\bar{x}_i)$.

The total birth rate $\bar{B}_i$ at the grid point x_i can be expressed as:

$$\begin{gathered}\bar{B}_i = N_{i-1}^B \cdot \lambda_i^-(\bar{x}_{i-1}) \cdot Hs(\bar{x}_{i-1} - x_{i-1}) + N_i^B \cdot \lambda_i^-(\bar{x}_i) \cdot Hs(x_i - \bar{x}_i) + \\ N_i^B \cdot \lambda_i^+(\bar{x}_i) \cdot Hs(\bar{x}_i - x_i) + N_{i+1}^B \cdot \lambda_i^+(\bar{x}_{i+1}) \cdot Hs(x_{i+1} - \bar{x}_{i+1}),\end{gathered} \tag{4.36}$$

where $Hs(x)$ is the Heaviside step function, which is defined as:

$$Hs(x) = \begin{cases} 0 & x < 0 \\ 0.5 & x = 0 \\ 1 & x > 0 \end{cases} \tag{4.37}$$

For the approximation of the death term $\bar{D}_i$ no further calculations are needed.

The main distinction between the fixed pivot and the CA method are related in considering of birth events and in the length of the domain which can contribute to birth event. The advantage of CA is that the birth events are initially collected and just in the next step reassignment occurs. By the fixed pivot technique each birth is immediately reassigned to the neighbor cells, which can lead to a larger numerical error (Kumar, 2006)

The cell average method has been implemented into SolidSim-Dynamics as a solver for the fluidized bed agglomerator unit named *FBAgglomeratorPBMCA*. In this unit the continuous aggregation process was considered. The particle volume (v) has been used as an internal property coordinate. It is assumed that during coalescence the total volume remains constant. In this case the number of new-born particles in the interval i can be found by Eq. (4.38). The particle flux into the cell i depends on the number of particles in the classes of the contact partners (N_j, N_k) and the coalescence kernel $\beta_{j,k}$. The different types of kernels, which can be used in this model, are listed in Table A.3.

$$N_i^B = \sum_{\substack{j,k \\ v_{i-\frac{1}{2}} \le v_j + v_k \le v_{i+\frac{1}{2}}}}^{j>k} \beta_{j,k} \cdot N_j \cdot N_k + \sum_{\substack{j \\ v_{i-\frac{1}{2}} \le 2 \cdot v_j \le v_{i+\frac{1}{2}}}} \frac{1}{2} \beta_{j,j} \cdot {N_j}^2 \tag{4.38}$$

The average volume $\bar{v}_i$ can be approximated as:

Dieses Werk ist copyrightgeschützt und darf in keiner Form vervielfältigt werden noch an Dritte weitergegeben werden.
Es gilt nur für den persönlichen Gebrauch.

$$\bar{v}_i = \frac{V_i^B}{N_i^B}, \tag{4.39}$$

whereby the total volume of newborn particles V_i^B is equal to:

$$V_i^B = \sum_{\substack{j,k \\ v_{i-\frac{1}{2}} \le v_j + v_k \le v_{i+\frac{1}{2}}}}^{j>k} \beta_{j,k} \cdot N_j \cdot N_k \cdot (v_j + v_k) + \sum_{\substack{j \\ v_{i-\frac{1}{2}} \le 2 \cdot v_j \le v_{i+\frac{1}{2}}}} \beta_{j,j} \cdot {N_j}^2 \cdot v_j \tag{4.40}$$

The death (sink) term $\bar{D}_i$ characterizes the particles which are removed as a result of the aggregation with the other particles and it is estimated as:

$$\bar{D}_i = \sum_{j=1}^{N_{cl}} \beta_{i,j} \cdot N_i \cdot N_j \tag{4.41}$$

To implement implicit transformation of the material stream during calculation of the agglomerator model, the movement matrix for the mass fractions has been estimated. Therefore, the PBM has been reformulated into the mass derived form.

If the particle diameter d_i is used as a property coordinate and Δd_i is the width of the cell i, then the number of particles can be obtained as:

$$N_i = \Delta d_i \cdot N_{tot} \cdot q_{0,i} = \frac{6 \cdot M_{tot} \cdot q_{3,i} \cdot \Delta d_i}{\pi \cdot \rho_p \cdot d_i^3} \tag{4.42}$$

where ρ_p is the particle density; q_0 and q_3 are the number and the mass density distributions accordingly; N_{tot} is the total number of particles and M_{tot} is the total holdup mass. Regarding to the Eq. (4.32) and (3.17) the change of the mass density distribution can be expressed as the differential equation (4.43).

$$\frac{dq_{3,i}}{dt} = \frac{(\bar{B}_i - \bar{D}_i) \cdot \pi \cdot \rho \cdot d_i^3}{6 \cdot M_{tot} \cdot \Delta d_i} \tag{4.43}$$

To derive the entries of the movement matrix, the Eq. (4.43) is numerically solved by the Euler method. Afterwards in each successful solver step, the movement matrix is applied to transform the stream which describes the holdup in the apparatus. The movement matrix can be represented as:

$$Mov = I - Mov^D \cdot \Delta t + Mov^B \cdot \Delta t, \tag{4.44}$$

where I is the identity matrix; Δt is the simulation time step; Mov^D and Mov^B are the components of the transformation matrix derived from the death and the birth terms

Dieses Werk ist copyrightgeschützt und darf in keiner Form vervielfältigt werden noch an Dritte weitergegeben werden.
Es gilt nur für den persönlichen Gebrauch.

accordingly. The mass fractions which are induced by the death event and moved from the source interval *src* into the destination interval *dst* are estimated as:

$$Mov^{D}_{src,dst} = \begin{cases} 0, & src \neq dst \\ \dfrac{\pi \cdot \rho \cdot d^{3}_{dst}}{6 \cdot M_{tot} \cdot \Delta d_{dst}} \cdot \displaystyle\sum_{j=1}^{N_{cl}} \beta_{src,j} \cdot N_j \cdot N_{src}\,, & src = dst \end{cases} \tag{4.45}$$

The entries of the two-dimensional matrix Mov^{B} can be found as:

$$Mov^{B}_{src,dst} = \frac{\bar{B}^{src}_{dst} \cdot \pi \cdot \rho \cdot d^{3}_{dst}}{M_{tot} \cdot \Delta d_{dst}} \tag{4.46}$$

where N_{src} is a number of particles in the source class and $\bar{B}^{src}_{dst}$ is the particle number flux from the interval *src* to the interval *dst*. This flux is derived from the Eq. (4.36) and equal to:

$$\begin{aligned} \bar{B}^{src}_{dst} = {} & N^{B,src}_{dst-1} \cdot \lambda^{-}_{dst}(\bar{v}_{dst-1}) \cdot Hs(\bar{v}_{dst-1} - v_{dst-1}) + N^{B,src}_{dst} \\ & \cdot [\lambda^{-}_{dst}(\bar{v}_{dst}) \cdot Hs(v_{dst} - \bar{v}_{dst}) + \lambda^{+}_{dst}(\bar{v}_{dst}) \cdot Hs(\bar{v}_{dst} - v_{dst})] \\ & + N^{B,src}_{dst+1} \cdot \lambda^{+}_{dst}(\bar{v}_{dst+1}) \cdot Hs(v_{dst+1} - \bar{v}_{dst+1}) \end{aligned} \tag{4.47}$$

Here, $N^{B,src}_{dst}$ is the flux of particles from the class *src* into the class *dst*. The terms $N^{B,src}_{dst-1}$ and $N^{B,src}_{dst+1}$ are particle fluxes into the neighbor classes, which afterwards are reassigned to the class *dst*. The term $N^{B,src}_{dst}$ is calculated as:

$$N^{B,src}_{dst-1} = \sum_{v_{dst-\frac{1}{2}} \leq v_i + v_{src} \leq v_{dst+\frac{1}{2}}}^{i \neq src} \beta_{i,src} \cdot N_i \cdot N_{src} \cdot \frac{N_{src}}{N_i + N_{src}} + \Upsilon_{src,dst}\,, \tag{4.48}$$

where the conditional term $\Upsilon_{src,dst}$ is expressed as:

$$\Upsilon_{src,dst} = \begin{cases} \dfrac{1}{2} \cdot \beta_{src,src} \cdot N^{2}_{src}, & v_{dst-\frac{1}{2}} \leq 2v_{src} \leq v_{dst+\frac{1}{2}} \\ 0, \quad v_{dst-\frac{1}{2}} > 2v_{src} & or \quad 2v_{src} > v_{dst+\frac{1}{2}} \end{cases} \tag{4.49}$$

Dieses Werk ist copyrightgeschützt und darf in keiner Form vervielfältigt werden noch an Dritte weitergegeben werden.
Es gilt nur für den persönlichen Gebrauch.

5. Multiscale treatment of solids processes

One of the demands on the processing of solids processes is caused due to the necessity to consider subprocesses on various time and length scales. This happens, because for many processes like agglomeration, comminution, attrition the key phenomenon is on the scale of individual particles, while the point of interest is the global macroscopic production process. Clift (1996) has distinguished three relevant scales, where such processes can be described: scale of the individual particle, sub-particle phenomena, such as adhesion or fracture, and scale of process equipment.

In the area of industrial solids processes most of the simulation tools use empirical or semi-empirical models, which describe the process on the macroscale. As a result of the simplifications in these models the numerical solution can be obtained in acceptable time. The main disadvantage of such macro models is a poor consideration of material microproperties and apparatus geometries. The calculations can be performed in a strictly limited parameter space, where the experimental validation is performed. Due to the big influence of material microproperties, even two similar solid materials can have totally dissimilar behavior. Therefore, the development of a generalized macromodel, which can be used for different types of material outside the parameter space, for which the experimental data exists, is very complicated and in many cases is an impossible task.

5.1 General concept and interscale communications

The possible way to increase the quality of process simulation is the usage of the multiscale simulation approach. Here, with the purpose to obtain a more detailed process description, the submodels which are relevant at different time and length scales can be combined by interscale communication into one multiscale model. Such multiscale models can be classified according to the spatial relationship between balance volumes that comprise the model. One can distinguish between multidomain, embedded, parallel, serial, simultaneous and multidomain model with interface zone types of communication (Ingram et al., 2003).

In recent years many authors have tried to use multiscale modeling methodology in the area of solids processes applying it to different processes and apparatuses such as drum granulators (Ingram and Cameron, 2005), fluidized bed reactors (Balaji et al., 2010), crystallizers, gas-solid fluidization (Ge et al., 2011), etc. However, none of the already developed concepts can be

Dieses Werk ist copyrightgeschützt und darf in keiner Form vervielfältigt werden noch an Dritte weitergegeben werden.
Es gilt nur für den persönlichen Gebrauch.

effectively applied for the calculation of the fluidized bed granulation process or extended to other solids processes.

According to Werther et al. (2011) the models of different apparatuses and processes in solids industry can be distinguished by detailing levels and application purposes, whereby each level can only be applied to some specific application of modeling. In Figure 5.1 the proposed classification of models by various application areas is given.

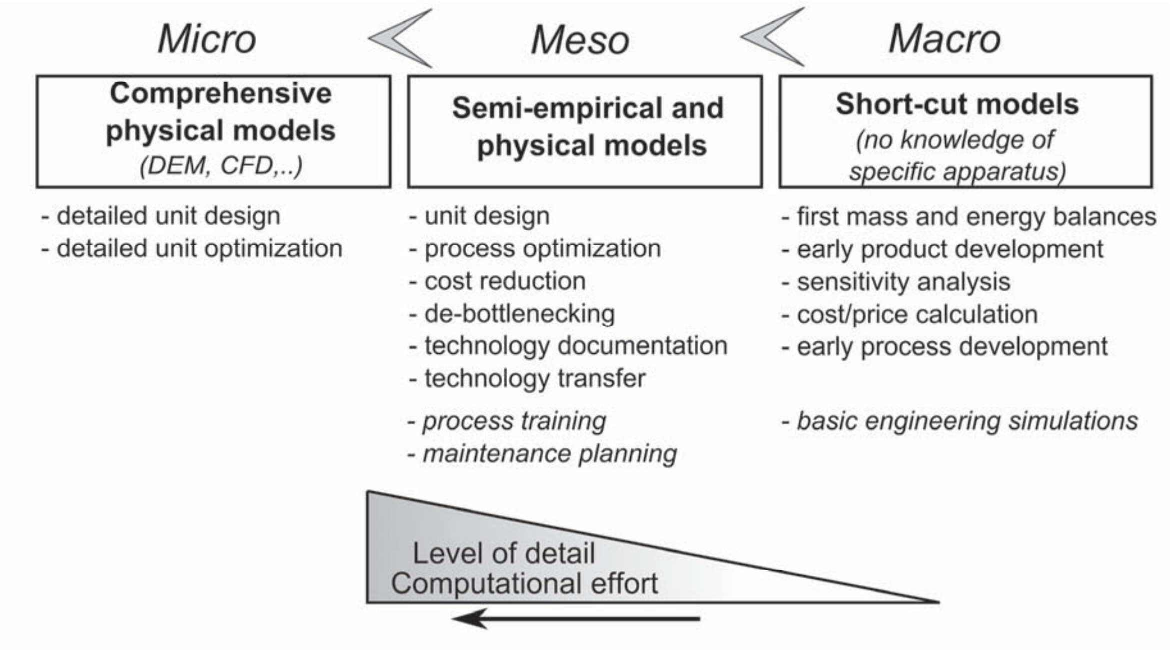

Figure 5.1: Models classification according to application area

The mostly used names for the scales definitions are micro, meso and macroscale. In this work the definition of the macroscale is used on the level of the global production process. On the microscale the separate particles and interactions between them are considered. The mesoscale is used as an intermediate submodel between micro and macro descriptions of the process. An example of a possible description of a circulating fluidized bed apparatus at different time and length scales is shown in Figure 5.2 (Werther et al., 2011).

Dieses Werk ist copyrightgeschützt und darf in keiner Form vervielfältigt werden noch an Dritte weitergegeben werden.
Es gilt nur für den persönlichen Gebrauch.

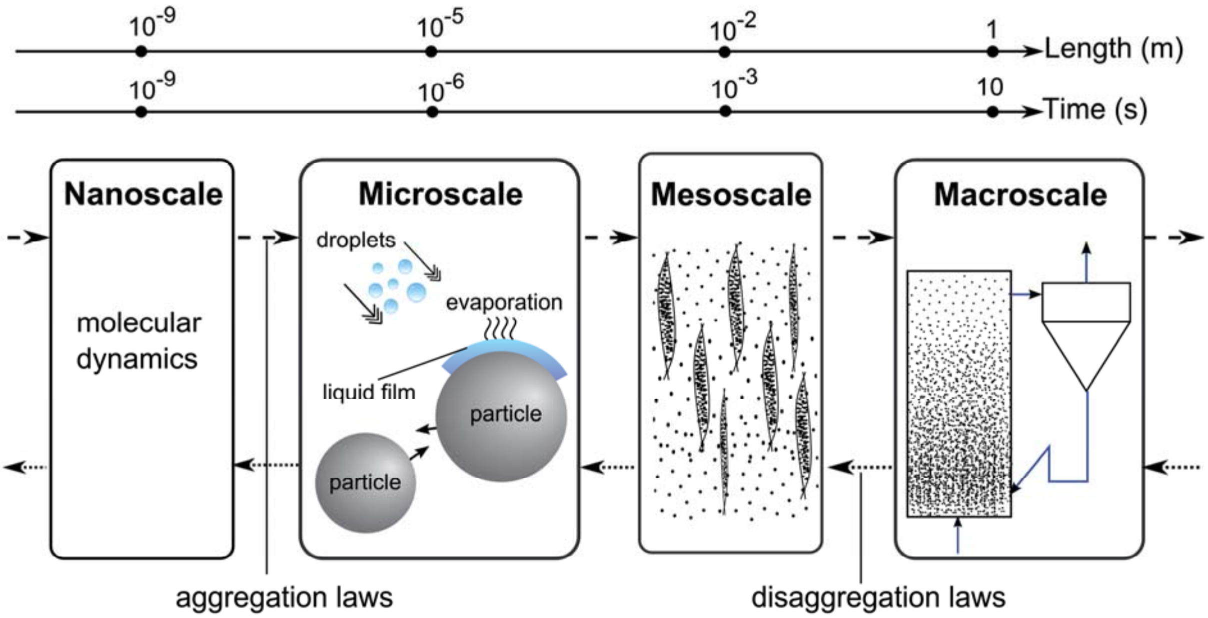

Figure 5.2: Multiscale model of a circulating fluidized bed

The specific material properties can be effectively considered on the microscale process description, where the usage of the discrete element method (DEM) is a state of the art (Zhu et al., 2008). By the DEM each particle is considered as a separate entity, for which Newton's equations of motions are solved in each simulation time step (Cundall and Strack, 1979).

Coupling of a DEM with a computational fluid dynamic (CFD) system using an Euler-Lagrange coupling approach allows to predict particle motions under the influence of the fluid field. In Figure 5.3 a general coupling scheme between CFD and DEM is shown. The DEM takes into account each particle as separate entity, detects impacts and collisions between particles, calculates contact forces between particles, between particles and walls and afterwards updates particle positions by solving Newton's second law. Simultaneously for the CFD calculation of the fluid phase, the apparatus is discretized into volume cells, for which the gas flow field is described by the Navier-Stokes equation of motion. The particles are considered in the CFD system as cells porosities. The gas velocity profile and pressure gradients in each cell, which are received from CFD simulations, are then used within the DEM code for the calculation of the drag force which acts on every particle.

Dieses Werk ist copyrightgeschützt und darf in keiner Form vervielfältigt werden noch an Dritte weitergegeben werden.
Es gilt nur für den persönlichen Gebrauch.

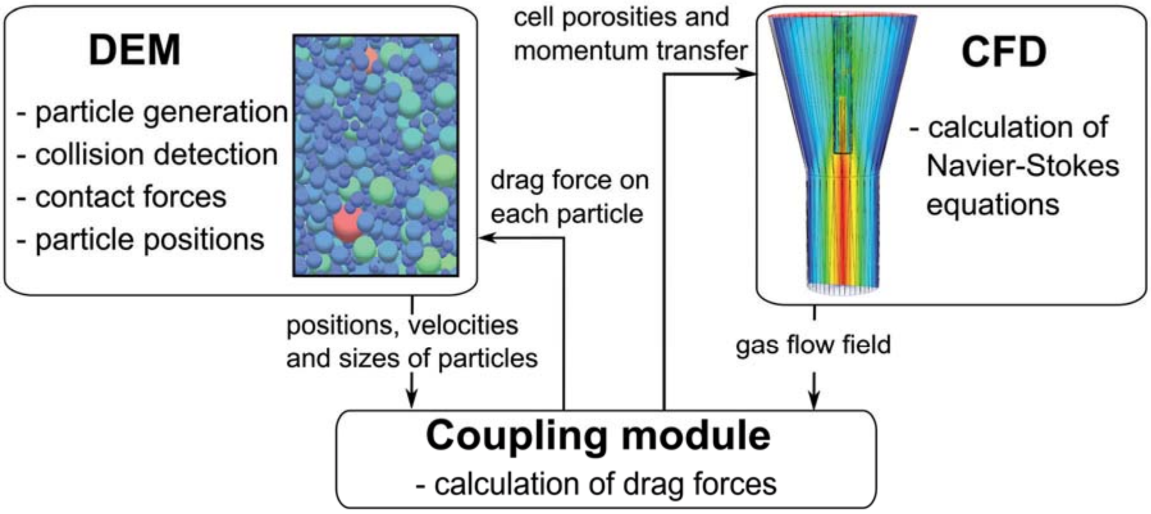
DEM
- particle generation
- collision detection
- contact forces
- particle positions
cell porosities and momentum transfer
drag force on each particle
CFD
- calculation of Navier-Stokes equations
positions, velocities and sizes of particles
gas flow field
Coupling module
- calculation of drag forces

Figure 5.3: Coupling scheme between DEM and CFD systems

The main limitation factor of the application of the DEM method is a huge computational effort. To perform adequate simulations the number of modeled particles should be very large and for some cases it easily exceeds several millions of particles. That is why, even the usage of the high performance graphical processor units (GPU) does not allow calculation of a whole production process on the microscale.

In this contribution a novel multiscale simulation environment for the modeling of fluidized bed growth and aggregation processes has been developed. The developed environment architecture allows to obtain specific material parameters from the microscale and afterwards to use them in the PBM on the macroscale.

The multiscale models of the FB consist of several submodels which are distributed between three different scales. The sketch view of the interscale coupling network is depicted in Figure 5.4. The arrows in the scheme represent the directions of the communications and the set of main transferred parameters.

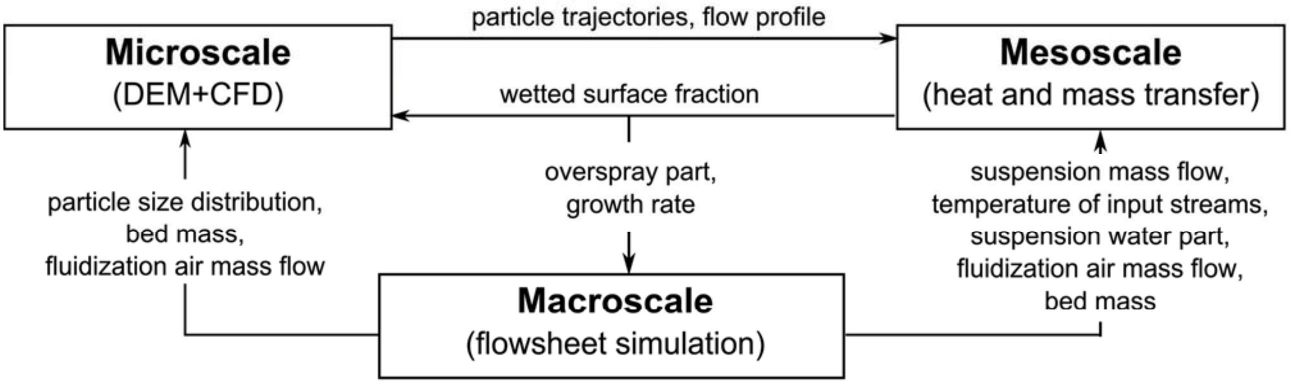
particle trajectories, flow profile
Microscale
(DEM+CFD)
Mesoscale
(heat and mass transfer)
wetted surface fraction
overspray part, growth rate
particle size distribution, bed mass, fluidization air mass flow
suspension mass flow, temperature of input streams, suspension water part, fluidization air mass flow, bed mass
Macroscale
(flowsheet simulation)

Figure 5.4: General scheme of interscale coupling

Dieses Werk ist copyrightgeschützt und darf in keiner Form vervielfältigt werden noch an Dritte weitergegeben werden.
Es gilt nur für den persönlichen Gebrauch.

On the microscale the process is modeled on a relatively short time interval in order of several seconds. Here, the simultaneous co-simulation of the gas and the solid phases are performed with help of the Discrete Element Method (DEM) coupled with a CFD package (Figure 5.3). Due to the high computational effort, the dimensions of the apparatus are scaled down and the original number of particles is drastically decreased. The modeling on this scale allows to predict the dynamics of the particles in the apparatus and to consider the influence of material properties such as restitution coefficient, modulus of elasticity, stiffness, etc. As results from the microscale the following characteristics are obtained and saved for the further usage on the upper scales:

- particle trajectories;
- fluid profile;
- frequency and velocity of interparticle collisions;
- frequency and velocity of collisions between particles and apparatus walls;
- coalescence characteristics (impact velocity, contact duration, sticking probability (Dosta et al., 2011), etc.);
- particles residence time in specified zones.

The submodel on the mesoscale serves as an intermediate entity between micro and macroscales. It is used to predict the following parameters:

- heat transfer between particles, gas and liquid film;
- wetted surface fraction of granules;
- liquid evaporation from particle surface;
- gas temperature and humidity;
- size-dependent growth rate (Dosta et al., 2012);
- wetting of particles through one or several nozzles (Fries et al., 2011).

A more detailed description of the microscale and mesoscale models is given in the next chapters.

The macroscale modeling is performed in SolidSim-Dynamics and is based on the population balance model (Eq. (4.3)). On this scale the global process structure is simulated on the long-time interval in the order of hours.

In order to implement the interscale communications and to avoid discrepancies between different submodels an advanced calculation algorithm has been developed. In Figure 5.5 the general flowchart of this algorithm is shown.

Dieses Werk ist copyrightgeschützt und darf in keiner Form vervielfältigt werden noch an Dritte weitergegeben werden.
Es gilt nur für den persönlichen Gebrauch.

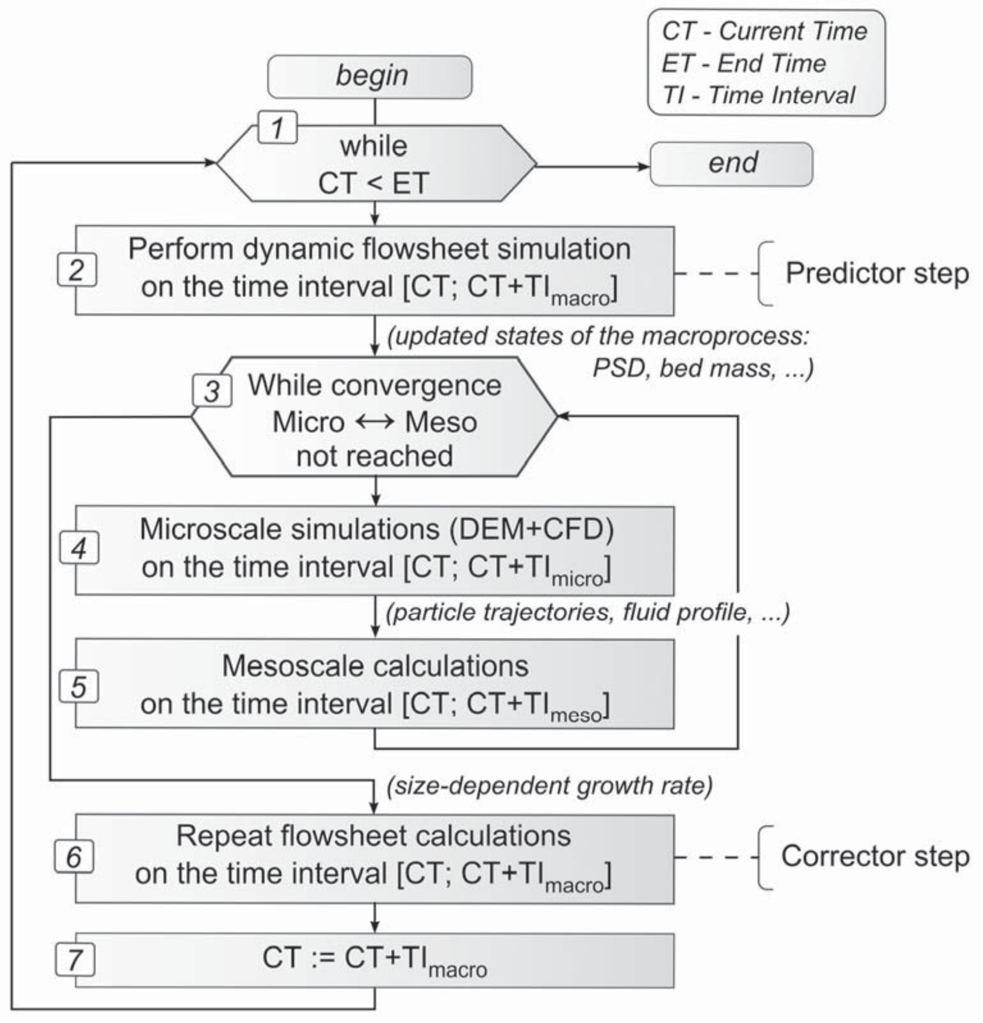
CT - Current Time
ET - End Time
TI - Time Interval
begin
1
while CT < ET
end
2
Perform dynamic flowsheet simulation on the time interval [CT; CT+TI$_{macro}$]
Predictor step
(updated states of the macroprocess: PSD, bed mass, ...)
3
While convergence Micro ↔ Meso not reached
4
Microscale simulations (DEM+CFD) on the time interval [CT; CT+TI$_{micro}$]
(particle trajectories, fluid profile, ...)
5
Mesoscale calculations on the time interval [CT; CT+TI$_{meso}$]
(size-dependent growth rate)
6
Repeat flowsheet calculations on the time interval [CT; CT+TI$_{macro}$]
Corrector step
7
CT := CT+TI$_{macro}$

Figure 5.5: Flow-chart of the multiscale calculation algorithm

The global (macroscopic) simulation time is divided into a set of smaller time intervals (TI_{macro}). Afterwards the algorithm starts on the macroscale, where the time progression of the PSD in the apparatus and transient behavior of other macroscopic parameters are approximated (*Block 2*). According to the results received in the *Block 2* (bed mass, PSD, inlet and outlet mass streams, etc.) the microscale model is generated and calculations are performed on the time interval TI_{micro} (*Block 4*). The magnitude of the TI_{micro} in most cases satisfies the following inequality:

$$\frac{TI_{macro}}{TI_{micro}} \gg 1 \tag{5.1}$$

As result, the particle trajectories, the fluid profile in the apparatus and other significant parameters related to particle and gas dynamics are obtained from the microscale. In the next step this data is transferred into the mesoscale model, where the thermodynamics in the apparatus are calculated (*Block 5*). The simulations in the *Block 5* are performed for the time

Dieses Werk ist copyrightgeschützt und darf in keiner Form vervielfältigt werden noch an Dritte weitergegeben werden.
Es gilt nur für den persönlichen Gebrauch.

interval in order of minutes (TI_{meso}). However, the granules and the gas characteristics were previously obtained (*Block 4*) for a much shorter time interval. Therefore, it is assumed that particles cyclically repeat their trajectories on the time interval TI_{meso}.

The new values of the process parameters, which are obtained after the processing on the mesoscale, have a decisive influence on the behavior of a microscale model. One of such parameters is a wetted surface fraction (φ), which describes the amount of the liquid on the particle surfaces as expressed in Eq. (4.17). Larger values of a wetted surface fraction cause a higher amount of energy which dissipates during interparticle contact and, as a consequence, they have a significant effect on the particle dynamics (Antonyuk et al., 2009). Therefore, to avoid inequality between the values on the different scales, the calculations in the *Block 4* and the *Block 5* should be iteratively repeated until the interscale convergence is reached (*Block 3*). The convergence analysis is based on the Eq. (3.8), where a set of transferred parameters is used as a vector of state variables y_i.

In the final stage, the correction procedure is started and the calculations of the macroscale model are repeated (*Block 6*) for the same time interval as in the *Block 2* $[CT; CT+TI_{macro}]$. For the simulations in the corrector step, more predicted process parameters, such as size-dependent particle growth (Dosta et al., 2012) or coalescence kernel (Dosta et al., 2011), are used.

From the programming point of view, the developed multiscale environment consists of several commercial and freeware packages. In Figure 5.6 the general architecture is illustrated.

Dieses Werk ist copyrightgeschützt und darf in keiner Form vervielfältigt werden noch an Dritte weitergegeben werden.
Es gilt nur für den persönlichen Gebrauch.

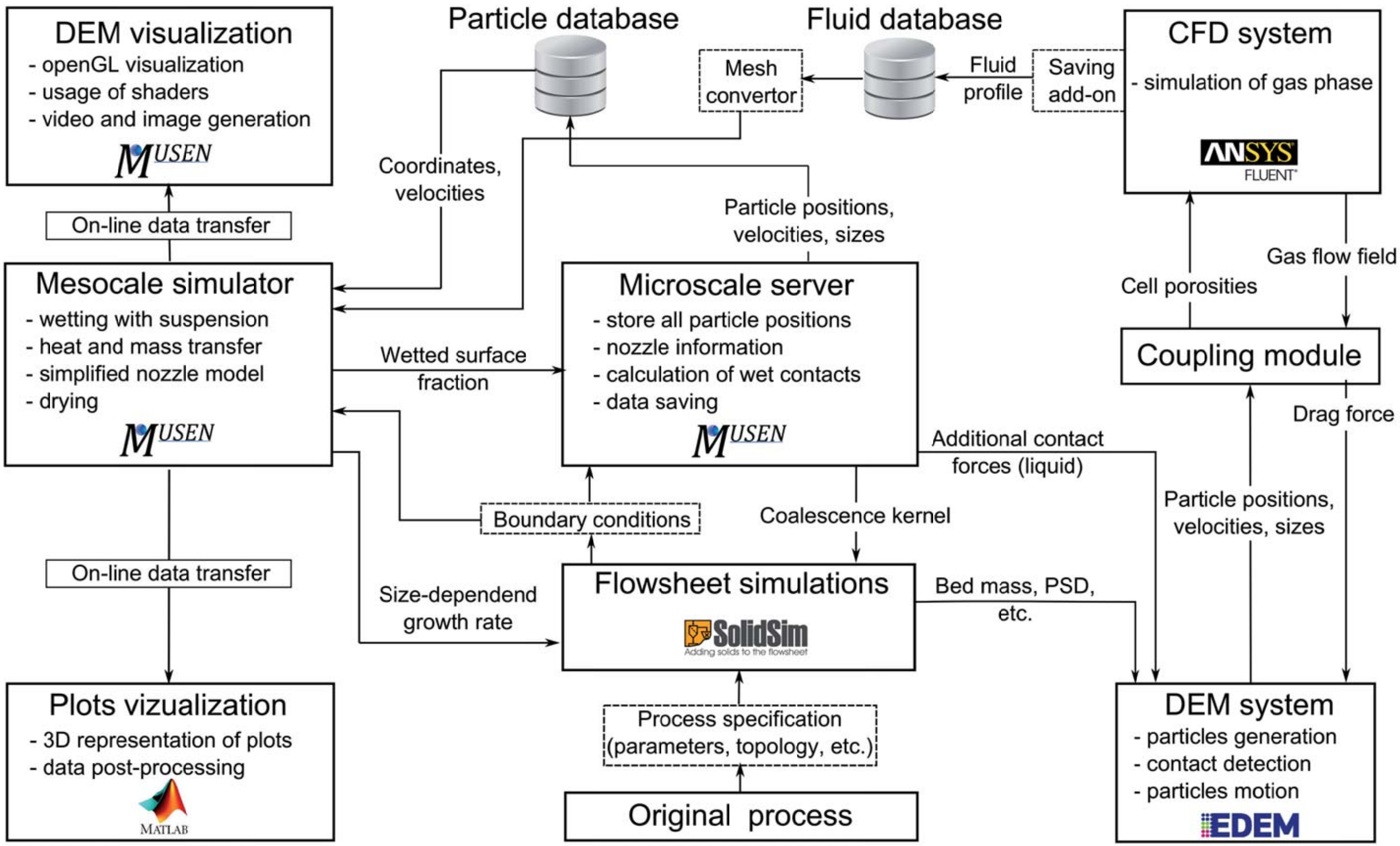

Figure 5.6: Programming architecture of the multiscale simulation environment

Dieses Werk ist copyrightgeschützt und darf in keiner Form vervielfältigt werden noch an Dritte weitergegeben werden.
Es gilt nur für den persönlichen Gebrauch.

The macroscale modeling is performed in the flowsheet simulation system of solids processes SolidSim-Dynamics. In this program the user specifies the process structure and through a set of Windows-based dialogs defines the main process parameters.

For the microscale calculations two commercial programs: EDEM (DEM Solutions) and Fluent (ANSYS Inc.) are used. In order to implement multiscale methodology these programs have been extended with additional components. Firstly, the saving add-on has been included into Fluent. This add-on is written in C++ programming language and it is used to save gas profiles into the database on the hard drive. Secondly, the EDEM has been extended with a supplementary communication package, which is used to realize bidirectional on-line data transfer with a microscale server of the MUlitscale Simulation Environment named MUSEN (Dosta et al., 2012). The microscale server is a stand-alone Windows application which is developed to:

- receive information (position, velocity, etc.) about particles;
- predict viscous and capillary forces which are caused by the existence of the liquid film on the particle surface;
- save particle trajectories into the external database;
- implicitly or explicitly define different zones with various wetted surface fraction;
- specify specific process parameters through a graphical user interface.

The mesoscale simulator shown in Figure 5.6 is a part of MUSEN package and it is applied to predict the heat and mass transfer, which occurs in the fluidized bed and to calculate a particle wetting through one or several nozzles. On this scale the equations of energy and mass balances are solved for each particle separately. Therefore, the required information about particles and fluid is loaded in advance from the databases. Afterwards the received simulation results are transmitted into the flowsheet simulation system SolidSim-Dynamics and into the microscale server.

The representation of the mesoscale and the microscale results are performed in the specially developed high-quality hardware accelerated visualization subsystem. This novel software is a subpart of the MUSEN environment and it is based on the rendering method that takes advantage of modern graphics hardware to perform interactive representation of large particle assemblages. The exemplary scenes which were obtained with a novel tool are shown in Figure 4.3, Figure 5.10 and Figure 6.16.

One of the main advantages of the developed multiscale approach is a detachment of a process description into three different scales and processing of the models on separate time intervals with further data extrapolation, which sufficiently minimizes the volume of necessary

Dieses Werk ist copyrightgeschützt und darf in keiner Form vervielfältigt werden noch an Dritte weitergegeben werden.
Es gilt nur für den persönlichen Gebrauch.

computations. The models illustrated in Figure 5.4 are expressed in terms of systems of ODE's, PDE's or DAE's. Due to the different nature of the described processes, these equations have sufficient difference of the rate of change of process variables with respect to time. The typical simulation step which is used in the discrete element method for the simulation of a fluidized bed granulator with 1 mm particles is on the order of µs. At the same time the internal solver step on the order of seconds or even minutes is used for the processing on the macroscale.

To perform the simulation of the FB growth process with high detailing grade, the population balance model presented above in Eq. (4.11), was expanded into the multiscale model by the inclusion of the process description on the lower scales. This model has been implemented and added into the SolidSim-Dynamics library of dynamic units (as *FBGranulatorMult*).

The multiscale simulation of the pure aggregation process has also been implemented. For this purpose the model *FBAgglmeratorMult* was added into SolidSim-Dynamics.

5.2 Modeling on the microscale

The Discrete Element Method (DEM) (Cundall and Strack, 1979) is used as basis for the microscale simulation. With help of it, the physic-chemical material properties and details of the geometry of the apparatus are included into the model.

In each simulation time step of the DEM the new coordinates and the rotational motion are predicted by solving of the Newtonian equation. In Eq. (5.2) the general form of this equation is shown:

$$m\frac{d^2x}{dt^2} = F_D + F_G + \sum_{i=1}^{N_{cp}} F_{cp,i} + \sum_{i}^{N_{CW}} F_{cw,i} - V_i \nabla P_G. \tag{5.2}$$

Here F_D and F_G are the drag and the gravity forces accordingly, $F_{cp,i}$ and $F_{cw,i}$ are forces induced by the contacts with other particles and apparatus walls, P_G is a gas phase pressure, N_{cp} and N_{CW} are the number of contacts between particles and between particles and walls accordingly.

To describe the dynamics of interparticle interactions the hard and soft sphere methods can be used. In the case of the hard sphere model the deformation is not explicitly incorporated into the model equations. Moreover, it is assumed that all collisions are binary and that they occur instantaneously. This type of the model cannot be effectively used for simulation of a system with high particle concentration (fluidized bed) or with low value of restitution coefficient.

Dieses Werk ist copyrightgeschützt und darf in keiner Form vervielfältigt werden noch an Dritte weitergegeben werden.
Es gilt nur für den persönlichen Gebrauch.

In a fluidized bed process as well as in many other processes including gas-solid contacts, the gas flow plays an important role. Therefore, to consider the influence of the flow on the process, the DEM is coupled with a Computational Fluid Dynamics (CFD) model. For the CFD calculation of the fluid phase the entire process volume is discretized to the mesh cells, where the gas flow field is described using the volume-averaged Navier-Stokes equation of motion. The motion of the particles in the apparatus is estimated using a coupled solution of the CFD and DEM systems. The general coupling scheme is shown in Figure 5.3.

In the case of a soft-sphere approach it is assumed that any two particles are in contact when there is a physical overlap between them. There exist different mathematical models to describe the forces and moments which act in the interparticle contact. Most of the widely used models, which has a good agreement with experimentally data, are the Hertz-Mindlin contact models. The normal component of force is described by the Hertz model which is supplemented with a damping term according to Tsuji et al. (1992). The tangential component described by the model which was proposed by Mindlin and Deresiewicz (1953). However, the Hertz-Mindlin model was developed to describe the contacts between dry surfaces and cannot be effectively applied for the simulation of a process in which the liquid phase plays an important role. Thus, a set of supplementary forces should be included in order to perform simulation of a fluidized bed granulation process. These forces should consider viscous and capillary forces due to the existence of the liquid film on the particle surfaces.

One possible way to consider the liquid phase is to increase the amount of the energy which is dissipated during the collision. This can be realized by variation of the restitution coefficient with the further parameter fitting to the experimental data (Antonyuk et al., 2009). This coefficient describes the amount of the energy which dissipates during the contact. It is defined as a square root of the ratio between kinetic energy after impact to the kinetic energy before impact. However, only a fitting of the restitution coefficient without the improvement of the contact models does not allow to obtain an adequate prediction of the real contact forces and the particle dynamics after injection of the liquid into the granulator. The main difference between “dry” and “wet” contacts is caused by the fact that the capillary F_{cap} and the viscous F_{vis} forces act on the particles before and after the physical overlap of the solid phases. Therefore, the interaction distance, where the contact detection and the force calculation take place, was increased according to the thickness of the liquid film and to the maximal length of liquid bridge.

In Figure 5.7 the forces in the different collisions modes induced by the liquid film are illustrated.

Dieses Werk ist copyrightgeschützt und darf in keiner Form vervielfältigt werden noch an Dritte weitergegeben werden.
Es gilt nur für den persönlichen Gebrauch.

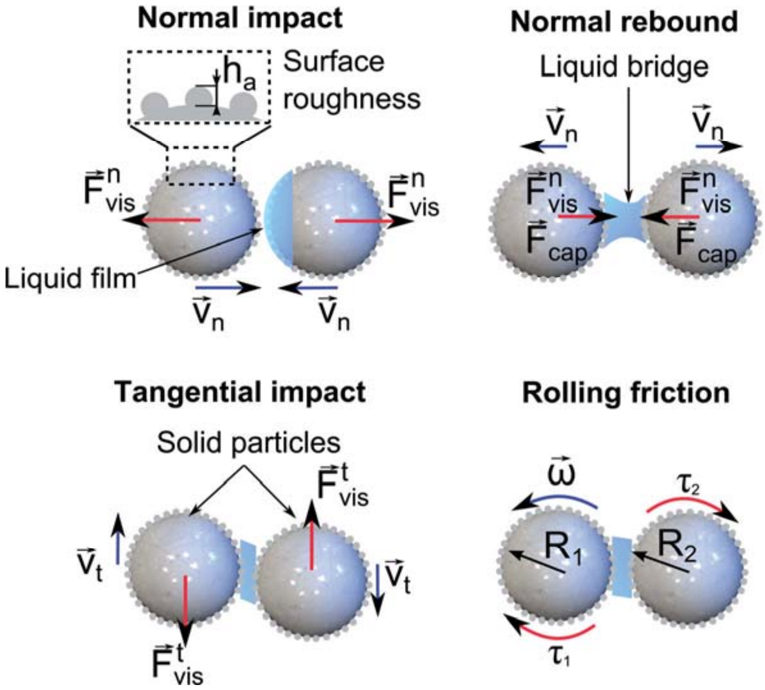

Figure 5.7: Different types of impact of wetted particles

For the simulation of wetted particles the following assumptions were made:

- no penetration of liquid into the particle pores;
- all particles are covered with the liquid film which has constant thickness L_f;
- a smooth particle surface;
- ideally spherical particles.

The normal and the tangential components of the viscous force were calculated using Eq. (5.3) and Eq. (5.4) respectively (Adams and Edmondson, 1987), (Popov, 2010).

$$F^n_{vis} = \frac{6 \cdot \pi \cdot \eta \cdot \bar{R}^2 \cdot v_{n,rel}}{L}, \tag{5.3}$$

$$F^t_{vis} = 2 \cdot \pi \cdot \eta \cdot \bar{R} \cdot v_{t,rel} \cdot \ln\left(1 + \frac{\bar{R}}{2L}\right), \tag{5.4}$$

$$\bar{R} = R_1 \cdot R_2 / (R_1 + R_2), \tag{5.5}$$

where R_1 and R_2 are the radii of the contact partners; $v_{n,rel}$ and $v_{t,rel}$ describe the normal and tangential components of relative impact velocity; η is the liquid viscosity. The distance between particle surfaces L was limited by a minimum value of $L = 2 \cdot h_a$, where h_a is the particle roughness.

Dieses Werk ist copyrightgeschützt und darf in keiner Form vervielfältigt werden noch an Dritte weitergegeben werden.
Es gilt nur für den persönlichen Gebrauch.

The capillary force F_{cap} is approximated according to the model of Pitois et al. (2000). This force depends on the surface tension σ, the volume of the liquid bridge V and the solid/liquid contact angle θ and it is calculated by the Eq. (5.6).

$$F_{cap} = 2 \cdot \pi \cdot \bar{R} \cdot \sigma \cdot cos\theta \cdot \left(1 - \left(1 + \frac{2 \cdot V}{\pi \cdot \bar{R} \cdot L^2}\right)^{-0.5}\right) \tag{5.6}$$

During the fluidized bed granulation process the granule surfaces are just partially covered with a liquid film. Therefore, "dry" and “wet” collisions simultaneously occur in the apparatus. To describe the different collision types the probabilities of various events are calculated. According to these probabilities, each new collision is randomly arranged to one of the collision types as it is shown in Figure 5.8. Three categories of contacts are distinguished: between totally dry, between totally wet and between dry and wet surfaces.

If ϕ is a current value of wetted surface fraction (Eq. (4.17)), then the probability that two particles impact as totally dry granules is equal to $(1 - \phi)^2$, and the probability that contact between dry and wet surfaces will occurs is equal to $2 \cdot \phi \cdot (1 - \phi)$. The probability of a totally wet contact is approximated as ϕ^2.

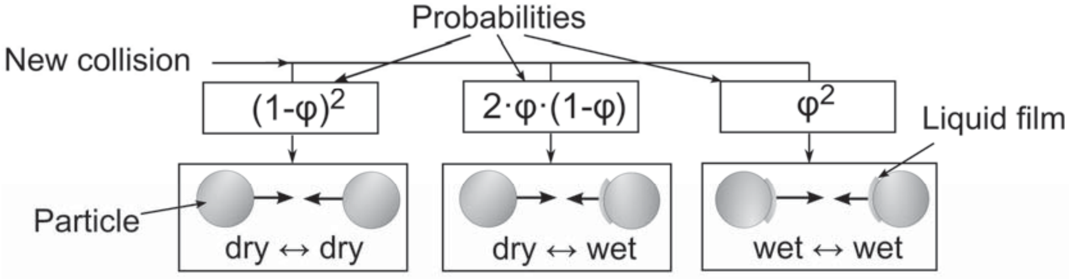

Figure 5.8: Probabilities of different collision types

The wet collision is considered to be finished when the rupture of the liquid bridge occurs. It happens when the distance between granules is larger than a critical bridge length. If L_{f1} and L_{f2} are the thicknesses of the liquid layers on the contact partners, then the critical bridge length is calculated according to $L_{crit} = 2(L_{f1} + L_{f2})$. Each further contact between the same particles is arranged again, according to the scheme shown in Figure 5.8.

The equations of capillary and viscous forces Eq. (5.3) – Eq. (5.6) are solved on the microscale server of MUSEN. Here, the values of wetted surface fraction can be specified for different apparatus zones. This can be done explicitly through a graphical user interface or implicitly through a data exchange with the mesoscale simulator.

Dieses Werk ist copyrightgeschützt und darf in keiner Form vervielfältigt werden noch an Dritte weitergegeben werden.
Es gilt nur für den persönlichen Gebrauch.

5.3 Modeling on the mesoscale

With help of the mesoscale submodel the calculations related to the particle wetting by a liquid solution, and the particle drying due to the liquid evaporation from the surface are performed. The mesoscale simulations are executed at the same length scale as the microscale, i.e. for the same apparatus geometry. However, due to the relatively slow mass transfer, a much larger time scale (in order of minutes) was employed.

As the input data into the mesoscale model, the particle trajectories as well as the gas profile, which are obtained from the DEM+CFD simulations, are used. The representative particle motion interval is chosen on the microscale and for the further mesoscale calculations it is assumed that the particles repeat their trajectories. Following this approach, the time-consuming microscale processing can be avoided for the relative larger time interval.

Coating of particles with a liquid film plays a central role during spray granulation. To simulate this process a new model of the nozzle has been developed and implemented (Dosta et al., 2010). The spraying zone of every nozzle in the apparatus is represented as a cone-shaped region, which is discretized through the height as it is illustrated in Figure 5.9. The amount of liquid which is deposited on each hold-up particle depends on:

- suspension mass stream $\dot{M}_{susp}$;
- water content in suspension X_w;
- porosity in the upper layers of a cone zone;
- the particle cross-cut surface A_{cs};
- the surface of the current layer A_{lev};
- distance between nozzle and particle.

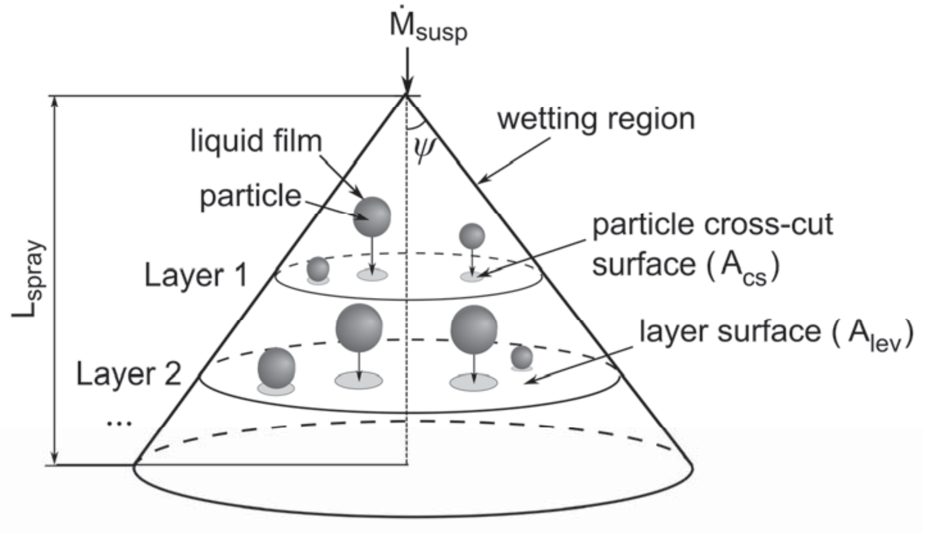

Figure 5.9: Schematic representation of the nozzle zone model

Dieses Werk ist copyrightgeschützt und darf in keiner Form vervielfältigt werden noch an Dritte weitergegeben werden.
Es gilt nur für den persönlichen Gebrauch.

The region where the wetting occurs is described with a conical geometry of the spraying zone. This spraying cone is determined by a length L_{spray}, an angle ψ and a direction (upwards or downward) as it is shown in Figure 5.9.

When a particle with index i is located within the region of the layer j, then the suspension mass stream onto this particle ($\dot{M}_{susp,i}$) is approximated according to:

$$\dot{M}_{susp,i} = \dot{M}_{susp}^{j} \cdot \frac{A_{cs,i}}{A_{lev,j}}, \tag{5.7}$$

where $A_{lev,j}$ is the cross-cut surface of the layer j; $A_{cs,i}$ is a particle cross-cut surface area; $\dot{M}_{susp}^{j}$ is the suspension stream in the layer j. The value of $\dot{M}_{susp}^{j}$ is calculated for each layer as expressed in the Eq. (5.8).

$$\dot{M}_{susp}^{j} = \dot{M}_{susp}^{j-1} \cdot \left(1 - \frac{\sum_{i=1}^{N_{p,j}} A_{cs,i}}{A_{lev,j}}\right), \tag{5.8}$$

where $N_{p,j}$ is the number of particles which are located in the layer with index j.

In order to calculate the wetting process, it is assumed that all particles are covered by a liquid film with constant thickness L_f, which does not depend on the process parameters. Hence, the maximal mass of the liquid film M_f^{max} which can cover the particle with radius R is determined as:

$$M_f^{max} = 4\pi \cdot (R + L_f)^2 \cdot L_f \cdot \rho_{susp}, \tag{5.9}$$

where ρ_{susp} is the suspension density.

The part of the suspension mass stream which does not collide with any of the particles is nevertheless considered in the energy and mass balance. It is assumed that the total drying of these droplets occurs that results in the increase of the gas humidity. Afterwards, these droplets leave the apparatus as overspray.

In Figure 5.10 an application example of the nozzle model is shown. Here, it is assumed that all particles do not change their positions. The particles in Figure 5.10 are colored according to the mass of deposited liquid. From analysis of the received results, the conclusion can be drawn that the granules which are placed closer to a nozzle have a larger mass of the liquid film.

Dieses Werk ist copyrightgeschützt und darf in keiner Form vervielfältigt werden noch an Dritte weitergegeben werden.
Es gilt nur für den persönlichen Gebrauch.

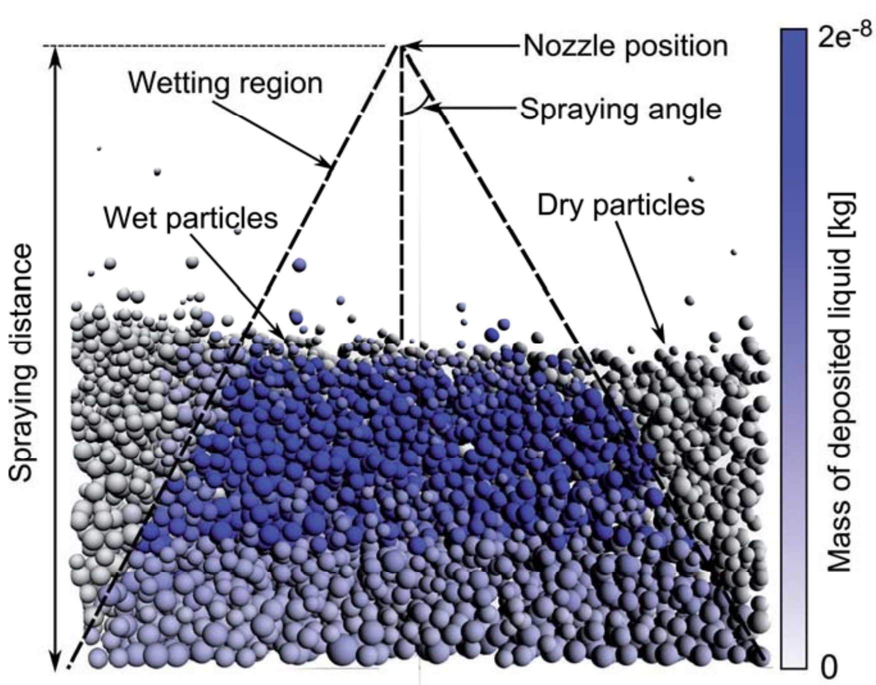

Figure 5.10: Example of application of the nozzle model

Additionally to the wetting, the evaporation process is calculated on the mesoscale. For this purpose the system of the differential equations for the description of air temperature ϑ_a, mass of the liquid film M_f, temperature of the liquid film ϑ_f, particle temperature ϑ_p and air humidity Y_a has been formulated. The formulated equations are based on the mass and energy balances, whereby the following enthalpy ($\dot{H}$) and heat ($\dot{Q}$) streams are considered:

- between particle and liquid film ($\dot{Q}_{pf}$);
- enthalpy streams of suspension ($\dot{H}_{susp}$) and vapor ($\dot{H}_{vap}$);
- between air and liquid film ($\dot{Q}_{af}$);
- between air and particle ($\dot{Q}_{ap}$).

The change of the liquid film temperature and mass of the liquid film are calculated by ordinary differential equations Eq. (5.10) and Eq. (5.11) respectively. The developed model considers that particles can be simultaneously located in the wetting regions of one or several nozzles. Therefore, the accumulated mass stream from all nozzles is used in the Eq. (5.11), where N_{noz} is the total number of active nozzles. Moreover, it is assumed that there is no penetration of liquid into the particle micropores.

$$\frac{d\vartheta_f}{dt} = \frac{\dot{Q}_{pf} + \dot{Q}_{af} + \dot{H}_{susp} - \dot{H}_{vap}}{M_f \cdot c_{p,f}} - \frac{\vartheta_f}{M_f}\frac{dM_f}{dt}, \tag{5.10}$$

Dieses Werk ist copyrightgeschützt und darf in keiner Form vervielfältigt werden noch an Dritte weitergegeben werden.
Es gilt nur für den persönlichen Gebrauch.

$$\frac{dM_f}{dt} = \sum_{i=1}^{N_{noz}} \dot{M}_{susp,i} - \dot{M}_{vap} \tag{5.11}$$

For the calculation of heat transfer between air and liquid film ($\dot{Q}_{af}$) and between particle and liquid film ($\dot{Q}_{pf}$) Eq. (5.12) and Eq. (5.13) are used accordingly. The heat transfer coefficients α_{af} and α_{pf} are obtained for each separate particle with the help of a model of Gnielinski (1980). The Reynolds number, which is needed for the approximation of transfer coefficients, depends on the relative velocity between particle and fluid and is obtained using the results received from the microscale.

$$\frac{d\dot{Q}_{af}}{dt} = \alpha_{af} \cdot A_f \cdot (\vartheta_a - \vartheta_f) \tag{5.12}$$

$$\frac{d\dot{Q}_{pf}}{dt} = \alpha_{pf} \cdot A_f \cdot (\vartheta_p - \vartheta_f) \tag{5.13}$$

The time-progression of the particle temperature is given by:

$$\frac{d\vartheta_p}{dt} = \frac{\dot{Q}_{ap} - \dot{Q}_{pf}}{M_p \cdot c_{p,p}}, \tag{5.14}$$

where the heat transfer between air and particle is expressed as:

$$\dot{Q}_{ap} = \alpha_{ap} \cdot (A_p - A_f) \cdot (\vartheta_a - \vartheta_p) \tag{5.15}$$

In the case when the particle is totally covered by the liquid film the heat transfer between air and particle is equal to zero.

The vapor mass flow from the particle surface ($\dot{M}_{vap}$) depends on the mass transfer coefficient β, surface of the liquid film A_f, air humidity Y_a and saturation humidity Y_{sat}. The value of $\dot{M}_{vap}$ is approximated with Eq. (5.16).

$$\dot{M}_{vap} = \beta \cdot A_f \cdot (Y_{sat} - Y_a) \tag{5.16}$$

As a main result from the mesoscale simulation, the growth rate $G_{e,i}^{meso}$, which is specific for each separate particle, is obtained with help of Eq. (5.17).

$$G_{e,i}^{meso} = \frac{(1 - K_w) \cdot \dot{M}_{vap,i}}{2 \cdot \rho_{susp} \cdot \pi \cdot R_{p,i}^2 \cdot K_w}, \tag{5.17}$$

where K_w is the water mass content in the suspension and $R_{p,i}$ is the radius of the particle with index i. Finally the growth rates specific for the each granule are averaged for each class of the

Dieses Werk ist copyrightgeschützt und darf in keiner Form vervielfältigt werden noch an Dritte weitergegeben werden.
Es gilt nur für den persönlichen Gebrauch.

PSD. Afterwards these data are transferred into the flowsheet simulation system SolidSim-Dynamics.

The gas profile received from the microscale calculations is used to determine the relative velocities between particle and fluid and to calculate the gas properties such as temperature (ϑ_a) and humidity (Y_a). For the CFD calculations on the microscale and for the mesoscale simulations the apparatus is discretized into different types of discrete cells (mesh), as it is schematically shown in Figure 5.11.

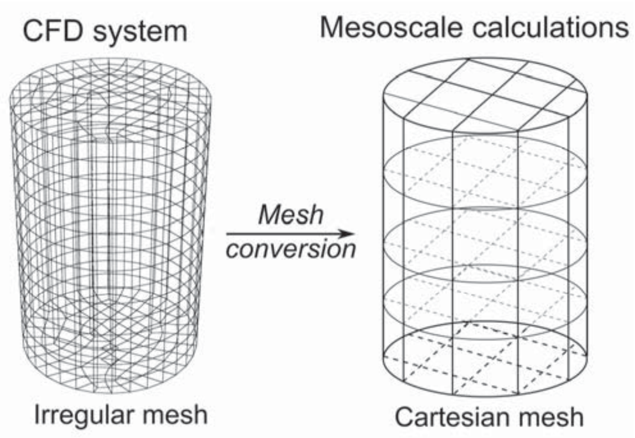

Figure 5.11: Example of a mesh conversion

The CFD calculations are performed on the irregular grid. Therefore, the data which are received from the CFD system are converted into the Cartesian grid type, which is used on the mesoscale. For this purpose the convertor tool is used (Figure 5.6).

Dieses Werk ist copyrightgeschützt und darf in keiner Form vervielfältigt werden noch an Dritte weitergegeben werden.
Es gilt nur für den persönlichen Gebrauch.

6. Applications of a novel system for fluidized bed granulation

6.1 Validation of a novel simulation system

To verify the correctness of the developed modeling environment various test simulations have been performed. The continuous fluidized bed granulation process according to Radichkov et al. (2006) was used, as one of the simulation benchmarks. The flowsheet of this process is shown in Figure 6.1. The illustrated scheme consists of a FB granulator, a stack of two screens and a mill.

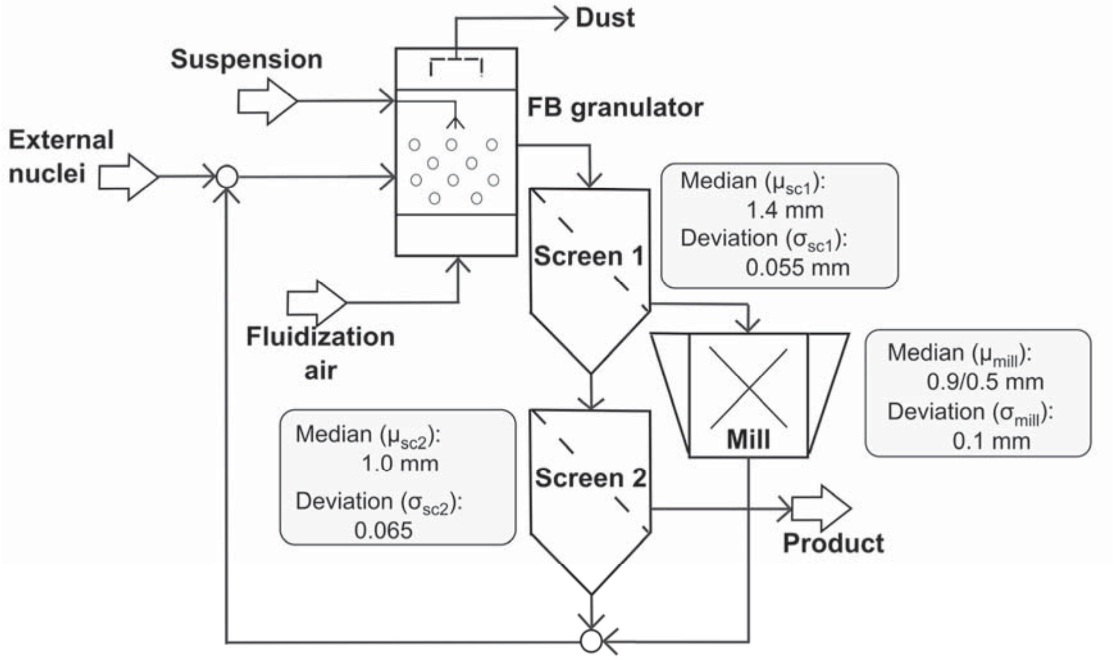
Dust
Suspension
FB granulator
External nuclei
Median (μ_{sc1}): 1.4 mm
Deviation (σ_{sc1}): 0.055 mm
Screen 1
Fluidization air
Median (μ_{mill}): 0.9/0.5 mm
Deviation (σ_{mill}): 0.1 mm
Mill
Median (μ_{sc2}): 1.0 mm
Deviation (σ_{sc2}): 0.065
Screen 2
Product

Figure 6.1: Flowsheet of the granulation process

Inside the granulator the suspension is sprayed onto the bed material and due to the drying of suspension on the particle surface continuous granule growth occurs. Considering the ideal solid mixing in the apparatus, all particles will discharge from the FB with the same probability. The output particulate flow, which is continually leaving the apparatus, enters the stack of two screens. The oversize of the first screen is milled and mixed with the undersize of the second screen and with the external nuclei stream. Finally, the accumulated material stream is recycled back into the fluidized bed apparatus. As a product of the process the middle fraction of screens is taken.

Dieses Werk ist copyrightgeschützt und darf in keiner Form vervielfältigt werden noch an Dritte weitergegeben werden.
Es gilt nur für den persönlichen Gebrauch.

For the modeling of the fluidized bed apparatus the *FBGranulatorPBM* unit from the SolidSim-Dynamics library has been used. The dynamic change of the PSD in this apparatus is predicted with a one-dimensional population balance model – Eq. (4.11). It was assumed that there is no attrition ($R_{attr} = 0$) and the overspray part of the suspension K_{os} is equal to 0. Thus, the particle growth rate has been approximated with Eq. (4.12), where the effective mass stream is obtained as:

$$\dot{M}_e(t) = \dot{M}_{susp}(t) \cdot (1 - K_w) \tag{6.1}$$

The particle size distribution of the particulate flow leaving the mill and the separation function of the screen unit were defined with a normal distribution (Eq. (3.7)). The exact parameters of the mill and screen units are shown in Figure 6.1. The initial PSD of the bed material in the granulator and the PSD of the external nuclei stream were determined by a Gaussian normal function (Eq. (3.7)). The values of the median μ and the deviation σ of the hold-up material in the apparatus and external nuclei stream are $\mu_b = 1\text{mm}$, $\sigma_b = 0.1\text{ mm}$ and $\mu_{ext} = 1\text{ mm}$, $\sigma_{ext} = 0.15\text{ mm}$ accordingly.

Due to the presence of the recycled solid stream, the process which is illustrated in Figure 6.2 can exhibit complex and in some cases even unsteady behavior (Heinrich et al., 2002). On the one hand, this leads to the undesired permanent fluctuations in the product quality. On the other hand, such oscillations can be effectively used to receive different products with varied distributions (Schütte et al., 1998).

One of the key parameters which has a decisive influence on the transient process behavior is the milling diameter. In the case of fine milling the production can have an unstable regime in form of constant self-sustained oscillations of the particle size distribution.

In Figure 6.2 and Figure 6.3 the comparison of new and previously received (Radichkov et al., 2006) simulation results for the coarse ($\mu_{mill} = 0.9\text{mm}$) and for the fine milling ($\mu_{mill} = 0.5\text{ mm}$) are shown accordingly. In these plots the time progression of Sauter diameter (d_{32}) of the bed material in the granulator are illustrated. The value of d_{32} has been approximated with Eq. (4.25).

Dieses Werk ist copyrightgeschützt und darf in keiner Form vervielfältigt werden noch an Dritte weitergegeben werden.
Es gilt nur für den persönlichen Gebrauch.

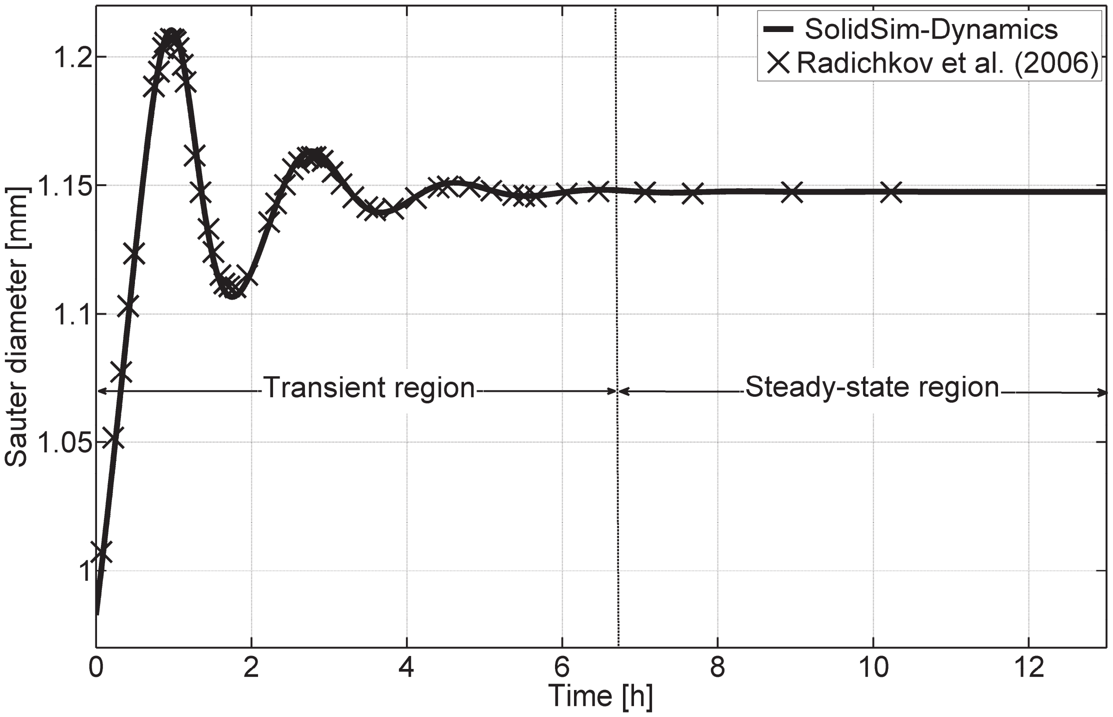

Figure 6.2: Comparison of the simulation results: coarse milling

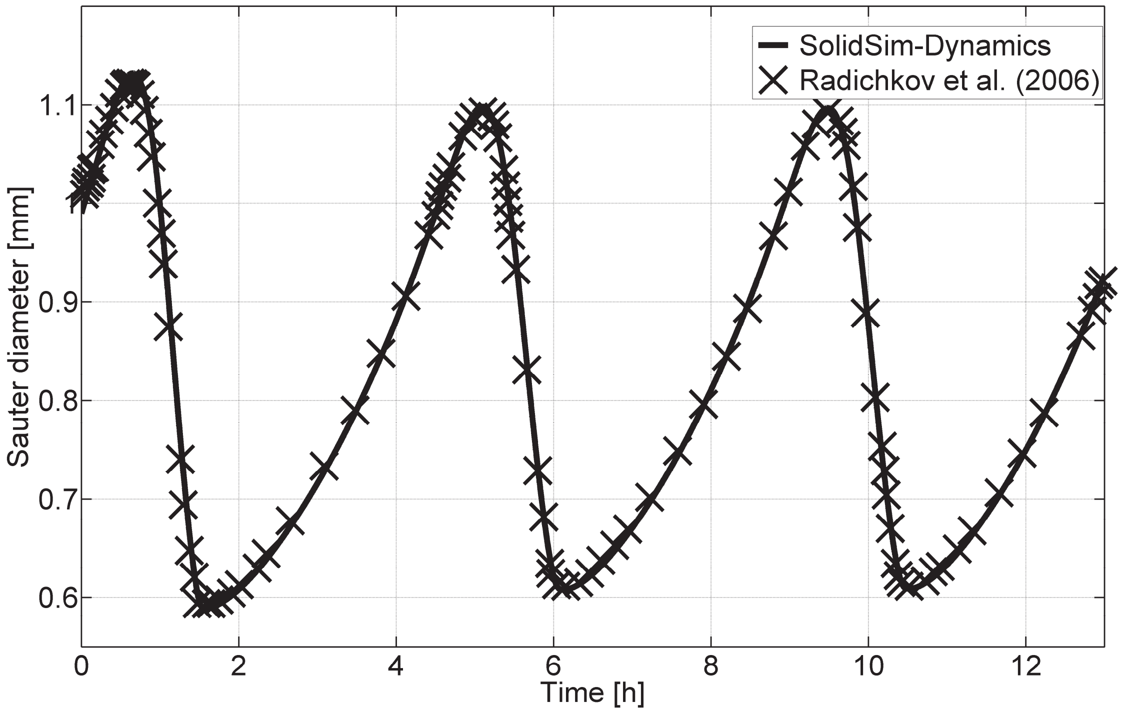

Figure 6.3: Comparison of the simulation results: fine milling

The coarse milling of granules leads to the damped oscillations, as it is depicted in Figure 6.2. In the initial phase (time period from 0 to 6.5 h) the process reveals oscillating behavior. However, after 6.5 h the stable steady-state region is reached.

Dieses Werk ist copyrightgeschützt und darf in keiner Form vervielfältigt werden noch an Dritte weitergegeben werden.
Es gilt nur für den persönlichen Gebrauch.

In the case study with the fine milling ($\mu_{mill} = 0.5\ \mathrm{mm}$) the process reveals transient behavior with self-sustained oscillations. This can be rationalized in the following way. The growth process occurs in the time period from 0 up to 0.7 h. As a result, the mass stream of the oversize of the first screen is enlarged. This leads to an increase of the fraction of fine milled particles, which are re-feeded into the granulator. The presence of a large number of fine particles in the FB leads to the larger surface of bed material and, as a consequence, to the slowing down of the growth rate. The small growth rate, simultaneously with the re-feeded material stream of fine particles, causes a sufficient decrease of a Sauter diameter in the apparatus (0.7-1.8 h). Afterwards, the continuous growth occurs up to 5.2 h. From the time point 5.2 h a steep decrease of Sauter diameter occurs again.

Comparing the results illustrated in Figure 6.2 and Figure 6.3, the conclusion can be drawn that there is no considerable difference between previously received results obtained from Matlab calculations, and new results obtained with SolidSim-Dynamics. Into both programs the identical mathematical models of different apparatuses have been implemented and the same process parameters have been used. The main difference between the both simulations is the type of the used modeling approach. The Matlab (Matlab) simulations have been performed with help of an equation-oriented approach and for the modeling in SolidSim-Dynamics the sequential-modular method has been applied.

The process which is shown in Figure 6.4 has been created in accordance to an industrial production process and it has been used as a next test example to verify correctness of the novel simulation environment. This process possesses a similar transient behavior as flowsheet which is depicted in Figure 6.1. However, the new flowsheet has a more complex structure and consists of an interconnection of three FB granulators. This flowsheet has been modeled in the SolidSim-Dynamics and in the equation-oriented Aspen Custom Modeler (ACM) program (Aspen). Afterwards the received results were compared in order to validate the correctness of the new environment (Figure A.3 and Figure A.4).

Dieses Werk ist copyrightgeschützt und darf in keiner Form vervielfältigt werden noch an Dritte weitergegeben werden.
Es gilt nur für den persönlichen Gebrauch.

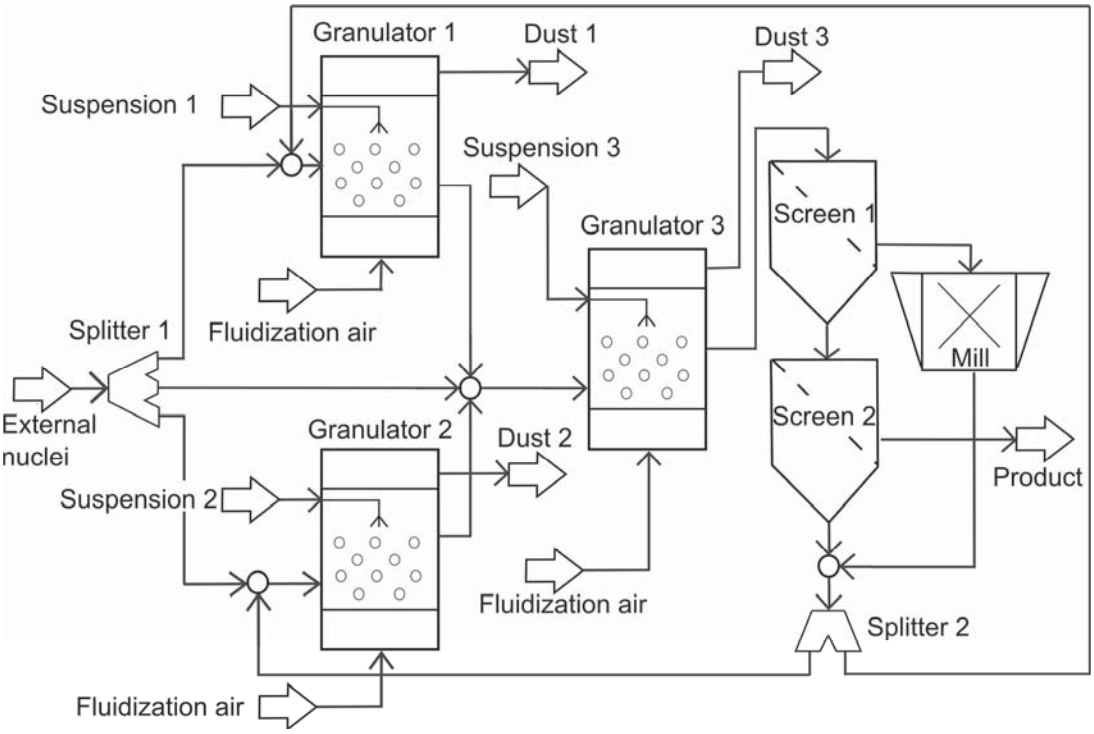

Figure 6.4: Flowsheet of the process which consists of three FB granulators

The external nuclei stream in Figure 6.4, which enters the process in the unit *Splitter 1*, is divided into three equal fractions. The output streams from the first and the second FB's are mixed with a fraction of the external nuclei stream and they are used as input nuclei stream of the third granulator. The output stream from the *Granulator 3* enters the stack of two screens and the mill. Similar to the scheme illustrated in Figure 6.1, the oversized fraction of the first screen is milled and mixed with the undersize of the second one. The unit *Splitter 2* divides the inlet material stream into two equal mass fractions.

For the modeling of the flowsheet in Figure 6.4, the following models have been applied:

- one-dimensional PBM for all FB granulators Eq. (4.11);
- normal Gaussian distribution Eq. (3.7) to describe the output PSD from the mill, the initial PSD of the holdup materials and size distribution of external nuclei stream;
- modified model of Molerus and Hoffmann (1969) to determine the separation function of both screens.

To describe the separation effect of the screens, the following expression has been used (Heinrich et al., 2002):

$$T(d) = \frac{1}{1 + \left(\frac{d_{sc}}{d}\right)^2 \cdot \exp\left(k_{sc}\left[1 - \left(\frac{d}{d_{sc}}\right)\right]\right)}, \tag{6.2}$$

Dieses Werk ist copyrightgeschützt und darf in keiner Form vervielfältigt werden noch an Dritte weitergegeben werden.
Es gilt nur für den persönlichen Gebrauch.

where $T(d)$ determines the probability with which a particle of diameter d remains on the screen, k_{sc} is a separation efficiency and d_{sc} is a separation diameter. Consequently, the probability that a particle will pass through the screen equals to $[1 - T(d)]$.

The key parameters, which were used for the test simulation, are listed in Table 6.1.

Table 6.1: Main process parameters of the flowsheet illustrated in Figure 6.4

	Granulator 1	Granulator 2	Granulator 3
Initial hold-up mass, kg	100	200	500
Initial PSD median diameter, mm	1.5	1.5	1.5
Initial PSD standard deviation, mm	0.2	0.2	0.2
Attrition rate, kg/m^2	1e^{-3}	1e^{-3}	1e^{-3}
Suspension mass flow, kg	100	200	500
Overspray part of suspension, –	0	0	0
	Screen 1		Screen 2
Separation diameter, mm	2		1.5
Separation efficiency, –	30		20

In Figure 6.5 the time-progression of the mass density distribution in the first granulator is shown. This transient behavior has been obtained for the case of fine milling ($\mu_{\text{mill}} = 1.1\ \text{mm}$, $\sigma_{\text{mill}} = 0.14\ \text{mm}$). From the analysis of simulation results the conclusion can be drawn that the process depicted in Figure 6.4 can reveal unsteady behavior in form of self-sustained oscillations. The comparison between results received from ACM and the SolidSim-Dynamics system is shown in Figure A.3 and Figure A.4.

Dieses Werk ist copyrightgeschützt und darf in keiner Form vervielfältigt werden noch an Dritte weitergegeben werden.
Es gilt nur für den persönlichen Gebrauch.

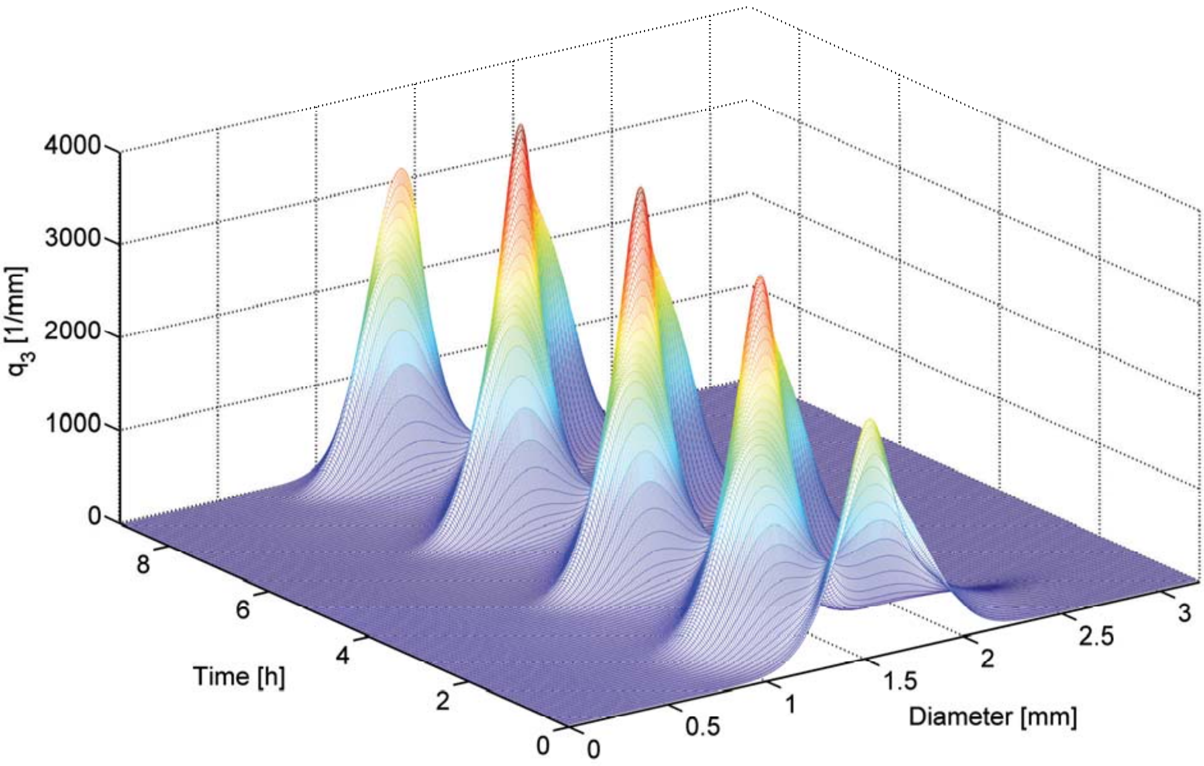

Figure 6.5: Time progression of the PSD in the first granulator

The modeling methods which were implemented into the SolidSim-Dynamics environment were additionally verified on a set of pure mathematical models. As benchmark software the Simulink (Matlab) package was used. Simulink is an environment for the multidomain simulation and model-based design for dynamic and embedded systems.

In Figure 6.6 the structure of the abstract test scheme which has been calculated in the SolidSim-Dynamics and Simulink systems is shown. This structure represents the model where the main process variable is defined as:

$$y = \frac{1}{2}\sin\left[\sin(t) + 2 + \frac{1}{2}y\right] \tag{6.3}$$

Dieses Werk ist copyrightgeschützt und darf in keiner Form vervielfältigt werden noch an Dritte weitergegeben werden.
Es gilt nur für den persönlichen Gebrauch.

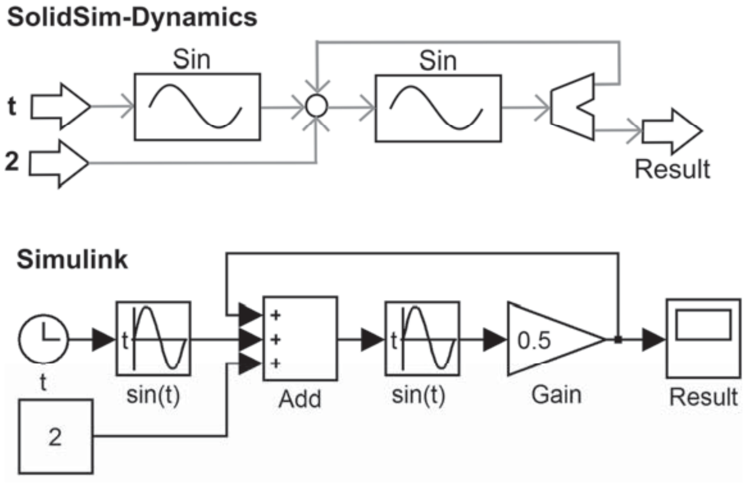

Figure 6.6: Equivalent flowsheet structure in the SolidSim-Dynamics and Simulink systems

The comparison between obtained results is illustrated in Figure 6.7. It can be observed that both environments give the same results.

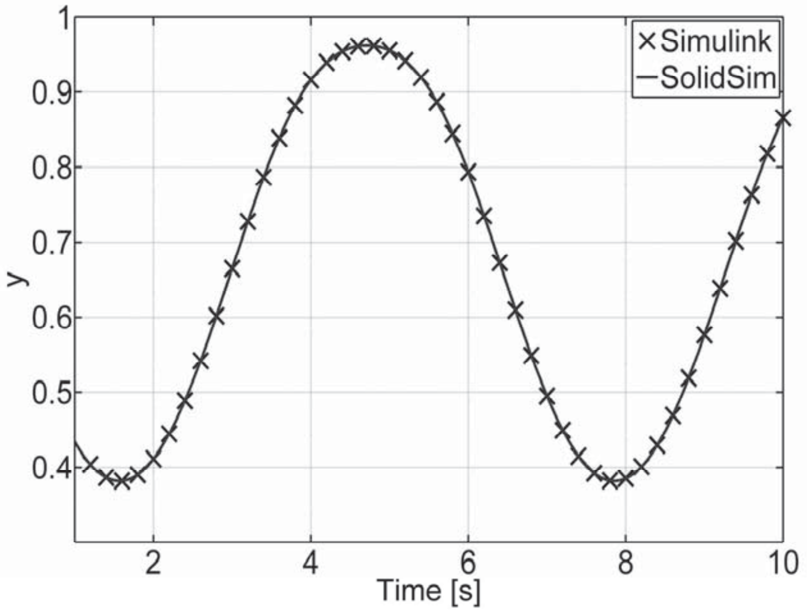

Figure 6.7: Comparison between results obtained with Simulink and SolidSim-Dynamics

Dieses Werk ist copyrightgeschützt und darf in keiner Form vervielfältigt werden noch an Dritte weitergegeben werden.
Es gilt nur für den persönlichen Gebrauch.

6.2 Simulation of a complex granulation model

A complex mathematical model of the fluidized bed granulation process, which consists of the PBM and thermodynamic equations, is implemented into the SolidSim-Dynamics as the unit *FBGranulatorPBMHM*. This model was used for the simulation of the process which is depicted in Figure 6.8.

The flowsheet presented in Figure 6.8 has a similar structure with the process shown in Figure 6.4. However, in distinction with the previous one, here, one of classification steps is applied directly in the apparatus. This is realized due to the presence of classification air. The fine fraction of the bed material does not leave the apparatus. Just the granules which are large enough to overcome the drag force will be discharged out of the granulator.

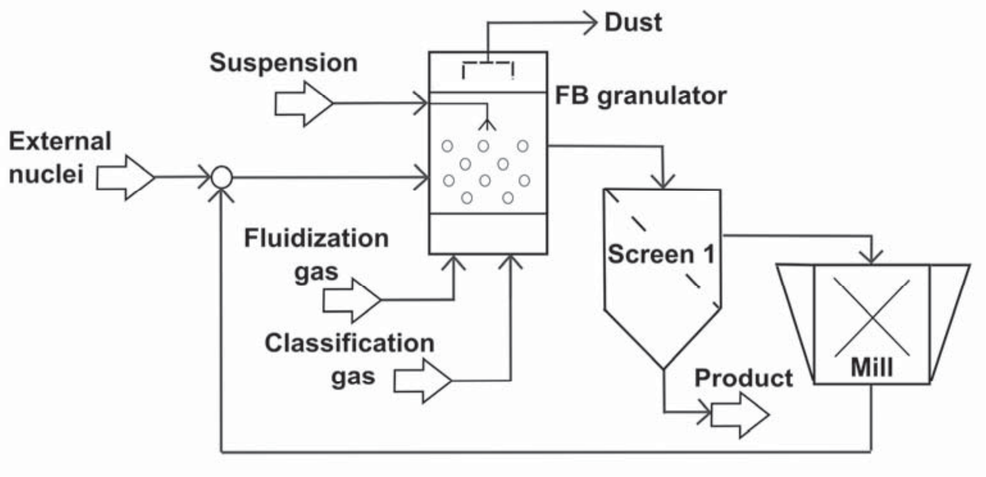

Figure 6.8: Flowsheet of the granulation process with internal classification

In the Table 6.2 the main process parameters are listed.

Dieses Werk ist copyrightgeschützt und darf in keiner Form vervielfältigt werden noch an Dritte weitergegeben werden.
Es gilt nur für den persönlichen Gebrauch.

Table 6.2: Main parameters of the process with internal classification

FB granulator		
initial bed mass	1000	kg
apparatus diameter	2	m
initial PSD median	1	mm
initial PSD standard deviation	0.1	mm
discharge tube diameter	0.1	m
Fluidization air		
volume flow	6.11	m^3/s
temperature	120	°C
Suspension		
mass flow	0.55	kg/s
temperature	30	°C
water content	40	%
Classification air		
temperature	100	°C
volume flow	0.038	m^3/s

Case study A: Start-up phase

In the first case study the process behavior in the start-up phase was investigated. During this study all values of input parameters like fluidization gas, mass flow, temperature, humidity, suspension flow, etc. remain constant.

From the analysis of the results depicted in Figure 6.9.a the increasing of Sauter diameter of the PSD in the apparatus can be observed. Granules were enlarged from 1 mm to 1.12 mm in the time period from zero to approximately one hour. This happens due to the relatively high volume flow of classification gas, which does not allow a fine fraction to leave the apparatus.

In Figure 6.9.b the time-progression of the output mass stream from the FB is shown. Proportionally to the particle growth, the enlargement of the output mass stream occurs. However, the same growth dynamic for the output stream can be observed also for the time period from 1 to 1.5 h, when the PSD in the apparatus has shifted to the finer fractions. The reason of this is an influence of the recycled stream. In the time point 1h the coarse fraction of the output mass steam from granulator has a relatively high magnitude. This leads to the formation of a high mass stream, which is separated by the screen as an oversize, and after milling is recycled back into the FB. Due to the processes described above, the mass of the

Dieses Werk ist copyrightgeschützt und darf in keiner Form vervielfältigt werden noch an Dritte weitergegeben werden.
Es gilt nur für den persönlichen Gebrauch.

bed increases and, as a consequence, an increase of the mass stream from the apparatus can be observed.

The injection of the liquid and deposition of the suspension onto the particles leads to the occurrence of a higher amount of the particle surfaces which are covered with a liquid film. This can be observed from the time progression of the wetted surface fraction in Figure 6.9.c. The value 1.28 which is reached after 1h indicates that 1.28% of particle surfaces are covered with a liquid film.

Due to the endothermic evaporation process the particle temperature is continually decreased during the entire simulated time interval from 0 to 3 h.

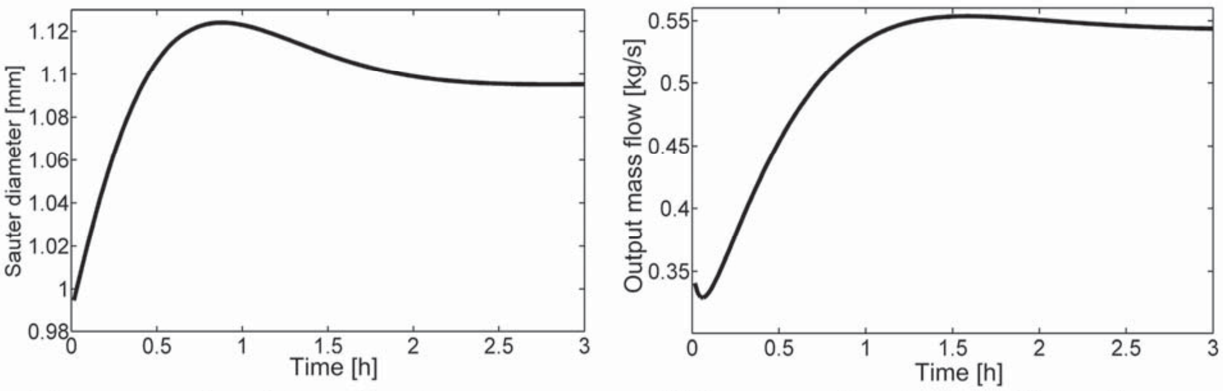

a) Time progression of Sauter diameter *b) Time progression of output solid mass flow*

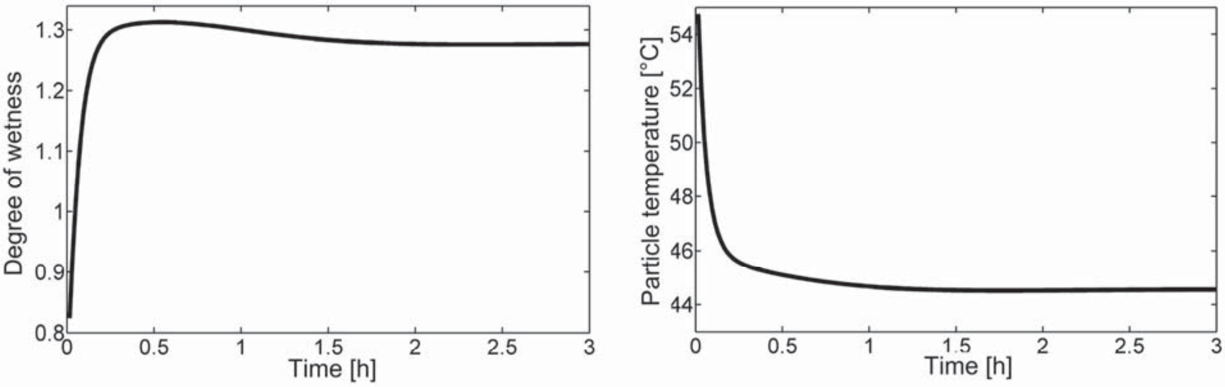

c) Time progression of wetness degree *d) Time progression of particle temperature*

Figure 6.9: Dynamic behavior of main process parameters in the start-up phase

Dieses Werk ist copyrightgeschützt und darf in keiner Form vervielfältigt werden noch an Dritte weitergegeben werden.
Es gilt nur für den persönlichen Gebrauch.

Case study B: Perturbation of classification air flow

As a further case study, the influence of the classification gas mass stream was investigated. In practice this is one of the main control parameters which is continually or stepwise adjusted during granulation to obtain specific product properties. In Figure 6.10 the changes of the classification mass flow, which have been simulated in this study, are shown. The presented perturbations are of continuous manner in order to avoid a restart of the simulation, and they are started after the steady state is reached.

In the time interval between 11 and 12 hours the increase of the classification stream from value 0.358 kg/s to 0.408 kg/s occurs. This leads to a greater resistance force in the classification tube and, as a consequence, to coarser particles in the granulator. With an enlargement of the particles in the apparatus, the bed mass and surface of the bed material is also growing. The increase of the total surface of the bed material, simultaneously with a constant injection of suspension, results in a smaller wetted surface fraction (1.15% in the time point 15h).

In Figure 6.10.d the oscillations of the output mass stream from the FB are depicted. Due to the higher classification gas mass flow 0.041 kg/s only a smaller part of a holdup can leave the apparatus and, as a consequence, the bed mass grows. Afterwards, due to the particle growth and the increased bed mass the output mass flow reaches the value 0.53 kg/s.

A similar behavior can be observed by the second perturbation of the classification gas in the time point of approximately 23 h. In the case of decreasing of gas flow in the time 39h the investigated parameters show reverse behavior.

Dieses Werk ist copyrightgeschützt und darf in keiner Form vervielfältigt werden noch an Dritte weitergegeben werden.
Es gilt nur für den persönlichen Gebrauch.

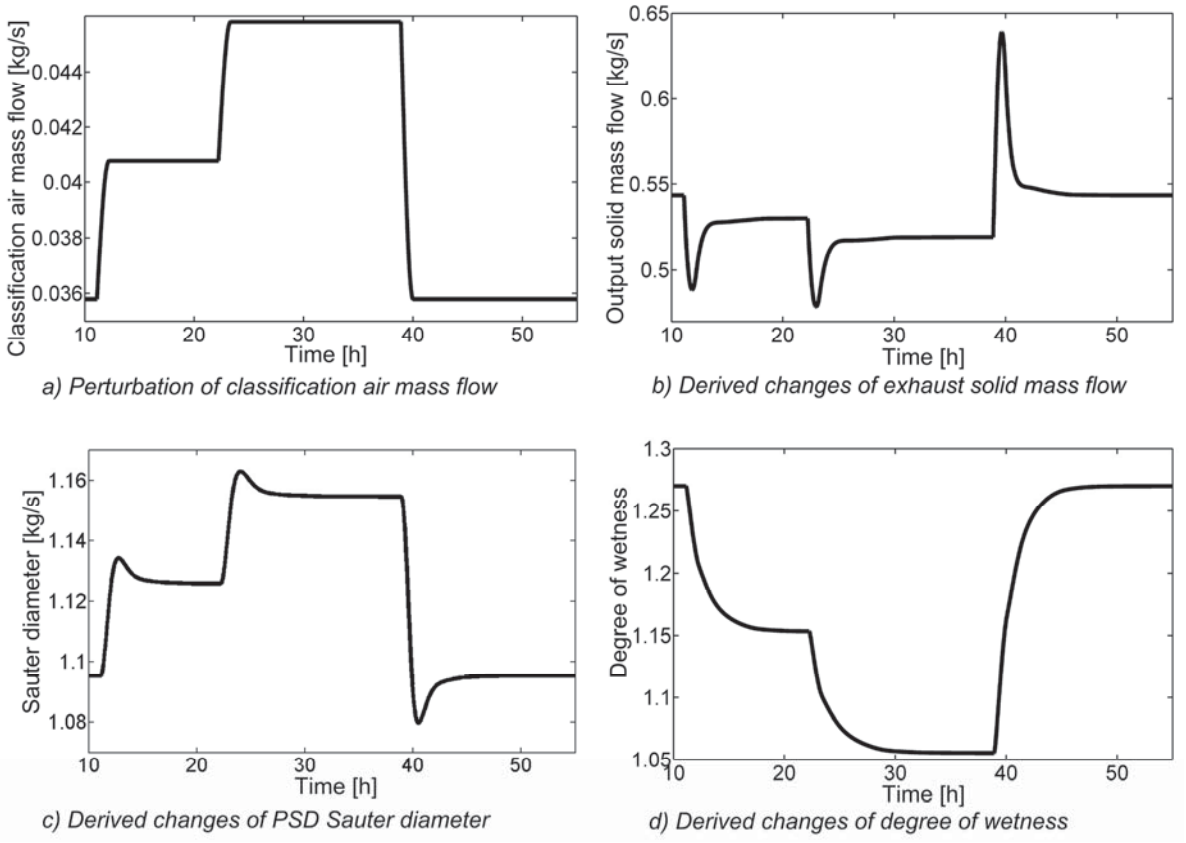

a) Perturbation of classification air mass flow

b) Derived changes of exhaust solid mass flow

c) Derived changes of PSD Sauter diameter

d) Derived changes of degree of wetness

Figure 6.10: Influence of process parameter perturbation (classification air mass flow)

Case study C: Perturbation of external nuclei flow

The influence of the external nuclei mass flow was investigated in the third case study. In some time points the external nuclei mass flow was increased from 0 up to 0.3 kg/s, as it is shown in Figure 6.11.a. The PSD of external flow was described by a Gaussian function Eq. (3.7) with median 0.3 mm and standard deviation 0.05 mm. The influence of the change of external nuclei flow on some process parameters is depicted in Figure 6.11.b, Figure 6.11.c and Figure 6.11.d. From the analysis of the simulation results it can be seen that an increase of mass flow of the fine external solid causes a decrease of the PSD in the granulator and, as a consequence, a decrease of the solid mass flow recycled to the granulator and output flow from it. Also such change leads to the larger bed mass and bigger product mass flow.

Dieses Werk ist copyrightgeschützt und darf in keiner Form vervielfältigt werden noch an Dritte weitergegeben werden.
Es gilt nur für den persönlichen Gebrauch.

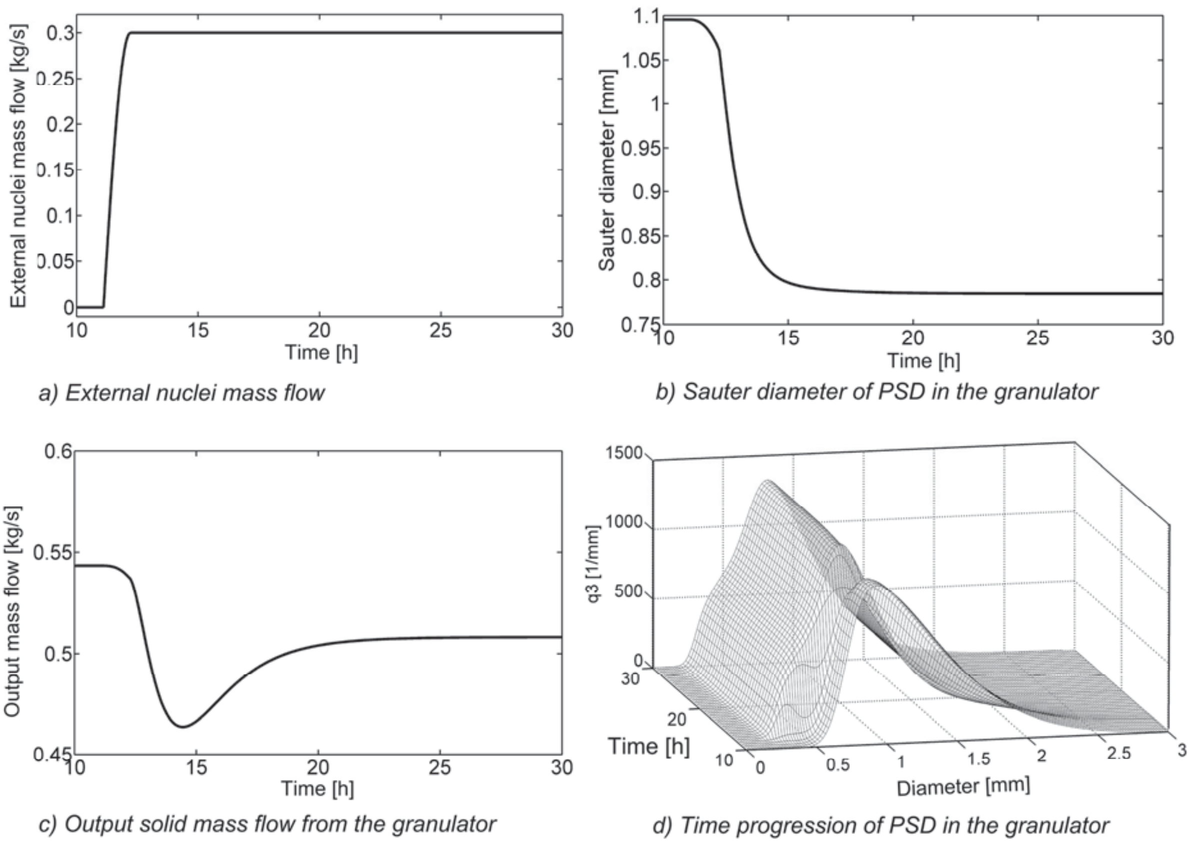

a) External nuclei mass flow

b) Sauter diameter of PSD in the granulator

c) Output solid mass flow from the granulator

d) Time progression of PSD in the granulator

Figure 6.11: Influence of external nuclei mass flow

The received simulation results show that the granulation processes with structures illustrated in Figure 6.1, Figure 6.4 and Figure 6.8 can have the constant or damped oscillations of the main process parameters. Similar patterns have been observed by agglomeration or crystallization processes. In order to increase the production efficiency and to provide constant quality of product material, the time regions of the transient behavior should be minimized. One possible way how the stability could be achieved is an implementation of control strategies. Palis and Kienle (2012) in their work have developed and implemented controllers to stabilize a fluidized bed spray granulation process. An alternative stabilization approach is a modification of the process structure. For example, inclusion of a bunker into a scheme allows to provide constant mass streams through the mill. As a result, the unsteady region can be drastically decreased compared to the source scheme.

Dieses Werk ist copyrightgeschützt und darf in keiner Form vervielfältigt werden noch an Dritte weitergegeben werden.
Es gilt nur für den persönlichen Gebrauch.

6.3 Multiscale process calculation

The developed multiscale approach was used for the detailed calculation of the granulation process. The structure of this process is illustrated in Figure 6.12. This scheme is similar to the process represented in Figure 6.1. The distinction between both flowsheets is that in the new scheme just about 40% of the output mass flow from the granulator reaches the stack of two screens, where the sieving occurs. Both screens have been simulated based on the Plitt separation model. The grade efficiency in this model is calculated as a function of a cut size (μ_{cut}) and of separation sharpness (α_{sc}) and is expressed as:

$$T(d) = 1 - \exp\left(-0.693 \cdot \left(\frac{d}{\mu_{cut}}\right)^{\alpha_{sc}}\right) \tag{6.4}$$

The main process parameters which have been used for the calculations are presented in the Appendix in Table A.4.

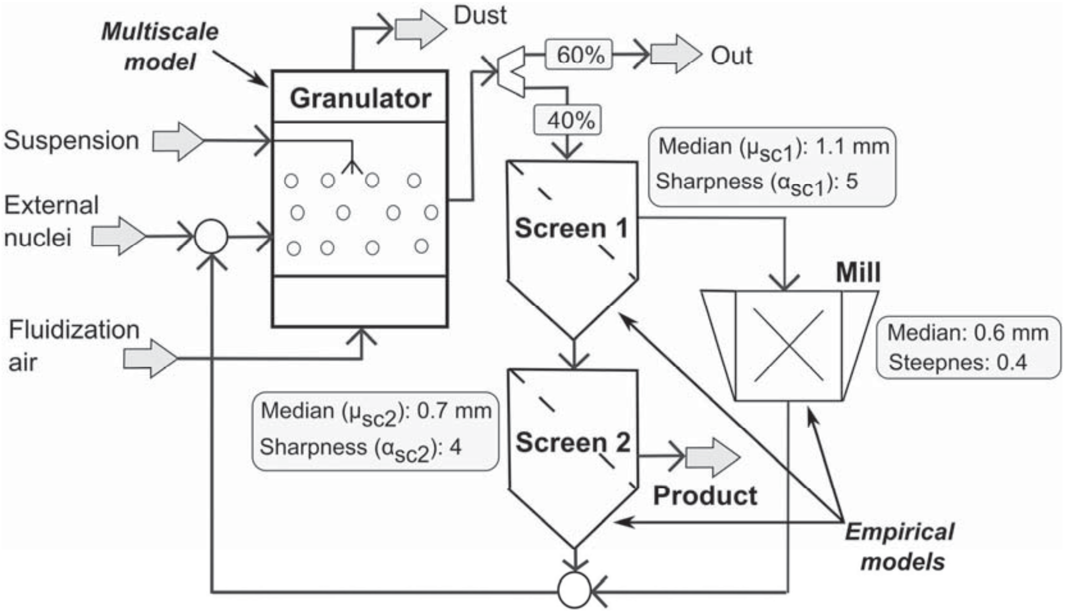

Figure 6.12: Flowsheet of the production process simulated by multiscale approach

The aim of the presented study was to obtain a more precise estimation of the steady-state regime. Therefore, instead of a fully dynamic simulation with a splitting of the whole simulation time into intervals (Figure 2.1), the prediction of a steady-state was done.

In the first step of the global calculation algorithm, the process was simulated in SolidSim-Dynamics up to the steady-state. In this calculation the semi-empirical model of the fluidized bed granulator (*FBGranulatorMult*) with the size-independent growth rate Eq. (4.12), Eq. (4.13) was used. The obtained time-progression of the PSD in the apparatus and mass streams in the scheme are plotted in Figure 6.13 and Figure 6.14. From the analysis of the received results

Dieses Werk ist copyrightgeschützt und darf in keiner Form vervielfältigt werden noch an Dritte weitergegeben werden.
Es gilt nur für den persönlichen Gebrauch.

the conclusion can be drawn that after approximately 3 hours the process reaches the steady-state. Afterwards, in order to perform a more accurate prediction of this steady-state, the calculations on the lower scales are started.

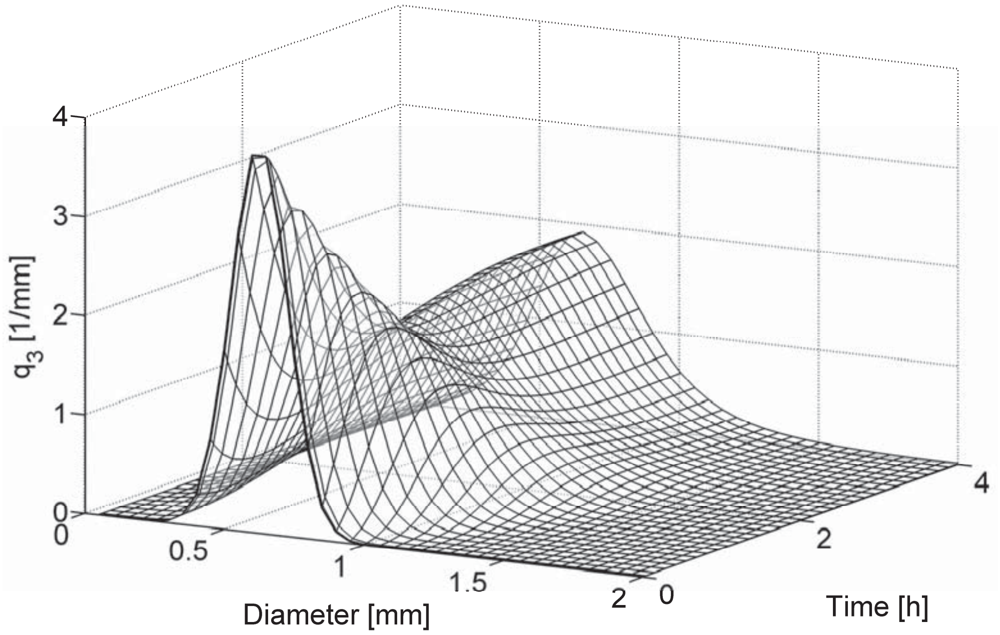

Figure 6.13: Time-progression of the PSD of the holdup material

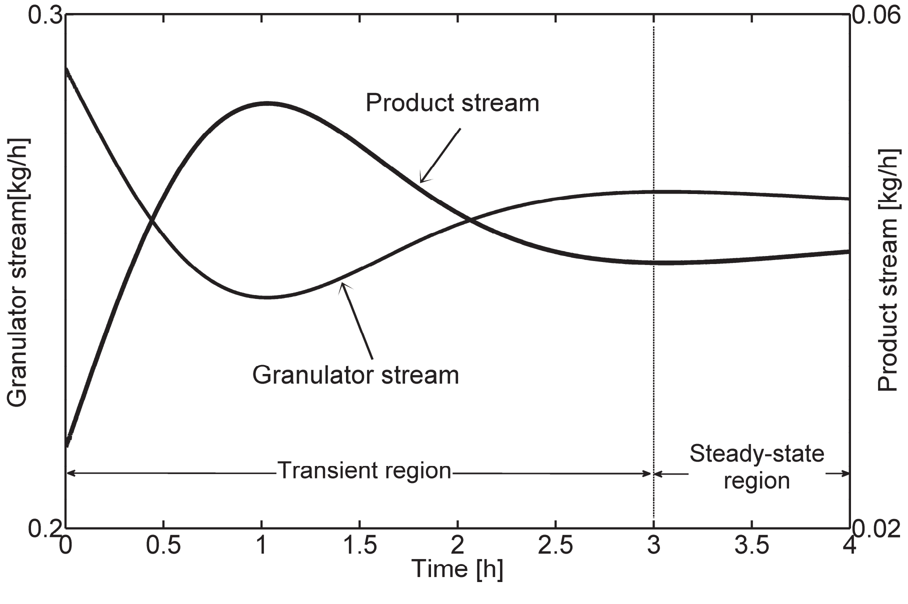

Figure 6.14: Transient behavior of the mass streams in the flowsheet

In Figure 6.15 the front and the top views of the apparatus, which was used for the iterative calculations on the micro and mesoscales, are schematically illustrated. The suspension in the apparatus is sprayed through the three symmetrically placed nozzles. The geometry of each wetting zone was described by a cone region.

Dieses Werk ist copyrightgeschützt und darf in keiner Form vervielfältigt werden noch an Dritte weitergegeben werden.
Es gilt nur für den persönlichen Gebrauch.

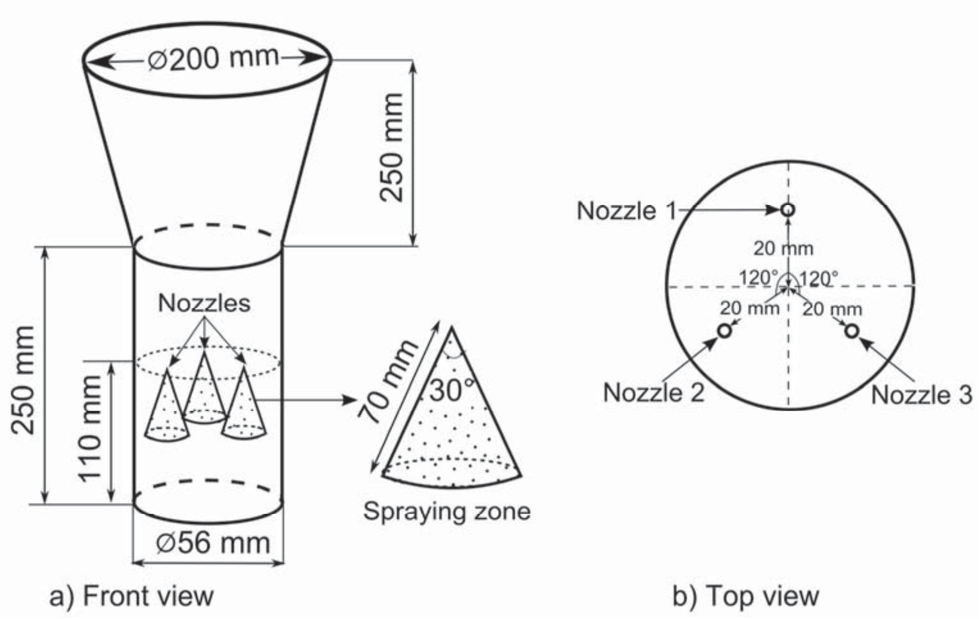

Figure 6.15: Apparatus geometry used for the micro and mesoscale simulations

On the microscale the DEM-CFD simulation with 25,000 spherical particles was performed for the time interval of 9 seconds. For the DEM calculations a fixed time step of 1 µs was applied. The received particle trajectories and fluid profiles have been saved into the databases and the control transferred into mesoscale model.

On the mesoscale the wetting and the drying were calculated for a time interval of 300 seconds. It was assumed that the particles cyclically repeat their trajectories. For the numerical solution of the mesoscale model the Euler method with variable time step size in the range between [1ms; 0.1s] was used. Afterwards, according to the main calculation algorithm (Figure 5.5), the interscale iterations had been repeated until the convergence was reached. As convergence criteria the averaged value of wet surface fraction was used.

In Figure 6.16 the screenshot illustrates the liquid distribution in the FB apparatus. The particles are colored according to the mass of the liquid film. It is assumed that the liquid film has a constant thickness of 0.1 mm.

Dieses Werk ist copyrightgeschützt und darf in keiner Form vervielfältigt werden noch an Dritte weitergegeben werden.
Es gilt nur für den persönlichen Gebrauch.

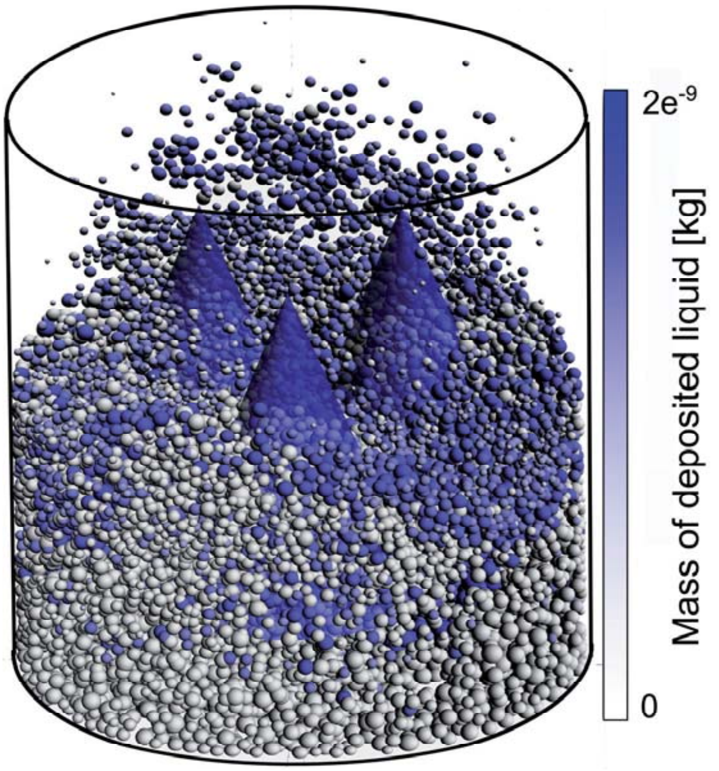

Figure 6.16: Screenshot of the liquid distribution in the fluidized bed apparatus

To couple mesoscale and macroscale models the normalized growth rate is used. It was obtained according to the Eq. (6.5), where $G_e^{meso}(d)$ is calculated by Eq. (5.17). This parameter is used in the PBM to qualitatively estimate the difference between growth rates of granules with different sizes. By solving of the implicit algebraic equation system in Eq. (6.6), the macroscopic growth rates $G_{e,i}^{macro}$ for different classes of the PSD are calculated.

$$G_{norm}^{meso}(d) = \frac{G_e^{meso}(d)}{d_{max} - d_{min}} \int_{d_{min}}^{d_{max}} G_e^{meso}(d) dd \tag{6.5}$$

$$\begin{cases} G_{norm}^{macro}(d) = G_{norm}^{meso}(d) \\ \sum G_{e,i}^{macro}(d) \cdot A_i(d) = \dfrac{2 \cdot \dot{M}_{susp} \cdot (1 - K_{os}) \cdot (1 - K_w)}{\rho_p} \\ G_{norm}^{macro}(d) = \dfrac{G_e^{macro}(d)}{d_{max} - d_{min}} \displaystyle\int_{d_{min}}^{d_{max}} G_e^{macro}(d) dd. \end{cases} \tag{6.6}$$

The overspray part of the suspension K_{os} was directly approximated from the mesoscale simulations, as it is expressed in Eq. (6.7). The overspray mass stream $\dot{M}_{os}$ describes the part of the suspension droplets which overcome the distance L_{spray} (Figure 5.9) and do not collide with any particle. For the investigated process the overspray part is equal to $K_{os} = 0.063$.

Dieses Werk ist copyrightgeschützt und darf in keiner Form vervielfältigt werden noch an Dritte weitergegeben werden.
Es gilt nur für den persönlichen Gebrauch.

$$K_{os} = \frac{\dot{M}_{os}}{\dot{M}_{susp}} \tag{6.7}$$

The normalized growth rate $G_{norm}^{meso}(d)$ obtained from the mesoscale calculations is plotted in Figure 6.17. From the analysis of the received results the conclusion can be drawn that in the investigated process the smaller particles have a higher growth rate. This occurs due to the top-down configuration of nozzles and the partial segregation of the bed material. The larger particles have a larger residence time in the bottom zones of the apparatus and, as a consequence, a smaller amount of the suspension droplets collides with these granules. On the contrary, the smaller granules are frequently located in the wetting zones, thus, they have a larger growth rate.

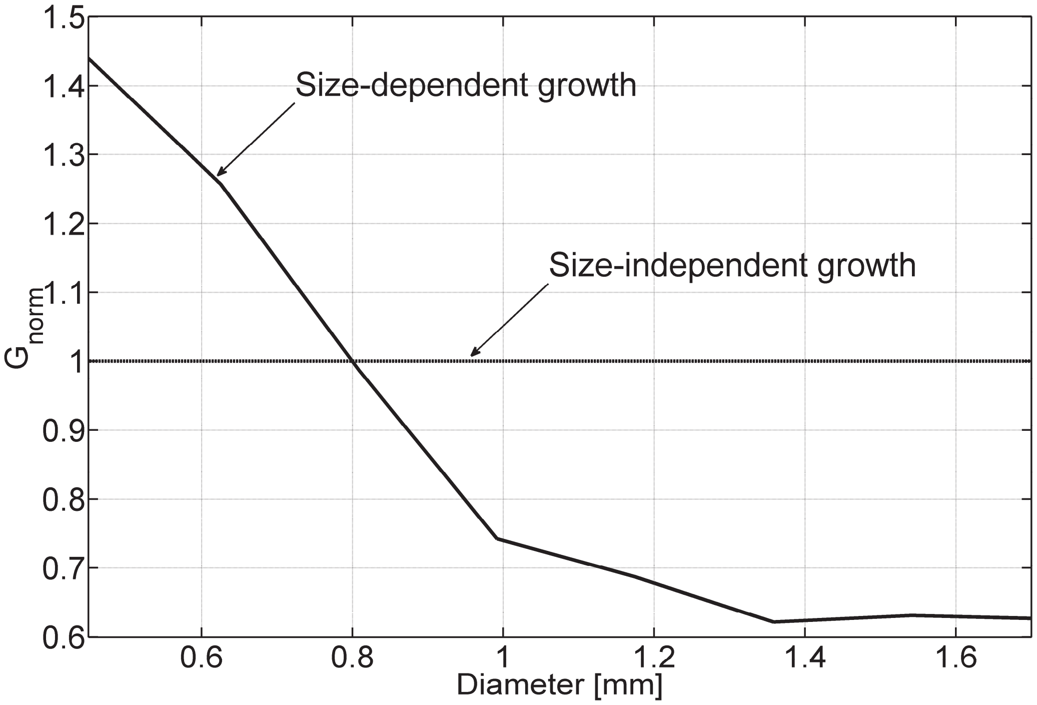

Figure 6.17: Normalized growth rate

In the final step of the main simulation algorithm (Figure 5.5) the flowsheet calculations were performed with more precise values of a growth rate and an overspray part of the suspension. In Figure 6.18 the comparison between the PSD, obtained with simplified empirical model and detailed multiscale model, is shown.

Dieses Werk ist copyrightgeschützt und darf in keiner Form vervielfältigt werden noch an Dritte weitergegeben werden.
Es gilt nur für den persönlichen Gebrauch.

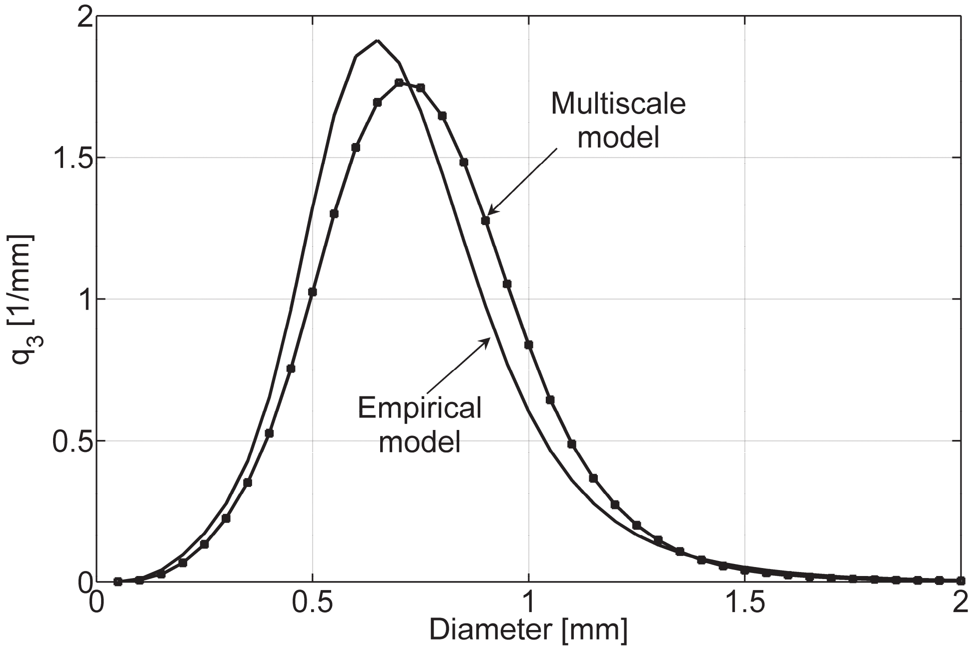

Figure 6.18: Comparison between steady-state results of empirical and multiscale models

From the analysis of the obtained simulation results the conclusion can be drawn that the consideration of the size-dependent growth, where smaller particles are growing faster, results in a coarser PSD in the FB. This happens due to the rapid enlargement of the fine fractions, which are supplied into the apparatus as a recycled stream and slowdown enlargement of coarse particles. This causes a smaller mass stream of the solid, which is milled as an oversize of the first screen and, as a consequence, a smaller amount of fine particles which are recycled into the granulator.

In the case study described above, the detailed modeling of the fluidized bed growth process has been performed. The proposed multiscale methodology allows to consider the influence of material parameters and apparatus geometry. For example, the influence of the nozzle positions on the PSD distribution of product material can be estimated.

The multiscale unit *FBGranulatorMult* implemented into SolidSim-Dynamics is a still simplified model with a large set of neglected effects. However, the proposed framework with process modeling on three different scales can be easily extended with new parameters or functional relationships.

Dieses Werk ist copyrightgeschützt und darf in keiner Form vervielfältigt werden noch an Dritte weitergegeben werden.
Es gilt nur für den persönlichen Gebrauch.

Conclusion

The work presented in this contribution was performed in order to develop and to implement novel methods, models and simulation strategies in the area of dynamic simulation of particulate systems. The proposed approaches were developed for general solids processes without limitation to specific process types. Nevertheless, fluidized bed spray granulation was used as a key investigated process, on which the new methods have been applied to.

The described work consists of four thematically subdivided main parts. From the analysis of the state of the art, which is presented in the first part, the conclusion can be drawn that nowadays despite the importance and the wide usage of solids processes, there is no software systems which are able to perform dynamic flowsheet simulation of solids processes. The complexity of the calculation of solids processes and the huge difference between description of solids and liquid-vapor systems were pointed out. Therefore, this work was focused not just on the development and implementation of a new simulation system, but also on a developing of new methods for the effective dynamic flowsheet simulation.

The actual state of research for the modeling of fluidized bed granulation is also given in the first part. The usage of the population balance model is an effective way to describe the particle growth. Additional coupling of the population balance with models of heat and mass transfer allows to describe the time-progression of the main process parameters. Nevertheless, for the macroscopic description of the granulation the empirical or semi-empirical models are used, where material microproperties or apparatus geometries are hardly considered. To perform more detailed simulation, the application of the multiscale approach was proposed.

For the dynamic flowsheet simulation the modular and equation-oriented approaches can be applied. Each of these methods has its own advantages, however, the performed analysis shows, that the usage of a modular approach is more effective for calculation of solids processes. This approach is implemented into the new system that gives a high flexibility by creating new models and allows the simultaneous usage of different solvers for the calculation of a whole flowsheet.

Another feature of the new simulation system is a splitting of the global calculation time into a set of smaller time intervals. In each iteration of the main calculation algorithm, the system is simulated on a small time interval with further analysis of reached convergence. The dividing of global time into a set of variable-size intervals increases the performance of a system and can be effectively used to parallelize calculations. The time is needed to perform calculations is one

Dieses Werk ist copyrightgeschützt und darf in keiner Form vervielfältigt werden noch an Dritte weitergegeben werden.
Es gilt nur für den persönlichen Gebrauch.

of the main efficiency criteria of a simulation system. Therefore, the minimization of computational volume and the possibility to use distributed computing were considered on the stage of designing a main calculation algorithm.

In order to implement the new models, the architecture of dynamic units was developed. According to the object-oriented methodology, the architecture was implemented as a set of parent virtual classes, from which every new dynamic unit should be inherited. This standardizes all dynamic units and through the usage of COM technology allows to use dynamic units in other simulation systems.

For the modeling of the fluidized bed spray granulation process, four new dynamic models have been implemented and added into the SolidSim-Dynamics library. Two of them are related to the Hounslow and Cell-average techniques and developed to simulate the pure aggregation process. The other two units describe the pure growth process with different detailing levels. To validate the new simulation system and to check the correctness of the implemented models, test calculations were performed. The results were compared with already published ones, which have been received with other software systems. The comparison showed good quantitative agreement between the calculated values and thus, showed the correctness of the new system for these cases.

The simulation of a granulation process by the usage of a complex fluidized bed model, where heat and mass transfer have been considered, gives the possibility to calculate the influence of different parameters on the whole process. For example, the information about the influence of perturbations of classification gas flow onto mass streams in the whole process was obtained. However, the usage of a semi-empirical model does not allow to make calculations on the entire parameter space. To perform more detailed simulations and to extend the parameter space, where models can be applied, a concept of the multiscale flowsheet simulation was developed.

The multiscale approach is based on the process description by a set of submodels on different time and length scales. These submodels are combined together by the interscale communications and are iteratively calculated according to the main simulation algorithm. On the highest hierarchy level the flowsheet system is used. Depending on the global process parameters, the microscale models are generated.

The process on the microscale is modelled by the Discrete Element Method (DEM), where each particle is considered as a separate entity. The coupling of the DEM with a CFD system allows to consider the influence of fluid, which plays a decisive role in fluidized bed systems. In order to take into account the influence of the liquid phase onto particle dynamics, a new

Dieses Werk ist copyrightgeschützt und darf in keiner Form vervielfältigt werden noch an Dritte weitergegeben werden.
Es gilt nur für den persönlichen Gebrauch.

contact model was implemented. Compared to the dry contact, this model is extended by supplementary viscous and capillary forces. As a result from the microscale calculations, the particle trajectories and fluid profiles are used and transmitted into the mesoscale.

The model on the mesoscale serves as a gateway between micro and macromodels. Here, the particle wetting with an injected suspension and the further drying of liquid from particle surfaces are simulated. To predict the wetting process, a novel nozzle model was developed. Finally, the results received from the mesoscale are used in the population balance model on the macroscale.

The developed flowsheet simulation system is applicable for general solids processes, without limitations on specific process structures or types of apparatuses. With the help of it the process engineers get a powerful tool for:

- performing dynamic simulations;
- developing control strategies;
- optimizing dynamic process;
- teaching the personnel;
- finding the answer to the question “what if”.

The multiscale approach, which has been developed in this work, is much more complex from a computational point of view. However, because of the rapid development of computer systems, this approach can become one of the most promising useful simulation approaches in the near future.

Dieses Werk ist copyrightgeschützt und darf in keiner Form vervielfältigt werden noch an Dritte weitergegeben werden.
Es gilt nur für den persönlichen Gebrauch.

References

Adams, M.J. and Edmondson, B. (**1987**). Forces between particles in continuous and discrete liquid media, in *Tribology in particulate technology*, Bristol: Adams Hilger.

Adetayo, A.A. and Ennis, B.J. (**1997**). A unifying approach to modeling coalescence mechanisms, *AIChE*, Vol. 43, pp. 927-934.

AggFlow (**2012**)., [Online], Available: www.aggflow.com.

Antonyuk, S., Heinrich, S., Deen, N., Kuipers, H. (**2009**). Influence of liquid layers on energy absorption during particle impact, *Particuology*, Vol. 7, pp. 245-259.

Antonyuk, S., Heinrich, S., Dosta, M. (**2009**). Energetic aspects of granule impact: Influence of the liquid layers, *Powder and Grains: Proceedings of 6th international conference on micromechanics of granular media*, pp. 796-799.

Ascher, U.M. and Petzold, L.R. (**1998**). *Computer methods for ordinary differential and differential algebraic equations*, Philadelphia: Society fo Industrial and Applied Mathematics.

Aspen (**2012**)., [Online], Available: www.aspentech.com.

Balaji, S., Du, J., White, C.M., Ydstie, B.E. (**2010**). Multi-scale modelling and control of fluidised beds for the production of solar grade silicon, *Powder Technology*, Vol. 199, pp. 23-31.

Balliu, N.E. and Cameron, I.T. (**2007**). Performance assessment and model validation for an industrial granulation circuit, *Powder Technology*, Vol. 179, pp. 12-24.

Balliu, N.E., Cameron, I.T., Newell, R. (**2004**). A comparative study of numerical methods for solving continuous population balance models for aggregation process, *Dev. Chem. Eng. Mineral Process.*, Vol. 12, pp. 277-291.

Barton, C.W. and Perkins, J.D. (**1988**). Experiences with SPEEDUP in the mineral processing industries, *Chemical Engineering Research and Design*, Vol. 66, pp. 408-418.

Biegler, L.T., Grossmann, I.E., Westerberg, A.W. (**1997**). *Systematic methods of chemical process design*, New Jersey: Prentice HALL PTR.

Borchardt, J., Klaus, E..G.F., Horn, D. (**1999**). Parallel modular dynamic process simulation, in *Scientific computing in chemical engineering*, New York: Springer Verlag.

Brochot, S., Villeneuve, J., Guillaneau, J.C., Durance, M.V., F., B. (**2002**). USIM PAC 3: Design and optimization of mineral processing plants from crushing to refining, in *Mineral processing plant design, practice and control*, Littleton, Colorado: Society for mining metal.

Brown, P.N., Hindmarsh, A.C., Petzold, L.R. (**1998**). Consistent initial conditions for differnt algebraic systems, *SIAM Journal on Scientific Computing*, Vol. 19, pp. 1495-1512.

CAPE-Open (**2012**)., [Online], Available: www.colan.org.

Dieses Werk ist copyrightgeschützt und darf in keiner Form vervielfältigt werden noch an Dritte weitergegeben werden.
Es gilt nur für den persönlichen Gebrauch.

Clift, R. (**1996**). Powder technology and particle science, *Powder Technology*, Vol. 88, pp. 335-339.

Crow, M.L. and Ilic, M.D. (**1990**). The waveform relaxation method for systems of differential equations, *Mathl. Comput. Modelling*, Vol. 19, pp. 67-84.

Cundall, P.A. and Strack, O.D.L. (**1979**). A discrete numerical model for granular assemblies, *Geotechnique*, pp. 47-65.

Detzner, H.-D. (**1995**). The Hamburg project METHA: large scale separation, dewatering and reuse of polluted sediments, *European Water Pollution Control*, Vol. 5, pp. 38-42.

Dosta, M., Antonyuk, S., Fries, L., Heinrich, S. (**2010**). Discrete element modelling of the fluidized bed granulation process by coupling of different simulation systems, *Proc. of the 17th International Drying Symposium*, pp. 506-512.

Dosta, M., Antonyuk, S., Heinrich, S. (**2012**). Multiscale simulation of the fluidized bed granulation process, *Chemical Engineering & Technology*, Vol. 35, no. 8, pp. 1373-1380.

Dosta, M., Fries, L., Antonyuk, S., Heinrich, S., Palzer, S. (**2011**). Multiscale simulation of fluidized bed agglomeration, *Proceedings of 5th International Granulation Workshop*.

Dosta, M., Heinrich, S., Werther, J. (**2010**). Fluidized bed spray granulation: Analysis of the system behaviour by means of dynamic flowsheet simulation, *Powder Technology*, Vol. 204, pp. 71-82.

Dosta, M., Mangold, M., Kienle, A., Svjantyj, V. (**2008**). Parallel simulation of molten carbonate fuel cell system, *ESCAPE 18*.

Ennis, B. (**1996**). Agglomeration and size enlargment session summary paper, *Powder Technology*, Vol. 88, pp. 203-225.

Evans, L.R. (**1989**). Simulation with respect to solid fluid systems, *Computers Chemical Engineering*, Vol. 13, pp. 343-350.

Flore, K., Schoenherr, M., Feise, H. (**2009**). Aspects of granulation in chemical industry, *Powder Technology*, Vol. 189, pp. 327-331.

Fries, L., Dosta, M., Antonyuk, S., Heinrich, S., Palzer, S. (**2011**). Moisture distribution in fluidized beds with liquid injection, *Chemical Engineering and Technology*, Vol. 34, pp. 1076-1084.

Gerstlauer, A., Gahn, C., Zhou, H., Rauls, M., Schreiber, M. (**2006**). Application of population balances in the chemical industry - current status and future needs, *Chemical Engineering Science*, Vol. 61, pp. 205-217.

Ge, W., Wang, W., Yang, N., Li, J., al., e. (**2011**). Meso-scale oriented simulation towards virtual process engineering (VPE) - The EMMS Paradigm, *Chemical Engineering Science*, Vol. 66, pp. 4426-4458.

Gnielinski, V. (**1980**). Wärme- und Stoffübertragung in Festbetten, *Chemie Ingenieur Technik*, Vol. 52, pp. 228-236.

Golovin, A.M. (**1963**). The solution of the coagulation equation for raindrops, *Sov. Phys. Dokl.*, Vol. 8, pp. 191-193.

Dieses Werk ist copyrightgeschützt und darf in keiner Form vervielfältigt werden noch an Dritte weitergegeben werden.
Es gilt nur für den persönlichen Gebrauch.

Gorosko, V.D., Rozenbaum, R.B., Todes, O.M. (**1958**). Приближенные закономерности гидравлики взвешенного слоя и стесненного падения, *Изв. вузов: Нефть и газ (Neft i Gas)*, Vol. 1, pp. 125-131.

Grainsoft (**2012**)., [Online], Available: www.grainsoft.de.

Grama, A., Gupta, A., Karypis, G., Kumar, V. (**2003**). *Introduction to parallel computing*, New York: Addison-Wesley.

Green, D.W. and Perry, R.H. (**2007**). *Perry's chemical engineers' handbook*, New York: McGraw-Hill Professional.

Groenewold, H. and Tsotsas, E. (**1999**). Predicting apparent sherwood numbers for fluidized beds, *Drying Technology: An International Journal*, pp. 1557-1570.

Grünewald, G. (**2011**). *Staubeinbindung und Keimbildung bei der Wirbelschicht-Sprühgranulation. Vom Prozessverständnis zur Modellierung*, Göttingen: Cuvillier Verlag.

Hampel, R. (**2010**). *Beitrag zur Analyse von kinetischen Einflüssen auf die Wirbelschicht-Sprühagglomeration*, Magdeburg: Fak. für Verfahrens- und Systemtechnik, Dissertation.

Hartge, E.-U., Pogodda, M., Reimers, C., Schwier, D., Gruhn, G., Werther, J. (**2006**). Flowsheet simulation of solids processes, *KONA*, Vol. 24, pp. 147-158.

Heinrich, S. (**2001**). *Modellierung des Wärme- und Stoffübergangs sowie der Partikelpopulationen bei der Wirbelschicht Sprühgranulation*, Düsseldorf: VDI-Verlag.

Heinrich, S. and Mörl, L. (**1999**). Fluidized bed granulation - a new model for the description of particle wetting and of temperature and concentration distribution, *Chemical Engineering and Processing*, Vol. 38, pp. 635-663.

Heinrich, S., Peglow, M., Ihlow, M., Henneberg, M., Mörl, L. (**2002**). Analysis of the start-up process in continuous fluidized bed spray granulation by population balance modelling, *Chemical Engineering Science*, Vol. 57, pp. 4369-4390.

Helget, A. (**1997**). *Modulare Simulation verfahrenstechnischer Anlage*, Düsseldorf: VDI-Verlag.

Hillestad, M. and Hertzberg, T. (**1986**). Dynamic simulation of chemical engineering systems by the sequential modular approach, *Computers and Chemical Engineering*, Vol. 10, pp. 377-388.

Hill, J.H. and M., N.K. (**1995**). New discretization procedure of the breakage equation, *AIChE*, Vol. 41, pp. 1204-1216.

Hindmarsh, A.C., Brown, P.N., Grant, K.E., Lee, S.L., Serban, R., Shumaker, D.E., Woodward, C.S. (**2005**). SUNDIALS: Suite of nonlinear and differential/algebraic equation solvers, *ACM Transactions on Mathematical Software*, pp. 363-396.

Hlavacek, V. (**1977**). Analysis of a complex plant steady-state and transient behavior, *Computers and Chemical Engineering*, Vol. 1, pp. 75-100.

Hounslow, M.J., Ryall, R.L., Marshall, V.R. (**1988**). A discretized population balance for nucleation growth and aggregation, *AIChE Journal*, pp. 1821-1832.

Hounslow, M.J. and Wynn, E.J.W. (**1992**). Modelling particulate processes: Full solutions and short cuts, *Computers and Chemical Engineering*, pp. 411-420.

Dieses Werk ist copyrightgeschützt und darf in keiner Form vervielfältigt werden noch an Dritte weitergegeben werden.
Es gilt nur für den persönlichen Gebrauch.

Hulburt, H.M. and Katz, S. (**1964**). Some problems in particle techology: A statistical mechanical formulation, *Chemical Engineering Science*, Vol. 19, pp. 555-574.

Ingram, G.D., Camerom, I.T., Hangos, K.M. (**2003**). Classification and analysis of integrating frameworks in multiscale modelling, *Chemical Engineering Science*, Vol. 59, pp. 2171-2187.

Ingram, G.D. and Cameron, I.T. (**2005**). Formulation and comparison of alternative multiscale models for drum granulation, *ESCAPE-15*.

Invensys (**2012**)., [Online], Available: ion.invensys.com.

Iveson, S.M., Litster, J.D., Hapgood, K., Ennis, B. (**2001**). Nucleation growth and breakage phenomena in agitated wet granulation process: a review, *Powder Technology*, Vol. 117, pp. 3-39.

Kapur, P.C. and Fuerstenau, D.W. (**1969**). Coalescence model for granulation, *Industrial and Engineering Chemistry, Process Design Devices*, Vol. 8, pp. 56-62.

Karypis, G. and Kumar, V. (**1998**). Multilevel k-way partition scheme for irregular graphs, *Journal of Parallel and Distributed Computing*, Vol. 48, pp. 96-129.

Kostoglou, M. and Karabelas, A.J. (**2002**). An assessment of low-order methods for solving the breakage equation, *Powder Technology*, Vol. 127, pp. 116-127.

Kulikov, V., Briesen, H., Grosch, R., Yang, A., Wedel, L., Marquardt, W. (**2005**). Modular dynamic simulation for integrated particulate processes by means of tool integration, *Chemical Engineering Science*, Vol. 60, pp. 2069-2083.

Kumar, J. (**2006**). *Numerical approximations of population balance equations in particulate systems*, Magdeburg: docupoint Verlag.

Kumar, J., Peglow, M., Warnecke, G., Heinrich, S., Mörl, L. (**2006**). Improved accuracy and convergence of discretized population balance for aggregation: The cell average technique, *Chemical Engineering Science*, Vol. 61, pp. 3327-3342.

Kumar, S. and Ramkrishna, D. (**1996**). On the solution of population balance equation by discretization - I. A fixed pivot technique., *Chemical Engineering Science*, pp. 1311-1332.

Le, P.K., Avontuur, P., Hounslow, M.J., Salman, A.D. (**2009**). The kinetics of the granulation process: Right from the early stages, *Powder Technology*, Vol. 189, pp. 149-157.

Lelarasmee, E. (**1982**). *The waveform relaxation method for time domain analysis of large scale integrated circuits: Theory and application*, University of California, Berkley: Dissertation.

Litster, J.D. and Sarwono, R. (**1996**). Fluidized drum granulation: studies of agglomerate formation, *Powder Technology*, Vol. 189, pp. 149-157.

Litster, J.D., Smit, D.J., Hounslow, M.J. (**1995**). Adjustable discretized population balance for growth and aggregation, *AIChE Journal*, Vol. 41, pp. 591-603.

Marquardt, W. (**1991**). Dynamic process simulation - Recent progress and future challenges, *Chemical Process Control CPC-IV, CACHE Publications*, pp. 131-180.

Matlab (**2012**). *Matlab*, [Online], Available: http://www.mathworks.com [2012].

Metsim (**2012**)., [Online], Available: www.metsim.com.

Dieses Werk ist copyrightgeschützt und darf in keiner Form vervielfältigt werden noch an Dritte weitergegeben werden.
Es gilt nur für den persönlichen Gebrauch.

Mindlin, R.D. and Deresiewicz, H. (**1953**). Elastic spheres in contact under varying oblique forces, *Journal of Applied Mechanics*, Vol. 20, pp. 327-344.

Mishra, B.K. (**2000**). Monte Carlo simulation of particle breakage during grinding, *Powder Technology*, Vol. 110, pp. 246-252.

Molerus, O. and Hoffmann, H. (**1969**). Darstellung von Windsichtertrennkurven durch ein stochastisches Modell, *Chemie Ingenieur Technik*, Vol. 41, pp. 340-344.

Mörl, L., Heinrich, S., Peglow, M. (**2007**). Fluidized bed spray granulation, in *Handbook of powder technology*, Amsterdam: Elsevier.

Morrison, R.D. and Richardson, J.M. (**2002**). JKSimMet: A simulator for analysis, optimization and design of comminution circuits, in *Mineral processing plant design, practice and control*, Society for mining metal.

Morton, W. (**2003**). Equation-oriented simulation and optimization, *Proc. Indian Nath. Sci. Acad.*, Vol. 69, pp. 317-357.

Motz, S., Mitrovic, A., Gilles, E.-D. (**2002**). Comparison of numerical methods for the simulation of dispersed phase systems, *Chemical Engineering Science*, Vol. 57, pp. 4329-4344.

Nagaiah, C., Warnecke, G., Heinrich, S., Peglow, M. (**2007**). Numerical simulation of temperature and concentration distributions in fluidized beds with liquid injection, *Chemical Engineering Science*, pp. 1567-1590.

Palis, S. and Kienle, A. (**2012**). Stabilization of continuous fluidized bed spray granulation with external calssification, *Chemical Engineering Science*, Vol. 70, pp. 200-209.

Piskunov, V.N., Golubev, A.I., Barrett, J.C., Ismailova, N.A. (**2002**). The generalized approximation method for modeling coagulaiton kinetics - Part 2: Comparison with other methods, *Journal of Aerosol Science*, Vol. 33, pp. 65-75.

Pitois, P., Moucheront, P., Chateau, X. (**2000**). Liquid bridge between two moving spheres: An experimental study of viscosity effects, *J. on Colloid and Interface Science*, Vol. 231, pp. 26-31.

Pogodda, M. (**2007**). *Development of an advanced system for the modeling and simulation of solids processes*, Aachen: Shaker Verlag.

Popov, V.L. (**2010**). *Contact mechanics and friction: physical principles and applications*, Berlin Heidelberg: Springer.

PSE (**2012**)., [Online], Available: www.psenterprise.com.

Qamar, S. (**2007**). *Modeling and simulation of population balances for particulate processes*, Magdeburg: Dissertation (Online-Ressource).

Radichkov, R., Müller, T., Kienle, A., Heinrich, S., Peglow, M., Mörl, L. (**2006**). A numerical bifurcation analysis of continuous fluidized bed spray granulation with external product classification, *Chemical Engineering and Processing*, Vol. 45, pp. 826-837.

Ramkrishna, D. (**2000**). *Population balances. Theory and applications to particulate systems in engineering*, London: Academin Press.

Ratschow, L. (**2009**). *Three dimensional simulaiton of temperature distributions in large scale circulating fluidized bed combustors*, Aachen: Shaker.

Dieses Werk ist copyrightgeschützt und darf in keiner Form vervielfältigt werden noch an Dritte weitergegeben werden.
Es gilt nur für den persönlichen Gebrauch.

Reppmann, D. (**1990**). *Experimentelle und theoretische Untersuchungen zur Eindüsung von Flüssigkeiten in eine Wirbelschicht*, Dissertation Mageburg.

Reynolds, G.K., Fu, J.S., Cheong, Y.S., Hounslow, M.J., Salman, A.D. (**2005**). Breakage in granulation: A review, *Chemical Engineering Science*, Vol. 60, pp. 3969-3992.

Ronsse, F., Pieters, J.G., Dewettinck, K. (**2007**). Combined population balance and thermodynamic modelling of the batch top-spray fluidised bed coating process. Part I - Model development and validation, *Journal of Food Engineering*, pp. 296-307.

Rossister, A.P. and Douglas, J.M. (**1986**). Design and optimization of solids processes. Part I - A hierarchical decision procedure for process synthesis of solids systems, *Chemical Engineering Research and Design*, Vol. 64, pp. 175-183.

Rumpf, H. (**1975**). *Mechanische Verfahrenstechnik*, München: C. Hanser.

Sastry, K.V. (**1975**). Similarity size distribution of agglomerates during their growth by coalescence in granulation of green pelletization, *International Journal of Mineral Processing*, Vol. 2, pp. 187-203.

Sastry, K.V. and Fuerstenau, D.W. (**1973**). Mechanisms of agglomerate growth in green pelletization, *Powder Technology*, Vol. 7, pp. 97-105.

Schopfer, G., Yang, A., von Wedel, L., Marquardt, W. (**2004**). CHEOPS: A tool-integration platform for chemical process modelling and simulation, *Int. J. Softw. Tools Technol. Transf.*, pp. 186-202.

Schubert, H. (**2003**). *Handbuch der Mechanischen Verfahrenstechnik, Band. 1*, Weinheim: Wiley-VCH Verlag.

Schütte, R., Ruhs, A., Pelgrims, I., Klasen, C.-J., Kaiser, L. (**1998**). Verfahren zur Herstellung von Granulat mit periodisch oszillierender Korngrößenverteilung und Vorrichtung zu seiner Durchführung., *German Patent DE 19639579 C1*.

Schuler, H. (**1995**). *Prozeßsimulation*, Weinheim: VCH-Verlaggeselschaft.

Secchi, A.R., Morari, M., Biscaia, E.C. (**1993**). The waveform relaxation method in the concurrent dynamic process simulation, *Computers and Chemical Engineering*, Vol. 17, pp. 453-465.

Shacham, M., Macchieto, S., Stutzman, F., Babcock, P. (**1982**). Equation oriented approach to process flowsheeting, *Computers and Chemical Engineering*, Vol. 6, pp. 79-95.

Smoluchowski, M. (**1917**). Versuch einer mathematischen Theorie der Koagulationskinetik kolloider Lösungen, *Zeitschrift für Physikalische Chemie*, Vol. 92, pp. 129-168.

Thornton, C., Yin, K.K., Adams, M.J. (**1996**). Numerical simulation of the impact fracture and fragmentation of agglomerates, *Journal of phsysics D: Applied physics*, Vol. 29, pp. 424-435.

Töbermann, J.-C. (**1999**). *Flowsheet simulation of solids processes - the development of a simulation system and its application to soil washing*, Aachen: Shaker.

Tsuji, Y., Tanaka, T., Ishida, T. (**1992**). Lagrangian numerical simulation of plug flow of cohesionless particles in a horizontal pipe, *Powder Technology*, Vol. 71, pp. 239-250.

Uhde Fertilizer Technology *http://www.uhde-fertilizer-technology.com/*, [Online] [2012].

Dieses Werk ist copyrightgeschützt und darf in keiner Form vervielfältigt werden noch an Dritte weitergegeben werden.
Es gilt nur für den persönlichen Gebrauch.

Uhlemann, H. (**1990**). Kontinuierliche Wirbelschicht-Sprühgranulation, *Chemie Ingenieur Technik*, Vol. 62, pp. 822-834.

Vaux, W.G. and Keairns, D.L. (**1980**). Particle attrition in fluid-bed processes, in R., G.J. and M., M.J. *Fluidization: International fluidization conference*, New-York: Plenum Press.

Werther, J., Hartge, E.-U., Gruhn, G. (**2004**). Fließschema-Simulation von Feststoffprozessen, *Chemie Ingenier Technik*, Vol. 76, pp. 709-713.

Werther, J., Heinrich, S., Dosta, M., Hartge, E.-U. (**2011**). The ultimate goal of modeling - simulation of system and plant performance, *Particuology*, Vol. 9, pp. 320-329.

Wintermantel, K. (**1999**). Process and product engineering - achievements, present and future challenges., *Chemical Engineering Science*, Vol. 54, pp. 1601-1620.

Wulkow, M., Gerstlauer, A., Niken, U. (**2001**). Modeling and simulation of crystallization processes using parsival, *Chemical Engineering Science*, Vol. 56, pp. 2575-2588.

Wynn, J.W. (**1996**). Improved accuracy and convergence of discretized population balance of Lister., *AIChE Journal*, Vol. 42, pp. 2084-2086.

Zank, J., Kind, M., Schlünder, E.-U. (**2001**). Particle growth and droplet deposition in fluidised bed granulation, *Powder Technology*, Vol. 120, pp. 76-81.

Zhu, H.P., Zhou, Z.Y., Yang, R.Y., Yu, A.B. (**2008**). Discrete particle simulation of particulate systems: A review of major applications and findings, *Chemical Engineering Science*, Vol. 63, pp. 5728-5770.

Ziff, R. (**1991**). New solutions to the fragmentation equation, *Journal of Physics A: Mathematical and General*, Vol. 24, pp. pp. 2821-2828.

Dieses Werk ist copyrightgeschützt und darf in keiner Form vervielfältigt werden noch an Dritte weitergegeben werden.
Es gilt nur für den persönlichen Gebrauch.

Appendix

A.1: Methods of CDAEModel class

In Table A.1 is given a short summary of methods, which were implemented into the *CDAEModel* class. The functions are listed without specification of the transferred parameters.

Table A.1: List of the methods implemented into the *CDAEModel* class

Method	**Description**
AddStateVariable()	Adds new entry into the list of simulated variables.
DeleteAllStateVariables()	Deletes all state variables which were previously defined.

SetIndependentVariable()
GetIndependentVariable()
	Both functions are used to change and obtain the magnitude of independent variable. In most cases the time property serves as an independent variable. However, the usage of other properties such as spatial coordinates is meaningful.

GetStateVariablesNumber()	Returns the number of calculated variables.

SetStateVariables()
GetStateVariables()
	Assigns the new and obtains old values of state variables.

GetStateDerivatives()	Returns the values of all derivatives.
InitializeDynamicUnit()	Performs initialization of the dynamic unit.
CalculateResiduals()	Calculates the values of residuals. This function plays a decisive role, because the equations of the original DAE system are defined here.
GetAllStVarHistory()	Returns the history of state variables for a specified time interval. This method is helpful for results analysis and further data post-processing.
GetVariableIndex()	By specified name of variable this function returns the index of it into the global data array.

Dieses Werk ist copyrightgeschützt und darf in keiner Form vervielfältigt werden noch an Dritte weitergegeben werden.
Es gilt nur für den persönlichen Gebrauch.

A.2: COM middleware interfaces used in SolidSim-Dynamics

Table A.2: Description of the main interfaces which are used in SolidSim-Dynamics

Interface name	Functionality
ICapeIdentification	Access to the object name and description.
ICapeParameter	Provides an access to the public parameters.
ICapeThermoCompounds	Interface to the data related to chemical compounds.
ICapeThermoMaterial	Provides an access to the discrete overall or phase properties.
ICapeThermoPhases	Allows to find out the number and properties of the phases in the material stream.
IDispatch	Automation interface which allows to obtain information about which properties and methods are supported by an object.
IDynamicThermoMaterial	Access to all operations which are related to time property.
ICapeUtilities	General interface which can be used for initialization and access to parameter collections.
ICapeUnit	Handles most of the interaction with the unit.
ICapeUnitEdit	Allows to display any graphical user interfaces of the unit.
ICapeUnitPort	Through this interface the access to units port can be obtained.
ICapeUnitReport	Allows to get an access to the unit model functions which are related to reporting.
IMaterialStreamCopy	Implements a copy operations with a stream data.
IMaterialStreamInitialization	This interface is used to perform data initialization.
IUnknown	Fundamental interface of COM middleware. Must be present in every COM object.

Dieses Werk ist copyrightgeschützt und darf in keiner Form vervielfältigt werden noch an Dritte weitergegeben werden.
Es gilt nur für den persönlichen Gebrauch.

A.3: Example of parallelization on the flowsheet level

As an illustrative example of the parallelization by the Jacobi WR method, the calculation of simple flowsheet is performed. The flowsheet is shown in Figure A.1.

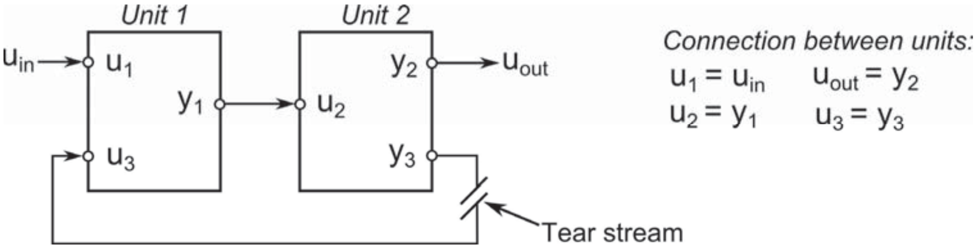

Figure A.1: Exemplary flowsheet

The represented flowsheet consists of two dynamic models, which are described by the following system of the differential-algebraic equations:

$$\begin{cases} \dfrac{dy_1}{dt} = \dfrac{u_3}{u_1}, & y_1(0) = 0.1 \\ y_2 = u_2 - 0.5, & u_{in} = 3 \\ \dfrac{dy_3}{dt} = -u_2, & y_2(0) = 0.8 \end{cases} \tag{A.1}$$

Suppose the example flowsheet is simulated on the time interval [0; 4] and both relative and absolute tolerances equal to 1e^{-3}. In the case of the usage of the Gauss-Seidel approach (implemented into sequential version of SolidSim-Dynamics) it is necessary to run 6 iterations to reach the convergence for the time interval [0; 4]. By the Jacobi WR method the number of iterations increases up to 9.

Figure A.1 shows the values of y_1 on different iterations of the Jacobi WR algorithm to compare the analytical solution. The variables y_1 and y_3 of the DAE system in Eq. (A.2) have the following analytical solution:

$$\begin{aligned} y_1 &= 0.1 \cdot \cos\frac{t}{\sqrt{3}} + \frac{0.8}{\sqrt{3}} \cdot \sin\frac{t}{\sqrt{3}} \\ y_3 &= -\frac{0.3}{\sqrt{3}} \cdot \sin\frac{t}{\sqrt{3}} + 0.8 \cdot \cos\frac{t}{\sqrt{3}} \end{aligned} \tag{A.2}$$

Dieses Werk ist copyrightgeschützt und darf in keiner Form vervielfältigt werden noch an Dritte weitergegeben werden.
Es gilt nur für den persönlichen Gebrauch.

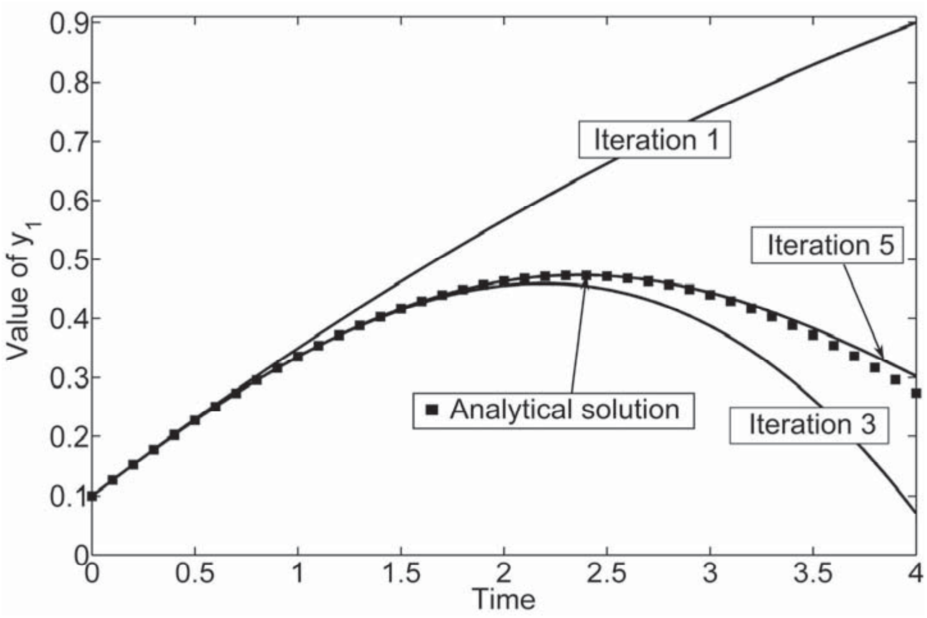

Figure A.2: Simulation results (Jacobi method)

From the analysis of received data, the conclusion can be drawn, that the usage of the Jacobi method causes a larger number of iterations. However, it allows to start concurrent calculations of the both units. The speedup f_{spd}, which can be received from the parallel simulation on two processor system, for this example can be calculated by:

$$f_{spd} = \frac{T_s}{T_p} = \frac{6 \cdot T_1 + 6 \cdot T_2}{9 \cdot \max\{T_1, T_2\} + 9 \cdot T_{tr}}, \qquad \text{(A.3)}$$

where T_1 and T_2 are the times necessary for the calculation of the first and the second models and T_{tr} is the time for the data transfer. If the time for data transfer is negligibly small and both units have equal calculation time, the speedup factor will be equal to 1.33.

Dieses Werk ist copyrightgeschützt und darf in keiner Form vervielfältigt werden noch an Dritte weitergegeben werden.
Es gilt nur für den persönlichen Gebrauch.

A.4: Types of coalescence kernels

To simulate the FB agglomeration process, within the SolidSim-dynamics system, different types of coalescence kernels have been introduced. The list of implemented kernels is given in Table A.3. All represented equations are empirical or semi-empirical models, which were received from the different theoretical calculations and experimental observations.

Table A.3: A short summary of different coalescence kernels given in the literature

Kernel $\beta(v,u)$	Reference
β_0	Kapur and Fuerstenau (1969)
$\beta_0 \cdot \left(u^{1/3} + v^{1/3}\right) \cdot \left(u^{-1/3} + v^{-1/3}\right)$	Smoluchowski (1917)
$\begin{cases} k, & w < w^* \\ 0, & w < w^*, \end{cases} \; w = \frac{(u \cdot v)^a}{(u+v)^b}$ where w^* - critical particle volume	Adetayo and Ennis (1997)
$\beta_0 \cdot \left(u^{1/3} + v^{1/3}\right) \cdot \left(u^{-1/3} + v^{-1/3}\right)$	Smoluchowski (1917)
$\beta_0 \cdot (u + v)$	Golovin (1963)
$\beta_0 \cdot \frac{\left(u^{2/3} + v^{2/3}\right)}{u^{-1} + v^{-1}}$	Sastry (1973)
$\beta_0 \cdot \left(u^{1/3} + v^{1/3}\right)^2 \cdot \left\lvert u^{1/6} - v^{1/6} \right\rvert$	Piskunov et al., (2002)

Dieses Werk ist copyrightgeschützt und darf in keiner Form vervielfältigt werden noch an Dritte weitergegeben werden.
Es gilt nur für den persönlichen Gebrauch.

A.5: Comparison of results obtained from SolidSim-Dynamics and ACM systems

In Figure A.3 and Figure A.4 the simulation results obtained from the SolidSim-Dynamics and Aspen Custom Modeler (ACM) systems are shown accordingly. In both figures the time-progressions of Sauter diameters in all three granulators are shown. Such transient behavior related to the process which is depicted in Figure 6.4.

From the analysis of simulation results the conclusion can be drawn, that each granulator has the same oscillation period of the main parameters. But, due to the different sprayed suspension mass flows and sequence of fluidized beds, they have different amplitudes and values of the PSD.

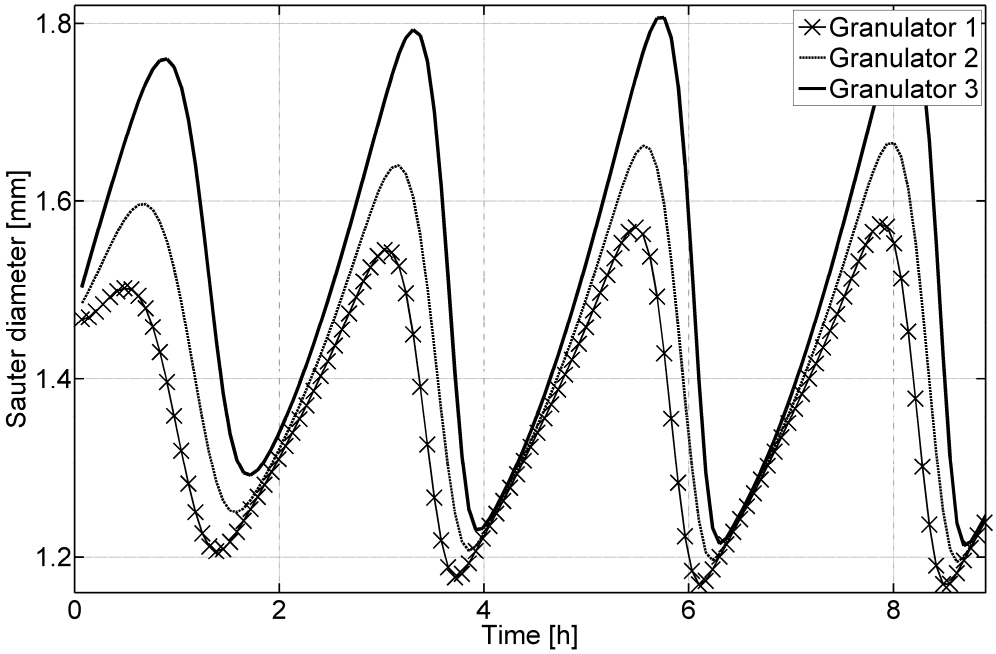

Figure A.3: Results obtained from SolidSim-Dynamics

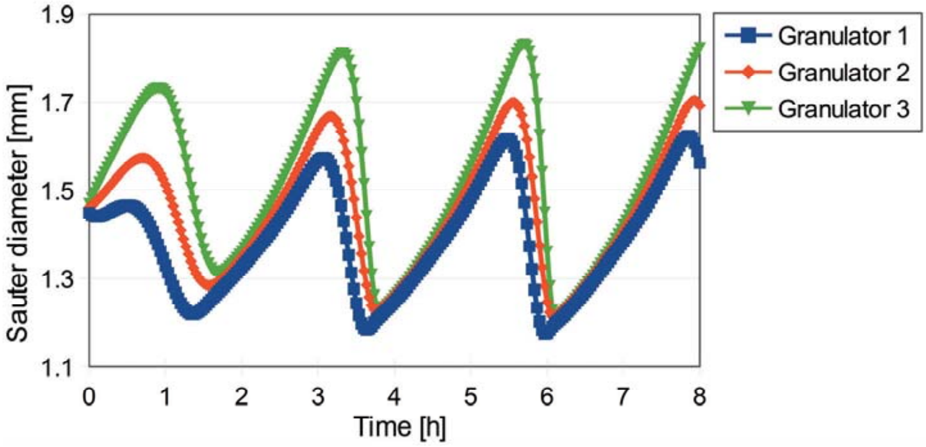

Figure A.4: Results obtained from ACM

Dieses Werk ist copyrightgeschützt und darf in keiner Form vervielfältigt werden noch an Dritte weitergegeben werden.
Es gilt nur für den persönlichen Gebrauch.

A.6: Approximations of heat and mass transfer

According to the empirical approximations of Gnielinski (Wärme- und Stoffübertragung in Festbetten, 1980) the Nusselt number for the packed bed can be calculated as:

$$Nu = 2 + \sqrt{Nu_{turb}^2 + Nu_{lam}^2}, \tag{A.4}$$

where values of Nu_{turb} and Nu_{lam} depend on values of Prandtl number (Pr) and Reynolds number (Re), which are obtained according to:

$$Nu_{lam} = 0.664 \cdot Pr^{1/3} \cdot \sqrt{Re}, \tag{A.5}$$

$$Nu_{turb} = \frac{0.037 \cdot Pr \cdot Re^{0.8}}{1 + 2.443 \cdot Re^{-0.1} \cdot (Pr^{2/3} - 1)} \tag{A.6}$$

The value of the Sherwood number is calculated according to Eq. (A.7) – (A.9). Here, Sc is the Schmidt number.

$$Sh = 2 + \sqrt{Sh_{turb}^2 + Sh_{lam}^2}, \tag{A.7}$$

$$Sh_{lam} = 0.664 \cdot Sc^{1/3} \cdot \sqrt{Re}, \tag{A.8}$$

$$Sh_{turb} = \frac{0.037 \cdot Sc \cdot Re^{0.8}}{1 + 2.443 \cdot Re^{-0.1} \cdot (Sc^{2/3} - 1)} \tag{A.9}$$

The porosity ε (void volume fraction) in the bed depends on Reynolds and Archimedes numbers (Ar) and is calculated according to (Gorosko et al., 1958):

$$\varepsilon = \left(\frac{18 \cdot Re + 0.36 \cdot Re^2}{Ar}\right)^{0.21} \tag{A.10}$$

The Reynolds number at the elutriation point (Re_{elu}) and Reynolds number at the point of the minimal fluidization (Re_{mf}) is approximated by (Gorosko et al., 1958):

$$Re_{elu} = \frac{Ar}{18 + 0.61 \cdot \sqrt{Ar}} \tag{A.11}$$

$$Re_{mf} = \frac{Ar}{1400 + 5.22 \cdot \sqrt{Ar}} \tag{A.12}$$

Dieses Werk ist copyrightgeschützt und darf in keiner Form vervielfältigt werden noch an Dritte weitergegeben werden.
Es gilt nur für den persönlichen Gebrauch.

A.7: Simulation parameters for the multiscale calculation of the granulation process

Table A.4: Main simulation parameters used for the multiscale process modeling

FB granulator		
initial bed mass	0.245	kg
initial PSD median	1	mm
initial PSD deviation	0.1	mm
Fluidization air		
Temperature	80	°C
Suspension		
mass flow	0.5	kg/h
temperature	60	°C
water content	50	%
External feed stream of nuclei		
mass flow	1	kg/h
temperature	30	°C
PSD median	0.6	mm
PSD standard deviation	0.1	mm

Dieses Werk ist copyrightgeschützt und darf in keiner Form vervielfältigt werden noch an Dritte weitergegeben werden.
Es gilt nur für den persönlichen Gebrauch.

List of publications

Peer-reviewed journal publications

M. Dosta, S. Antonyuk, S. Heinrich (**2012**).
Multiscale simulation of fluidized bed granulation process. *Chemical Engineering and Technology, Vol. 35, Issue 8, pp. 1373-1380.*

L. Fries, M. Dosta, S. Antonyuk, S. Heinrich, S. Palzer (**2011**).
Moisture distribution in fluidized beds with liquid injection. *Chemical Engineering & Technology, Vol. 34, Issue 7, pp. 1076-1084.*

J. Werther, S. Heinrich, M. Dosta, E.-U. Hartge (**2011**).
The ultimate goal of modeling - simulation of system and plant performance. *Particuology, 2011, Vol. 9, pp. 320-329.*

M. Dosta, S. Heinrich, J. Werther (**2010**).
Fluidized bed spray granulation: Analysis of the system behaviour by means of dynamic flowsheet simulation, *Powder Technology, Vol. 204, pp. 71-82.*

Conference proceedings

M. Dosta, S. Heinrich (**2011**).
SolidSim-Dynamics – система моделирования технологических процессов твердофазных материалов. *Экологические проблемы индустриальных мегаполисов: Сборник трудов, Донецк, 2011. ISBN 966-508-311-2, pp. 42-49.*

M. Dosta, L. Fries, S. Antonyuk, S. Heinrich, S. Palzer (**2011**).
Multiscale simulation of fluidised bed agglomeration process. *Proceedings of the 5th International Granulation Workshop, Lausanne, Switzerland, June 2011.*

M. Dosta, S. Antonyuk, L. Fries, S. Heinrich (**2010**).
Discrete Element Modelling of the fluidized bed granulation process by coupling of different simulation systems. *Proceedings of the 17th International Drying Symposium, Magdeburg, pp. 506-512.*

M. Dosta, S. Heinrich, M. Pogodda, C. Reimers (**2010**).
Analysis of various granulation process structures by dynamic flowsheet simulation of solids processes, *Proceedings of 6th World Congress on Particle Technology, Nürnberg, April, pp. 26-29*.

Dieses Werk ist copyrightgeschützt und darf in keiner Form vervielfältigt werden noch an Dritte weitergegeben werden.
Es gilt nur für den persönlichen Gebrauch.

J. Neuwirth, M. Jacob, S. Heinrich, M. Dosta, C. Reimers, M. Pogodda (**2010**).
Simulation of the fluidized bed spray granulation pilot plant GF/ProCell 25 with the flowsheet simulation software SolidSim. *Proceedings of the 17th International Drying Symposium, Magdeburg, pp. 571-576.*

L. Fries, M. Dosta, S. Antonyuk, S. Heinrich, S. Palzer (**2010**).
Moisture distribution in fluidized beds with liquid injection, *Proceedings of the 17th International Drying Symposium, Magdeburg, pp. 1093-1100*.

M. Dosta, S. Heinrich, J. Werther, C. Reimers, M. Pogodda (**2009**).
SolidSim-Dynamics – A novel software for the dynamic flowsheet simulation of solids processes. *Proceedings of the 4th International Granulation Workshop, 24- 26 June, Sheffield, England.*

S. Antonyuk, S. Heinrich, M. Dosta (**2009**).
Energetic Aspects of Granule Impact: Influence of the Liquid Layers. *Powders and Grains 2009: Proceedings of the 6th international conference on micromechanics of granular media. Vol. 1145, pp. 796-799*.

Dieses Werk ist copyrightgeschützt und darf in keiner Form vervielfältigt werden noch an Dritte weitergegeben werden.
Es gilt nur für den persönlichen Gebrauch.

Curriculum Vitae

Personal details

Date of Birth:	06.12.1983
Place of Birth:	Donetsk, Ukraine
Nationality:	Ukrainian
Email:	dostamax@gmail.com

Education

1990-1995	School №9, Donetsk, Ukraine
1995-1997	School №17, Donetsk, Ukraine
1997-2000	Donetsk Technical College, Ukraine
2000-2004	**B. Sc.**, Donetsk National Technical University, Faculty of Computer Science
2004-2005	**M. Sc.**, Donetsk National Technical University, Faculty of Computer Science

Experience

07.2003-10.2003, 09.2004	**Software engineer** (Industry practice), Aldec ADT, Katowice, Poland.
09.2005-10.2005	**Software engineer** (Industry practice), FA Donezkstal, Donetsk, Ukraine.
11.2005-10.2006	**Pro3 scholarship**, Max Planck Institute for Dynamics of Complex Technical Systems, Magdeburg, Germany.
01.2007-12.2007	**Scientific co-worker**, Max Planck Institute for Dynamics of Complex Technical Systems, Magdeburg, Germany.
Since 01.2008	**Scientific co-worker**, Hamburg University of Technology, Institute of Solids Process Engineering and Particle Technology, Germany.

Dieses Werk ist copyrightgeschützt und darf in keiner Form vervielfältigt werden noch an Dritte weitergegeben werden.
Es gilt nur für den persönlichen Gebrauch.

Dieses Werk ist copyrightgeschützt und darf in keiner Form vervielfältigt werden noch an Dritte weitergegeben werden.
Es gilt nur für den persönlichen Gebrauch.

Dieses Werk ist copyrightgeschützt und darf in keiner Form vervielfältigt werden noch an Dritte weitergegeben werden.
Es gilt nur für den persönlichen Gebrauch.

Dieses Werk ist copyrightgeschützt und darf in keiner Form vervielfältigt werden noch an Dritte weitergegeben werden.
Es gilt nur für den persönlichen Gebrauch.